

**Investigation of the Corrosion Behaviour of Electroless  
Nickel-Boron and Nickel-Phosphorus Coatings  
in Basic Solutions**

By

Nazila Dadvand

Submitted

In partial fulfillment of the requirement  
for the degree of

DOCTOR OF PHILOSOPHY

Major Subject: Metallurgical Engineering

at

DALHOUSIE UNIVERSITY

Halifax, Nova Scotia

July 12, 2002

© Copyright by Nazila Dadvand, 2002

---



National Library  
of Canada

Acquisitions and  
Bibliographic Services

395 Wellington Street  
Ottawa ON K1A 0N4  
Canada

Bibliothèque nationale  
du Canada

Acquisitions et  
services bibliographiques

395, rue Wellington  
Ottawa ON K1A 0N4  
Canada

*Your file* *Votre référence*

*Our file* *Notre référence*

The author has granted a non-exclusive licence allowing the National Library of Canada to reproduce, loan, distribute or sell copies of this thesis in microform, paper or electronic formats.

The author retains ownership of the copyright in this thesis. Neither the thesis nor substantial extracts from it may be printed or otherwise reproduced without the author's permission.

L'auteur a accordé une licence non exclusive permettant à la Bibliothèque nationale du Canada de reproduire, prêter, distribuer ou vendre des copies de cette thèse sous la forme de microfiche/film, de reproduction sur papier ou sur format électronique.

L'auteur conserve la propriété du droit d'auteur qui protège cette thèse. Ni la thèse ni des extraits substantiels de celle-ci ne doivent être imprimés ou autrement reproduits sans son autorisation.

0-612-77589-5

Canada

**Dalhousie University**  
**Faculty of Engineering**

DOCTOR OF PHILOSOPHY

The undersigned hereby certify that they have examined, and recommend to the Faculty of Graduate Studies for acceptance, the thesis entitled “Investigation of the corrosion behaviour of electroless nickel – boron and nickel - phosphorus coatings in basic solutions” by Nazila Dadvand in partial fulfillment of the requirements for the degree of Doctor of Philosophy.

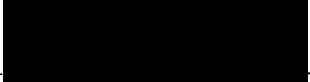
Dated: September 9, 2002

Supervisors:

  
\_\_\_\_\_  
Professor W.F. Caley

  
\_\_\_\_\_  
Professor G. J. Kipouros

External Examiner:

  
\_\_\_\_\_  
Professor J.R. Cahoon,  
University of Manitoba

Examiners:

  
\_\_\_\_\_  
Professor A.M. Al Taweel

  
\_\_\_\_\_  
Professor M.A. White

**Dalhousie University  
Faculty of Engineering**

DATE: Sept. 9/02

AUTHOR: Nazila Dadvand

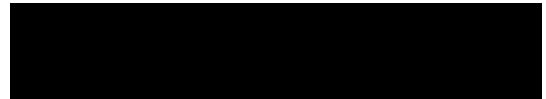
TITLE: Investigation of the Corrosion Behaviour of Electroless Nickel-  
Boron and Nickel-Phosphorus Coatings in Basic Solutions

MAJOR SUBJECT: Metallurgical Engineering

DEGREE: Doctor of Philosophy

CONVOCATION:

Permission is herewith granted to Dalhousie University to circulate and to have copied for non-commercial purposes, at its discretion, the above thesis upon the request of individuals or institutions.



The author reserves other publication rights, and neither the thesis nor extensive extracts from it may be printed or otherwise reproduced without the author's written permission.

The author attests that permission has been obtained for the use of any copyrighted material appearing in this thesis (other than brief excerpts requiring only proper acknowledgement in scholarly writing), and that all such use is clearly acknowledged.

# TABLE OF CONTENTS

TABLE OF CONTENTS	iv
LIST OF TABLES	ix
LIST OF FIGURES	x
LIST OF ABBREVIATIONS AND SYMBOLS	xvii
ACKNOWLEDGEMENTS	xviii
ABSTRACT	xix
<b>1. INTRODUCTION</b>	<b>1</b>
1.1 MODIFYING THE SURFACE WITHOUT CHANGING THE CHEMICAL NATURE OF THE SUBSTRATE	1
<i>1.1.1 Thermal treatment</i>	1
<i>1.1.1.1 Induction heating</i>	2
<i>1.1.1.2 Flame hardening</i>	2
<i>1.1.1.3 Laser hardening</i>	2
<i>1.1.1.4 Electron beam</i>	3
<i>1.1.2 Mechanical treatment</i>	3
1.2 MODIFYING THE SURFACE BY CHANGING THE CHEMISTRY OF THE SURFACE	3
<i>1.2.1 Anodising treatment</i>	4
<i>1.2.2 Ion implantation</i>	4

1.3	MODIFYING THE SURFACE BY ADDING A LAYER OF MATERIAL TO THE SURFACE	4
	<i>1.3.1 Laser alloying</i>	5
	<i>1.3.2 Laser cladding</i>	5
	<i>1.3.3 Thermal spraying</i>	8
	<i>1.3.3.1 Arc spraying</i>	8
	<i>1.3.3.2 Flame spraying</i>	8
	<i>1.3.3.3 Plasma spraying</i>	8
	<i>1.3.4 Electroplating</i>	9
	<i>1.3.5 Electroless plating</i>	11
	<i>1.3.6 Chemical vapour deposition (CVD)</i>	11
	<i>1.3.7 Physical vapour deposition (PVD)</i>	12
	<i>1.3.7.1 Vacuum evaporation</i>	12
	<i>1.3.7.2 Sputter deposition</i>	12
	<i>1.3.7.3 Arc vapour deposition</i>	13
	<i>1.3.7.4 Ion plating</i>	13
1.4	ELECTROLESS NICKEL PLATING	14
	<i>1.4.1 Sodium hypophosphite baths</i>	15
	<i>1.4.2 Aminoborane baths</i>	16
	<i>1.4.3 Sodium borohydride baths</i>	16
	<i>1.4.4 Hydrazine baths</i>	17
1.5	PROPERTIES OF ELECTROLESS NICKEL-PHOSPHORUS COATINGS	17
	<i>1.5.1 Structure</i>	17

1.5.2	<i>Internal stress</i>	20
1.5.3	<i>Uniformity and adhesion</i>	20
1.5.4	<i>Physical properties</i>	21
1.5.5	<i>Mechanical properties</i>	22
1.5.6	<i>Frictional properties</i>	23
1.5.7	<i>Solderability</i>	23
1.5.8	<i>Corrosion resistance</i>	23
1.5.8.1	<i>Effect of composition</i>	24
1.5.8.2	<i>Effect of heat treatment</i>	25
1.5.8.3	<i>Effect of coating porosity</i>	25
1.6	PROPERTIES OF ELECTROLESS NICKEL-BORON COATINGS	25
1.6.1	<i>Hardness and wear resistance</i>	29
1.6.2	<i>Corrosion resistance</i>	30
1.6.2.1	<i>Laboratory corrosion testing</i>	31
2.	<b>THEORETICAL CONSIDERATIONS</b>	47
2.1	ELECTROLESS NICKEL-PHOSPHORUS COATING PRODUCTION MECHANISM	47
2.2	ELECTROLESS NICKEL-BORON COATING PRODUCTION MECHANISM	52
2.2.1	<i>Anodic and cathodic reactions</i>	52
2.3	RESEARCH OBJECTIVES	57
3.	<b>EXPERIMENTAL PROCEDURES</b>	60
3.1	MATERIALS	60

3.2 INSTRUMENTATION	61
3.3 PRETREATMENT PROCESSES	63
<b><i>3.3.1 Pretreatment process for electroless nickel - phosphorus coating on aluminum alloy AA6061</i></b>	63
<b><i>3.3.1.1 Deoxidising and zincating the surface of aluminum alloy</i></b>	63
<b><i>3.3.2 Pretreatment process for electroless nickel-boron coating on aluminum alloy AA6061</i></b>	65
3.4 ELECTROLESS NICKEL-PHOSPHORUS DEPOSITION	66
<b><i>3.4.1 Preparation of EN-P solution</i></b>	66
3.5 ELECTROLESS NICKEL-BORON DEPOSITION	67
<b><i>3.5.1 Preparation of EN-B bath</i></b>	67
3.6 HARDNESS TESTING	68
3.7 CORROSION TESTING	68
<b><i>3.7.1 Preparation of working electrode for corrosion testing of EN-P coatings</i></b>	68
<b><i>3.7.2 Preparation of working electrode for corrosion testing of EN-B coating</i></b>	70
<b><i>3.7.3 Electrolysis cell</i></b>	71
<b>4. RESULTS AND DISCUSSION</b>	<b>74</b>
4.1 ELECTROLESS NICKEL-BORON PLATING ON AA6061	74
<b><i>4.1.1 Pretreatment process before EN-B coating</i></b>	74



4.1.1.1	<i>Intermediate electroless nickel - phosphorus deposition</i>	74
4.1.2	<i>Electroless nickel - boron plating</i>	98
4.1.3	<i>Hardness testing</i>	109
4.2	INVESTIGATION OF THE CORROSION BEHAVIOUR OF ELECTROLESS NICKEL-PHOSPHORUS COATINGS ON AA6061 IN BASIC SOLUTIONS	110
4.2.1	<i>Potentiodynamic study of the electroless nickel - phosphorus coated AA6061 aluminum alloy</i>	111
4.2.2	<i>Cyclic voltammetric study of the electroless nickel - phosphorus coated AA6061 samples</i>	124
4.3	INVESTIGATION OF THE CORROSION BEHAVIOUR OF ELECTROLESS NICKEL-BORON COATINGS IN BASIC SOLUTIONS	137
4.2.1	<i>Potentiodynamic study of the electroless nickel - boron coated brass samples</i>	137
4.2.1	<i>Potentiodynamic study of the electroless nickel - boron coated AA6061 samples</i>	159
5.	CONCLUSIONS	163
6.	REFERENCES	166
7.	APPENDICES	182

## LIST OF TABLES

<b>Table 1.1</b>	<b>Physical and mechanical properties of electroless nickel-boron and nickel-phosphorus deposits<sup>a</sup> [38].</b>	<b>28</b>
<b>Table 3.1</b>	<b>The composition of EN-P plating baths.</b>	<b>69</b>

## LIST OF FIGURES

Figure 1.1	Preplaced powder process [18].	6
Figure 1.2	Blown powder process (laser cladding) [18].	7
Figure 1.3	Electroplating setup [29].	10
Figure 1.4	Triangular waveform of potential ramp [94].	33
Figure 1.5	A typical cyclic voltammogram [94].	34
Figure 1.6	Cyclic voltammograms recorded for a clean nickel electrode electrode (first cycle in each case) in 1.0 mol dm <sup>-3</sup> NaOH at 25 <sup>o</sup> C. Values for lower limit: (—) -0.15 V; (-----) -0.3 V; (.....) -0.050 V. The upper limit was constant in each case at 0.5 V; Sweep rate is 0.041V/sec [95].	39
Figure 1.7	Effect of lower limit on the anodic peaks observed at Low potentials in the case of cyclic voltammograms recorded for an initially clean nickel electrode in 1.0 mol dm <sup>-3</sup> NaOH at 25 <sup>o</sup> C. upper limit, 1.55 V; sweep rate, 41 mV s <sup>-1</sup> . (a) Lower limit -0.2V; (—)1 <sup>st</sup> cycle; ( ---- ) 2 <sup>nd</sup> ; (.....) 3rd; ( .-.-.-. ) 10 <sup>th</sup> . (b) Lower limit -0.3V; ( — )1 <sup>st</sup> cycle; ( -----) 2 <sup>nd</sup> ; (.....) 6 <sup>th</sup> ; ( .-.-.-. ) 10 <sup>th</sup> [95].	40
Figure 2.1	Schematic of the initial steps of the electroless nickel deposition over a catalytic surface [122].	49
Figure 2.2	Outline of the research work.	59
Figure 3.1	Flow chart of deoxidizing and zincating treatment of AA6061.	64
Figure 3.2	Schematic diagram of the AA6061 substrate coated with EN-P.	70
Figure 3.3	An electrolysis cell for corrosion testing.	71
Figure 4.1	Effect of time on the thickness of coating deposited. The bath 76 contained nickel sulfate ( 0.171 M), sodium hypophosphite (0.29 M), glycine (0.53 M), thallium acetate (9.35x10 <sup>-4</sup> M), and acetic acid (0.16 M). The pH was adjusted at 4.87 using sodium	78

hydroxide solution. The temperature of the bath was fixed at  $85 \pm 0.01$  °C.

- Figure 4.2 Effect of nickel sulfate concentration on deposition rate of EN-P coating. The bath contained sodium hypophosphite (0.29 M), glycine (0.53 M), thallium acetate ( $9.35 \times 10^{-4}$  M), and acetic acid (0.16 M). The pH was adjusted at 4.87 using sodium hydroxide solution. The plating was performed at bath temperature of  $85 \pm 0.01$  °C for 2 h. 80
- Figure 4.3 Effect of sodium hypophosphite concentration on deposition rate of EN-P coating. The bath contained nickel sulfate (0.171 M), glycine (0.53 M), thallium acetate ( $9.35 \times 10^{-4}$  M), and acetic acid (0.16 M). The pH was adjusted at 4.87 using sodium hydroxide. The plating was performed for 2 h at bath temperature of  $85 \pm 0.01$  °C. 81
- Figure 4.4 Plot of logarithm of deposition rate versus logarithm of nickel sulfate concentration. The slope of the line is approximately 0.95. Therefore,  $\beta$  is 0.95. The bath contained sodium hypophosphite (0.29 M), glycine (0.53 M), thallium acetate ( $9.35 \times 10^{-4}$  M), and acetic acid (0.16 M). The pH was adjusted at 4.87 using sodium hydroxide. The plating was performed for 2 h at bath temperature of  $85 \pm 0.01$  °C. 82
- Figure 4.5 Plot of logarithm of deposition rate versus logarithm of sodium hypophosphite concentration. The slope of the line is approximately 1.24. Therefore,  $\alpha$  is 1.24. The bath contained nickel sulfate (0.171 M), glycine (0.53 M), thallium acetate ( $9.35 \times 10^{-4}$  M), and acetic acid (0.16 M). The pH was adjusted at 4.87 using sodium hydroxide. The plating was performed for 2 h at bath temperature of  $85 \pm 0.01$  °C. 83
- Figure 4.6 Schematic diagram of a 6-coordinated nickel ion in a given solution. 84
- Figure 4.7 Effect of glycine concentration on deposition rate of EN-P coating. The bath contained nickel sulfate (0.171 M), sodium hypophosphite (0.29 M), acetic acid (0.16 M), and thallium acetate ( $9.35 \times 10^{-4}$  M). The pH was adjusted at 4.87 using sodium hydroxide solution. The plating was performed for 2 h at a bath temperature of  $85 \pm 0.01$  °C. 86

- Figure 4.8 Plot of logarithm of deposition rate versus logarithm of glycine concentration. The slope of the line is approximately  $-0.10$ . Therefore,  $\delta$  is  $-0.1$ . The bath contained nickel sulfate (0.171 M), sodium hypophosphite (0.29 M), acetic acid (0.16 M), and thallium acetate ( $9.35 \times 10^{-4}$  M). The pH was adjusted at 4.87 using sodium hydroxide solution. The plating was performed for 2 h at a bath temperature of  $85 \pm 0.01$  °C. 87
- Figure 4.9 Effect of pH on deposition rate of EN-P. The bath contained nickel sulfate (0.171 M), sodium hypophosphite (0.29 M), glycine (0.53 M), acetic acid (0.16 M), and thallium acetate ( $9.35 \times 10^{-4}$  M). The plating was performed for 2 h at bath temperature of  $85 \pm 0.01$  °C. 89
- Figure 4.10 Plot of logarithm of deposition rate versus logarithm of hydrogen ion concentration. The slope of the line is approximately  $-0.47$ . Therefore,  $\gamma$  is  $-0.47$ . The bath contained nickel sulfate (0.171 M), sodium hypophosphite (0.29 M), glycine (0.53 M), acetic acid (0.16 M), and thallium acetate ( $9.35 \times 10^{-4}$  M). The plating was performed for 2 h at a bath temperature of  $85 \pm 0.01$  °C. 90
- Figure 4.11 Plot of logarithm of deposition rate versus logarithm of hydrogen ion concentration. The slope of the line is approximately  $-0.054$ . Therefore,  $\gamma$  is  $-0.054$ . The bath contained nickel sulfate (0.171 M), sodium hypophosphite (0.29 M), glycine (0.53 M), acetic acid (0.16 M), and thallium acetate ( $9.35 \times 10^{-4}$  M). The plating was performed for 2 h at bath temperature of  $85 \pm 0.01$  °C. 91
- Figure 4.12 Effect of temperature on rate of deposition of nickel-phosphorus coating. The bath contained nickel sulfate (0.171 M), acetic acid (0.16 M), sodium hypophosphite (0.29 M), glycine (0.53 M), and thallium acetate ( $9.35 \times 10^{-4}$  M). The pH of the bath was adjusted at 4.87 using sodium hydroxide solution and the plating was performed for 2 h. 94
- Figure 4.13 Temperature dependence plot of logarithm of deposition rate of nickel-phosphorus versus reciprocal of temperature (K). The bath contained nickel sulfate (0.171 M), acetic acid (0.16 M), sodium hypophosphite (0.29 M), glycine (0.53 M), and thallium acetate ( $9.35 \times 10^{-4}$  M). The pH of the bath was adjusted at 4.87 using sodium hydroxide solution and the plating was performed for 2 h. 95

- Figure 4.14** Effect of temperature on the phosphorus content of an EN-P deposit. The bath contained nickel sulfate (0.171 M), acetic acid (0.16 M), sodium hypophosphite (0.29 M), glycine (0.53 M), and thallium acetate ( $9.35 \times 10^{-4}$  M). The pH of the bath was adjusted at 4.87 using sodium hydroxide solution and the plating was performed for 2 h. 96
- Figure 4.15** Effect of pH on the phosphorus content of an EN-P deposit. The bath contained nickel sulfate (0.171 M), sodium hypophosphite (0.29 M), glycine (0.53 M), thallium acetate ( $9.35 \times 10^{-4}$  M), and acetic acid (0.16 M). The plating was performed for 2h at bath temperature of  $85 \pm 0.01$  °C. 97
- Figure 4.16** Effect of sodium borohydride concentration on deposition rate of EN-B. The bath contained nickel chloride (0.126 M), ethylenediamine (1.42 M), thallium acetate ( $9.35 \times 10^{-4}$  M), 2-butyl-1,4-diol ( $1.2 \times 10^{-3}$  M), and sodium hydroxide (1 M). Bath pH was 12, and the plating was performed for 2 h at a bath temperature of  $85 \pm 0.01$  °C. 101
- Figure 4.17** Effect of sodium borohydride concentration on boron content of EN-B coating. The bath contained nickel chloride (0.126 M), ethylenediamine (1.42 M), thallium acetate ( $9.35 \times 10^{-4}$  M), 2-butyl-1,4-diol ( $1.2 \times 10^{-3}$  M), and sodium hydroxide (1 M). Bath pH was 12, and the plating was performed for 2h at a bath temperature of  $85 \pm 0.01$  °C. 102
- Figure 4.18** Cross section of EN-B coating over intermediate over EN-P coated aluminum alloy (AA6061). 103
- Figure 4.19** SEM micrographs of Ni-P coatings with different thicknesses: (a) 1.4  $\mu\text{m}$ , (b) 3.5  $\mu\text{m}$ , (c) 7.5  $\mu\text{m}$ , and (d) 9  $\mu\text{m}$ . 104
- Figure 4.20** SEM micrographs of Ni-P and Ni-B coatings on Ni-P with different thicknesses: (a) Ni-P coating; 1.1  $\mu\text{m}$  thickness, (b) Ni-B coating; 8.7  $\mu\text{m}$ , (c) Ni-P coating; 2.3  $\mu\text{m}$ , and (d) Ni-B coating; 13.5  $\mu\text{m}$ . 106

- Figure 4.21** SEM micrographs of Ni-P and Ni-B coatings on Ni-P with different thicknesses: (a) Ni-P coating; 7.5  $\mu\text{m}$ , (b) Ni-B coating; 9.2  $\mu\text{m}$ , (c) Ni-P coating; 24  $\mu\text{m}$ , and (d) Ni-B coating; 11.8  $\mu\text{m}$ . 107
- Figure 4.22** SEM micrographs of Ni-B coatings (on Ni-P) with different thicknesses and magnifications: (a) 20  $\mu\text{m}$ ; 249X, (b) 9.4  $\mu\text{m}$ ; 25X, (c) 9.4  $\mu\text{m}$ ; 249X, and (d) 9.4  $\mu\text{m}$ ; 996X. The EN-B bath contained nickel chloride (0.126 M), ethylenediamine (1.42 M), sodium borohydride (0.095 M), thallium acetate ( $9.35 \times 10^{-4}$  M), 2-butyl-1,4-diol ( $1.2 \times 10^{-3}$  M), and sodium hydroxide (1M). Bath pH was 12, and the plating was performed for 2h at a bath temperature of  $85 \pm 0.01$   $^{\circ}\text{C}$ . The thickness of the intermediate EN-P coating was 5  $\mu\text{m}$ . The intermediate EN-P coated AA6061 was heat treated in vacuum at 220  $^{\circ}\text{C}$  for 9 h. 108
- Figure 4.23** Effect of heat treatment time on Vickers hardness of Ni-B coated AA6061 aluminum alloy. The coating was 39  $\mu\text{m}$  thick and contained 6.8 w% B. The heat treatment was performed at 220  $^{\circ}\text{C}$  in vacuum. 110
- Figure 4.24** Polarization curves of EN-P coated sample 1 (12.5 w% P) in 0.5 M NaOH at 5 mV/s scan rate; (a) first run, (b) second run, (c) third run, (d) fourth run. 112
- Figure 4.25** Polarization curves of EN-P coated sample 2 (8 w% P) in 0.5 M NaOH at 5 mV/s scan rate; (a) first run, (b) second run, (c) third run, (d) fourth run. 114
- Figure 4.26** Polarization curves of EN-P coated sample 3 (6 w% P) in 0.5 M NaOH at 5 mV/s scan rate; (a) first run, (b) second run, (c) third run, (d) fourth run. 116
- Figure 4.27** Polarization curves of EN-P coated sample 4 (2 w% P) in 0.5 M NaOH at 5 mV/s scan rate; (a) first run, (b) second run, (c) third run, (d) fourth run. 117
- Figure 4.28** Cyclic voltammogram of EN-P coated sample 1 in 0.5M NaOH at different scan rates; (a) 0.010 V/s, (b) 0.05 V/s, (c) 0.100 V/s, (d) 0.200 V/s, (e) 0.300 V/s, (f) 0.400 V/s, (g) 0.500 V/s. 126
- Figure 4.29** Cyclic voltammogram of EN-P coated sample 2 in 0.5M NaOH at different scan rates; (a) 0.010 V/s, (b) 0.050 V/s, 126

(c) 0.100 V/s, (d) 0.200 V/s, (e) 0.300 V/s, (f) 0.400 V/s,  
(g) 0.500 V/s.

- Figure 4.30 Cyclic voltammogram of EN-P coated sample 3 in 0.5M NaOH at different scan rates; (a) 0.010 V/s, (b) 0.050 V/s, (c) 0.100 V/s, (d) 0.200 V/s, (e) 0.300 V/s, (f) 0.400 V/s, (g) 0.500 V/s. 127
- Figure 4.31 Cyclic voltammogram of EN-P coated sample 4 in 0.5M NaOH at different scan rates; (a) 0.010 V/s, (b) 0.050 V/s, (c) 0.100 V/s, (d) 0.200 V/s, (e) 0.300 V/s, (f) 0.400 V/s, (g) 0.500 V/s. 127
- Figure 4.32 A schematic diagram of EN-P coated AA6061 covered by 128  $\beta$ -Ni(OH)<sub>2</sub> /  $\beta$ -Ni(OH)<sub>3</sub> and  $\alpha$ -Ni(OH)<sub>2</sub> /  $\gamma$ -Ni(OH)<sub>3</sub> layers.
- Figure 4.33 Peak potential difference vs. scan rate (mV/s). 130
- Figure 4.34 Cyclic voltammograms of EN-P coated sample 1 at 0.100 V/s scan rate for different upper voltage limits. 133
- Figure 4.35 Cyclic voltammograms of EN-P coated sample 2 at 0.100 V/s scan rate for different upper voltage limits. 133
- Figure 4.36 Cyclic voltammograms of EN-P coated sample 3 at 0.100 V/s scan rate for different upper voltage limits 134
- Figure 4.37 Cyclic voltammograms of EN-P coated sample 4 at 0.100 V/s scan rate for different upper voltage limits. 134
- Figure 4.38 Cyclic voltammogram of EN-P coated sample 4 after soaking in sulfuric acid (15% v/v) for 20 s in 0.5 M NaOH for different runs. 136
- Figure 4.39 Multiple cyclic voltammograms of EN-P coated sample 4 in 0.5 M NaOH at 0.100 V/s scan rate. 136
- Figure 4.40 Polarization curves of EN-B coated sample 1 in 0.5 M NaOH solution for no heat treatment. (a) first run, (b) second run, (c) third run, (d) 4<sup>th</sup> run, (e) 5<sup>th</sup> run, (f) 6<sup>th</sup> run, (g) 7<sup>th</sup> run, (h) 8<sup>th</sup> run, (i) 9<sup>th</sup> run, (j) 10<sup>th</sup> run, (k) 11<sup>th</sup> run. 140



- Figure 4.41 Polarization curves of EN-B coated sample 2 in 0.5 M NaOH solution for heat treatment duration of 24h. (a) first run, (b) second run, (c) third run, (d) 4<sup>th</sup> run, (e) 5<sup>th</sup> run, (f) 6<sup>th</sup> run, (g) 7<sup>th</sup> run, (h) 8<sup>th</sup> run, (i) 9<sup>th</sup> run, (j) 10<sup>th</sup> run, (k) 11<sup>th</sup> run. 144
- Figure 4.42 Polarization curves of EN-B coated sample 3 in 0.5 M NaOH solution for heat treatment durations of 96h. (a) first run, (b) second run, (c) third run, (d) 4<sup>th</sup> run, (e) 5<sup>th</sup> run, (f) 6<sup>th</sup> run, (g) 7<sup>th</sup> run, (h) 8<sup>th</sup> run, (i) 9<sup>th</sup> run, (j) 10<sup>th</sup> run, (k) 11<sup>th</sup> run. 149
- Figure 4.43 XRD spectra of various Ni-B coatings: (a) as-plated condition, (b) 5 h heat treatment, (c) 24 h heat treatment, (d) 48 h heat treatment, (e) 72 h heat treatment, (f) 96h heat treatment, (g) 120 h heat treatment (h) substrate (brass 70:30). 151
- Figure 4.44 Polarization curves of EN-P coated sample 3 in 0.5 M NaOH at 5 mV/s scan rate; a) first run, b) second run, c) third run, and d) fourth run. 158
- Figure 4.45 Polarization curves of EN-B coated AA6061 sample in 0.5 M NaOH solution for no heat treatment. (a) 1<sup>st</sup> run, (b) 2<sup>nd</sup> run, (c) 3<sup>rd</sup> run, (d) 4<sup>th</sup> run, (e) 5<sup>th</sup> run, (f) 6<sup>th</sup> run, (g) 7<sup>th</sup> run, (h) 8<sup>th</sup> run, (i) 9<sup>th</sup> run, (j) 10<sup>th</sup> run, (k) 11<sup>th</sup> run. 160

## LIST OF ABBREVIATIONS AND SYMBOLS

### Symbol

AAS	Atomic absorption spectrometry
AES	Auger electron spectroscopy
CVD	Chemical vapour deposition
CV	Cyclic voltammetry
DMAB	Dimethyl aminoborane
DSC	Differential scanning calorimetry
EN	Electroless nickel
EN-P	Electroless nickel-phosphorus
EN-B	Electroless nickel-boron
EPMA	Electron micro probe analysis
ESCA	Electron spectroscopy for chemical analysis
HPEN	High-phosphorus electroless nickel
PT	Potentiodynamic
PVD	Physical vapour deposition
SEM	Scanning electron microscopy
TEM	Transmission electron microscopy
VHN	Vickers Hardness Number
VSM	Vibrating sample magnetometry
W%	Weight percent
$\mu\text{m}$	Micrometer
nm	Nanometer

## **ACKNOWLEDGEMENTS**

The author of this thesis would like to acknowledge the guidance, words of encouragement and financial support offered from Dr. W. F. Caley and Dr. G. J. Kipouros during the completion of this work. Thanks are also extended to Darrell Adams for his technical support.

## ABSTRACT

One of the major drawbacks to using aluminum parts in automotive applications is poor wear resistance. Various techniques have been used to address this concern and the purpose of this work was to produce a hard and wear resistant Ni-B coating on AA6061. This was accomplished using an electroless nickel-boron (EN-B) bath preceded by a protective zincating/electroless nickel-phosphorus pretreatment. The experimental parameters for Ni-P and Ni-B baths were optimized, and the effect of various experimental parameters on the plating rate were examined. The phosphorus and boron contents of each deposit were measured using electron probe microanalysis (EPMA) and atomic absorption spectroscopy (AAS), respectively; the surface morphology of each coating was examined using scanning electron microscopy (SEM). Results showed that the surface morphology of the Ni-B coating varies with that of the intermediate EN-P coating. In turn the surface morphology of the intermediate EN-P coating depends on the thickness of the coating and the EN-P plating bath condition.

As well the corrosion behaviour of electroless nickel-phosphorus (EN-P) coatings with phosphorus content ranging from 2 to 12.5 w% was investigated using potentiodynamic (PT) and cyclic voltammetry (CV) techniques in 0.5 M sodium hydroxide. It was found that although the corrosion resistance of EN-P coatings generally decreased with an increase in phosphorus content the trend was observed only for samples where the difference in the P content was large. For example, a very low P EN coating (2 w%) was more resistant in alkaline solution than two medium P (6.5, 8 w%) samples, and these in turn were more resistant than the high P (12.5 w%) coated sample. However, when comparing the 6.5 and 8 w% samples the higher P content showed more resistance. This behaviour may be explained in terms of the two counteracting effects, activation and inhibition, of phosphorus on corrosion resistance. The activating effect is due to the lower protectiveness of the passivating film because of its lower thickness. As the P content increases, the inhibiting effect increases as a result of phosphate formation. As well, the corrosion products and cyclic voltammetric behaviour of the EN samples varied with bath pH.

Finally the corrosion behaviour of electroless nickel-boron (EN-B) coatings with boron content of 6 w% was also investigated using potentiodynamic technique in 0.5M sodium hydroxide, and the results were compared with those of nickel-phosphorus coating with phosphorus content of 6 w%.

The overall results are discussed with a view to providing an optimum process to inhibit the corrosion of AA6061.

# 1. INTRODUCTION

The surface of an aluminum alloy can be treated in a variety of ways to improve in-service lifetime performance, appearance or economics of production [1]. The purpose of modifying the surface may be to increase corrosion resistance, wear resistance or hardness, reduce frictional energy losses, act as a diffusion barrier, provide thermal or electrical insulation, exclude certain wavelengths of radiation, enhance radiation electronic interactions, or improve appearance [2]. Such modifications may involve changing the surface without changing the chemical nature of the substrate, changing the chemistry of the substrate surface, or adding material to the surface. Each of these is addressed in the following sections.

## 1.1 MODIFYING THE SURFACE WITHOUT CHANGING THE CHEMICAL NATURE OF THE SUBSTRATE

In this case, the existing metallurgy of the component is changed, by thermal or mechanical means, within the surface regions so that the hardness is increased [2,3].

### *1.1.1 Thermal treatment*

This case is applied to heat-treatable aluminum alloys, and instead of heating the entire component, only the surface is affected. As a result, bulk properties such as toughness are not affected and component distortion is minimized. Surface thermal treatment can be done by using induction, flame, laser, or electron beam techniques [4].

#### *1.1.1.1 Induction heating*

In this case the surface is heated by using a water-cooled induction coil. The process can be controlled accurately and can be automated. Usually a depth of several mm is hardened [5].

#### *1.1.1.2 Flame hardening*

By local application of an oxyacetylene flame (usually by hand) flame hardening can be achieved. Although the process is less well controlled, it is ideal for treating specific areas (those needing wear resistance) of complex-shaped components [6].

#### *1.1.1.3 Laser hardening*

In this case, a focused laser beam, scans over the surface of the sample. Due to the movement of the laser, initially heated regions become cooled rapidly due to heat conduction into the bulk of the sample so that the structure of the material in the surface changes. The beam scanning over the surface produces a narrow trace of increased hardness. By moving the laser beam over a sample with a slight movement in a lateral direction after the completion of each line, the whole surface of the sample or a selected portion can be hardened [7].

The advantage of using the laser beam is that precise areas of a metal can be heat treated without involving the entire sample [7]. The enhanced mechanical properties resulting from laser heat treatment depend

upon the specific composition of the metal or alloy. Laser hardening provides high wear and abrasion resistance with a minimum of distortion and cracking [7].

#### *1.1.1.4 Electron beam*

Electron Beam Hardening is similar to laser beam hardening. The heat source is a beam of high-energy electrons. The beam is manipulated using electromagnetic coils. The process can be highly automated, but needs to be performed under vacuum conditions since the electron beams dissipate easily in air. As in laser beam hardening, the surface can be hardened precisely both in depth and in location [8].

#### *1.1.2 Mechanical treatment*

Mechanical treatment involving cold working the surface using peening, shot blasting or other specialized machining processes provides a deformed layer in the sample. As a result the stored compressive energy increases and hardness, fatigue and stress corrosion resistance are increased as well [2].

## 1.2 MODIFYING THE SURFACE BY CHANGING THE CHEMISTRY OF THE SURFACE

In this case, new elements are diffused into the surface, usually at elevated temperature, so that the composition and properties of outer layers are changed relative to those of the bulk [2].



### ***1.2.1 Anodizing treatment***

Aluminum alloys form oxide films which are significantly harder than the substrate and reduce wear. In this case, the process of hard anodizing is carried out in an oxidizing acid at around zero degrees centigrade, so that a layer of oxide up to 500  $\mu\text{m}$  may be produced for corrosion protection

[9- 11].

### ***1.2.2 Ion implantation***

In this process, atoms of gaseous or metallic elements are ionized and passed to a high vacuum chamber, where they are accelerated through a mass separator. Selected ions are then further accelerated and implanted into the target component. The implanted species occupy interstitial sites and distort the lattice. The depth of effect is very shallow, 0.2  $\mu\text{m}$ , but the surface properties such as wear resistance, friction, and oxidation / corrosion resistance can be enhanced [12, 13].

## **1.3 MODIFYING THE SURFACE BY ADDING A LAYER OF MATERIAL TO THE SURFACE**

In this case, a material different from the bulk substrate is laid upon the surface. Unlike the first two categories, there is a clear boundary at the coating/substrate interface and the adhesion of the coating is a primary issue [14].

### ***1.3.1 Laser alloying***

In this process a high power focused laser melts the metal coating and a portion of underlying substrate. The melting occurs in a very short time, and only at the surface, so that the bulk of the material remains cool. Large temperature gradients exist across the boundary between the melted surface region and the underlying solid substrate. Therefore, rapid self-quenching and resolidification happens. Because of this rapid quench from the liquid phase, a variety of chemical and microstructural states such as solid solutions, metastable crystalline phases, and metallic glasses are retained. These include chemical profiles where the alloyed element is highly concentrated near the atomic surface giving a steep concentration gradient over nanometer scale depths as well as uniform profiles where the concentration is the same throughout the entire melted region [15-17].

### ***1.3.2 Laser cladding***

This process can be done in two ways: replaced powder process (Figure 1.1), and blown powder process (Figure 1.2). In the first case, a powdered material is distributed on the surface of the sample across the area to be treated. Then the laser beam is moved over the powder and the sample. Due to a sufficiently high beam intensity, and using an appropriate processing speed, a thin region near the surface at the position of the beam is molten [16, 18].

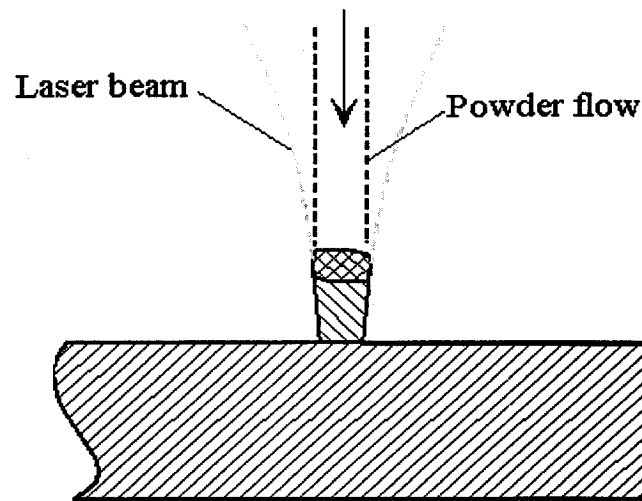


**Figure 1.1 Preplaced powder process [18].**

If the melting point of the powdered material is higher than the melting point of the sample the powder remains solid but is submerged in the liquid material of the sample. After the laser has moved on in the processing direction, the material resolidifies due to cooling by heat conduction into the bulk of the sample and then the powdered material is built into the lattice of the latter. This can be used for an improvement of certain sample properties such as wear or corrosion resistance and is called laser dispersing [18, 19]. If the melting point of the powdered material and the sample material are similar, then the powder is also molten and mixes with the molten surface of the sample. This results in laser alloying after resolidification [18, 19]. Finally, if the powdered film on the surface of the sample is relatively thick, then the molten powder will not be totally submerged into the molten surface of the sample, but will cover the initial surface. This process is called laser cladding [18, 19] and can be used to cover the surface of a material of low hardness with a layer of high hardness giving good wear resistance [18, 19].

In the second case, the powdered material is blown through a thin tube into the focus of the laser beam that moves over the surface of the sample, where laser cladding can be performed. In both process options, that of the preplaced powder and that of the blown powder process, the laser beam is moved along a straight line across the surface of the sample, thus producing a narrow and thin trace with added material. By arranging one trace over another processing of a desired area is possible. As a result the added material can be incorporated in the surface layer of the sample and thus only the part where wear resistance is required is treated, thereby saving material, time and finally cost [18-21].

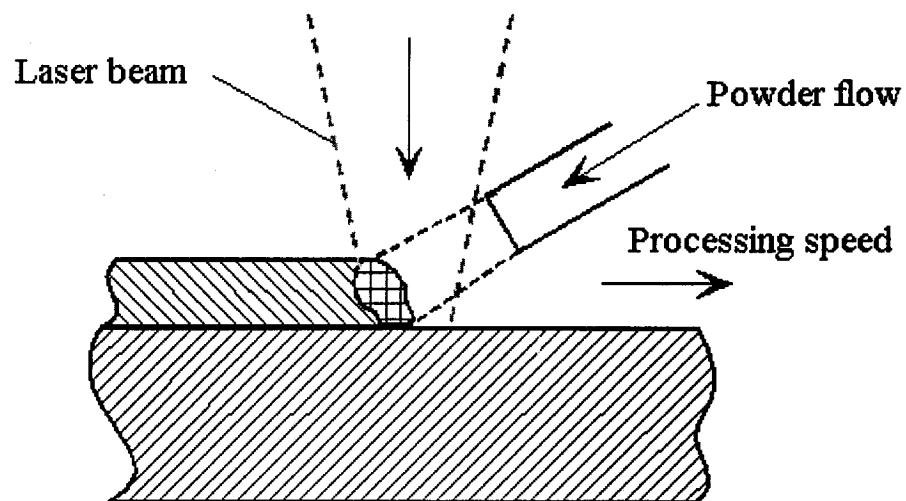


Figure 1.2 Blown powder process (Laser cladding) [18].

### *1.3.3 Thermal spraying*

The process involves heating metal, ceramic or mixtures of metal and ceramic powders to a semi-molten state and depositing them at high velocities on to the substrate. Thermal spraying can be performed using arc, flame, or plasma spraying [22-24]. A brief summary of each follows.

#### *1.3.3.1 Arc spraying*

In this process, the raw material in the form of a pair of metallic wires is melted by means of an electric arc. The molten material is atomized by compressed air and propelled towards the sample. The molten spray solidifies on the component surface to form an adherent coating. The coating has high porosity and low bond strength [25].

#### *1.3.3.2 Flame spraying*

In this process, the raw material in the form of a single wire, or powder is melted in an oxygen-fuel gas flame. This molten material is atomized by a cone of compressed air and propelled towards the sample. The molten spray solidifies on the sample surface to form a dense and adherent coating [26].

#### *1.3.3.3 Plasma spraying*

In this process, a plasma is created by an electric arc burning within the nozzle of a plasma gun. The arc gas is formed into a plasma as it exits the gun nozzle. Powdered particles are injected into this jet where they melt and

then strike the surface at high velocity to produce an adherent coating [27]. The coating is usually porous and often a number of layers must be applied to give a suitable product.

#### ***1.3.4 Electroplating***

The electroplating process employs soluble metal anodes. It requires the passage of direct current between two electrodes that are immersed in a conductive, solution of metal salts. The flow of direct current causes one of the electrodes (the anode) to dissolve and the other electrode (the cathode) to become covered with the metal from the anode [28].

A typical cell for the case of electroplating consists of anode, cathode, aqueous-metal solution, and a power supply. In the simplified example shown in Figure 1.3, the soluble anode is made of nickel, the cathode is made of another conductive material, and the aqueous-metal solution consists of nickel ( $\text{Ni}^{2+}$ ), hydrogen ( $\text{H}^+$ ), and sulfate ( $\text{SO}_4^{2-}$ ) ions. When the power supply is turned on, the positive ions in the solution are attracted to the cathode. The nickel ions that reach the cathode gain electrons and are deposited or plated onto the surface of the cathode forming the electrodeposit. Simultaneously, nickel is electrochemically dissolved from the anode, to produce nickel ions for the aqueous solution and electrons for the power supply. Hydrogen ions, that may also gain electrons from the cathode, form bubbles of hydrogen gas. The formation of hydrogen gas is undesirable since it lowers the plating efficiency (i.e., only a fraction of the total current is used to form the electrodeposit), the bubbles can obstruct the

deposition of the intended electrodeposit and the substrate and deposit may suffer from hydrogen embrittlement [28].

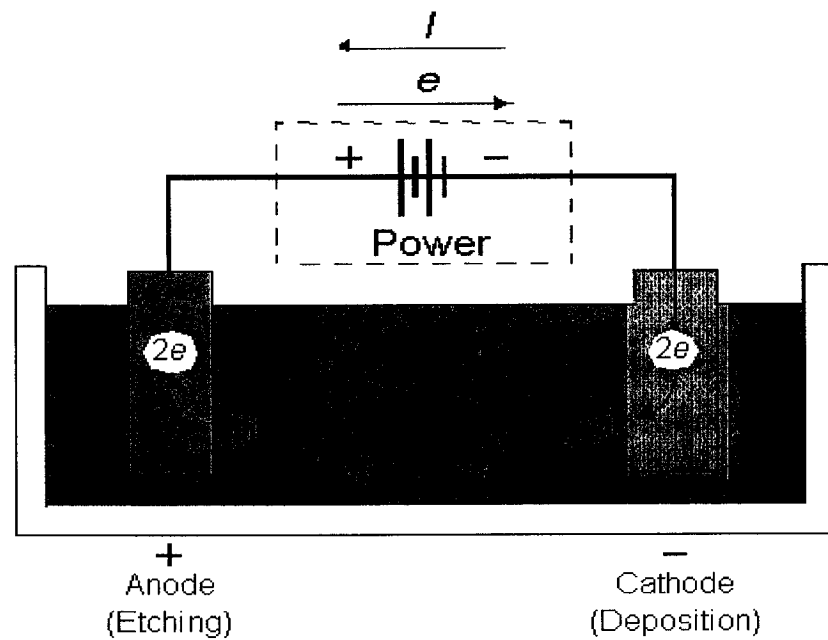


**Figure 1.3 Electroplating setup [29].**

Recently, increased attention has been directed at electrodeposition as an alternative to electroless deposition for producing Ni-P alloys. Electrodeposition offers a number of potential advantages [29]:

- Alloys with 14 to 15 w% phosphorus content – higher than that obtainable with electroless nickel – can be produced. The higher phosphorus content provides less tool wear.

- An order of magnitude greater deposition thickness can be produced.
- Noticeably less expensive than electroless deposition because electrodeposition is not a batch process and the thickness can be controlled.
- The possibility of reduced porosity is an advantage.

### ***1.3.5 Electroless plating***

Electroless plating is used to deposit a metal without the use of an electric current. The coating is deposited by an autocatalytic chemical reduction of metal ions by reducing agents. For electroless nickel plating sodium hypophosphite or sodium borohydride are used as reducing agents. Electroless nickel is a coating normally used because of excellent corrosion and wear resistance [30, 31].

### ***1.3.6 Chemical vapour deposition (CVD)***

CVD is a high-temperature (about 1000 °C) coating process that uses reactant gases, known as precursors, to react and plate out on the surfaces of the parts to be coated. In this non-line-of-sight process, reactant gases are fed into a chamber. Because of the typically high temperatures needed for this process, CVD is commonly used to coat ceramic based substrates. However, lower temperatures, sometimes in conjunction with a plasma assist, are possible if the substrate material distorts at higher temperatures. In terms of hardness, values as high as 2300 Vickers have been reported [32].



### ***1.3.7 Physical vapour deposition (PVD)***

PVD, which is a line-of-sight process that is performed inside a vacuum chamber, creates a vapour that coats a surface when it condenses. Line-of-sight means that only visible surfaces are coated. The two principle PVD processes are evaporation and sputtering. A combination of evaporation and sputtering is called ion plating. In the sputtering process, vapour is created by momentum transfer, where ions impact the target surface and knock atoms out. PVD can be run at relatively low temperatures, lower than 500 °C for high-speed steel or lower than 250 °C for 440 °C bearing steel. Depending on the coating material(s), coatings applied using the PVD process can be as hard as 2800 Vickers. PVD is currently the most popular process for tool coating, especially when the tool configuration can be compromised by high temperatures [33-35].

#### ***1.3.7.1 Vacuum evaporation***

Vacuum evaporation is a PVD process where material from a thermal vapourization source reaches the substrate without collision with the gas molecules in the space between the source and substrate [33, 36].

#### ***1.3.7.2 Sputter deposition***

Sputter deposition is the deposition of particles vapourized from a surface (sputter target) by the physical sputtering process [33]. Sputtering is a non-thermal vapourization process where surface atoms are physically ejected by momentum transfer from an energetic bombarding particle that is

usually a gaseous ion accelerated from a plasma or an ion gun. Sputter deposition can be performed in a vacuum or low-pressure gas (<5 mTorr) where the sputtered particles do not suffer gas-phase collisions [33].

#### *1.3.7.3 Arc vapour deposition*

In arc vapour deposition, the vapour source is the vapourization of the anode or cathode by a low-voltage, high-current electric arc in a good vacuum or low-pressure gas [33]. In cathodic arc configuration, the evaporation is from an arc that is moving over a solid cathodic surface [33]. In the anodic arc configuration, the arc is used to melt the source material that is contained in a crucible. The vapourized material is ionized as it passes through the arc plasma to form charged ions of the film to be deposited [33].

#### *1.3.7.4 Ion plating*

Ion plating uses concurrent or periodic energetic particle bombardment of the depositing film to modify and control the composition and properties of the deposited film and to improve surface coverage and adhesion [33]. The depositing material may be vaporized by evaporation, sputtering, arc erosion, or other vapourization technique [33]. It can be obtained also from the decomposition of a chemical-vapour precursor species. The energetic particles used for bombardment are usually ions of an inert or reactive gas or ions of the depositing material (film ions) [33, 37]. Ion plating can be done in a plasma environment where ions for

bombardment are extracted from the plasma, or it can be done in a vacuum environment where ions for bombardment are formed in a separate ion gun [33, 37].

#### 1.4 ELECTROLESS NICKEL PLATING

In an effort to produce a hard and wear resistant coating on AA6061 for automotive applications, electroless nickel plating has been used, because of the unique engineering properties of electroless nickel coatings, simplicity, and low labour costs [38-40]. Electroless nickel is normally used because of excellent corrosion and wear resistance [38, 41]. Some advantages and limitations of electroless nickel coatings include [38, 41]:

##### Advantages

- Uniformity in thickness
- High corrosion resistance
- High hardness (500-900 VHN)
- Good wear resistance
- Inherent lubricity
- Easy solderability and brazeability
- Adjustable electric and magnetic properties

##### Limitations

- High chemical cost
- Brittleness
- Need to copper plate aluminum alloys containing significant amounts of lead, tin, cadmium, and zinc before electroless nickel can be applied

- Slower plating rate, as compared to electrolytic methods.

Electroless nickel plating is the controlled electrochemical reduction of aqueous nickel ions onto a suitable catalytic surface [38]. The electroless nickel solution must contain: a reducing agent to supply electrons for reduction of nickel ions, a suitable complexing agent to control the free nickel ions and a stabilizer/inhibitor to control the reduction so that deposition occurs only onto the substrate to be plated. Energy in the form of heat is provided by heating the electroless nickel plating bath. Finally, the source of nickel ions is provided by adding a nickel salt, either a sulfate or chloride (the sulfate is preferred when the coatings are required for corrosion resistance applications) [38, 41].

Depending on the type of reducing agent used, the electroless nickel deposit can be nickel-phosphorus or nickel-boron [38, 41]. A number of different reducing agents have been used to prepare EN baths, including sodium hypophosphite, aminoboranes, sodium borohydride and hydrazine. Sodium hypophosphite produces Ni-P deposits whereas sodium borohydride and aminoboranes produce Ni-B deposits [38].

#### ***1.4.1 Sodium hypophosphite baths***

Most of the EN used commercially is deposited from solutions by reduction with sodium hypophosphite [38, 42, 43]. The principal advantages of these solutions over those in which reduction occurs with boron

compounds or hydrazine include lower cost, easier process control, and better corrosion resistance of the deposit.

#### ***1.4.2 Aminoborane baths***

The use of aminoboranes in commercial electroless nickel plating solutions has generally been limited to two compounds: N-dimethylamine borane (DMAB) and N-diethylaminoborane (DEAB). N-dimethylamine borane is readily soluble in aqueous media [38] but must be mixed with a short chain aliphatic alcohol, such as ethanol, before it can be dissolved in the plating solution [38]. Aminoborane baths are very useful for plating plastics and nonmetals, which is their primary application [38, 39, 42, 44, 45].

#### ***1.4.3 Sodium borohydride baths***

Sodium borohydride is one of the most powerful reducing agents for EN-B plating [38]. The coatings obtained by using this reducing agent exhibit excellent hardness, wear resistance and lubricity and have more consistent physical properties than deposits reduced with other boron compounds [38]. Unfortunately, because of the high operating pH of borohydride-reduced baths, they cannot be used for aluminum substrates [38, 39, 42, 46]. The properties of sodium-borohydride-reduced EN coatings are often superior to those of deposits reduced with other boron compounds or with sodium hypophosphite [38, 44].

#### ***1.4.4 Hydrazine baths***

Hydrazine has also been used to produce EN deposits. These baths operate at 90-95°C and pH 10-11. Because of the instability of hydrazine at high temperatures, however, these baths tend to be very unstable and difficult to control. Whereas the deposit from hydrazine reduced solutions is 97-99% Ni, it does not have a metallic appearance. The deposit is brittle and highly stressed with poor corrosion resistance [38, 42]. Unlike hypophosphite and boron reduced nickel, the hardness of the coatings from a hydrazine reduction is not increased by heat treatment. At present, hydrazine reduced EN has very little commercial use [38, 42].

### **1.5 PROPERTIES OF ELECTROLESS NICKEL-PHOSPHORUS COATINGS**

Nickel – phosphorus coatings are uniform, hard, relatively brittle, lubricious, easily solderable, and highly corrosion resistant. They can be precipitation hardened to very high levels through the use of low temperature treatments, producing wear resistance equal to that of commercial hard chromium coatings [38].

#### ***1.5.1 Structure***

The percentage of phosphorus in a coating depends on the formulation of the plating solution. The most widely studied composition range is from about 3 to 14 w% phosphorus. This range can be further divided into two regions, namely between 3-7 and 7-14 w% P [47-49]. It has been reported

that deposits in the lower range are crystalline whereas those in the higher range are amorphous [47, 50]. However, it has been suggested [47, 51] that deposits in the higher range could be a) a mixture of micro-crystalline and amorphous phases and b) a mixture of microcrystalline and amorphous phases along with various other phases like  $\text{Ni}_5\text{P}_4$ ,  $\text{Ni}_{12}\text{P}_5$  and  $\text{Ni}_5\text{P}_2$  [47]. Interestingly, Makhsoos et al. [52] report the entire range as being amorphous. The crystallization behaviour of these deposits has been the subject matter of various investigations and there appear to be conflicting opinions regarding structural aspects and the crystallization processes of these metastable conditions which may eventually form a stable structure of precipitated phosphide(s) in a nickel matrix [47]. The crystallization behaviour also depends on the phosphorus content. Differential scanning calorimetry (DSC) and TEM studies indicate that deposits with less than 7 w% phosphorus crystallize directly into  $\text{Ni}_3\text{P}$  from a supersaturated crystalline nickel solid solution. However, deposits with higher phosphorus contents form intermediate precipitates such as  $\text{Ni}_5(\text{P},\text{Ni})_2$  and  $\text{Ni}_3(\text{P},\text{Ni})$  from amorphous  $\text{NiP}$  before the final  $\text{Ni}_3\text{P}$  formation [53]. Other workers based on TEM and vibrating sample magnetometry (VSM) report the formation of various intermediate precipitates such as  $\text{Ni}_{12}\text{P}_5$ ,  $\text{Ni}_5\text{P}_2$ ,  $\text{NiP}_2$  and  $\text{Ni}_7\text{P}_3$  with  $\text{Ni}_3\text{P}$  as the final precipitate [47]. Tyagi et al [54] based on VSM conclude that deposits with phosphorus contents between 7 and 11 w% P first form crystalline nickel and subsequently precipitate  $\text{Ni}_3\text{P}$  from the phosphorus rich matrix [47, 54].

The broadening of x-ray line profiles obtained from the deposits is a definite indication of lattice disorder [47]. The measurement of crystallite size and microstrain in the lattice by x-ray line profile analysis can indicate the structural changes taking place in the deposits. By using x-ray line profile analysis along with DSC and microhardness measurements, it is possible to investigate the behaviour of these deposits, as a function of phosphorus content and annealing temperature. Kumar and Nair [47] showed that the structure of EN-P deposits with P contents ranging from 4.35 to 9.10 w% is a mixture of microcrystalline nickel and amorphous phases in the as-deposited condition. The lattice disorder in a microcrystalline nickel phase was significant and an increase in the phosphorus content increased the disorder. From x-ray line profile analysis they concluded that the crystallization behaviour of these deposits is essentially same for all compositions. First the deposits were annealed at 60, 100, 200, 300, 330, 360, 400, and 600 °C for 2 h, then the annealing temperature range was divided into three regions: room temperature to 100 °C, 100 to 300 °C, and 300 to 600 °C. Between room temperature and 100 °C, the change taking place in the structure was negligible. From 100 to 300 °C, only atomic rearrangements in the microcrystalline nickel phase seemed to be taking place without the formation of any intermediate precipitate. At 330 °C, complete crystallization occurred with the precipitation of Ni<sub>3</sub>P from the phosphorus rich amorphous matrix. Above this temperature Ni<sub>3</sub>P precipitates grew with a corresponding reduction in phosphorus content and lattice disorder in nickel [47].



Typical precipitation hardening type of behaviour of EN coatings has been reported [47] with microhardness values ranging from about 450 VHN in the as deposited state to a peak hardness of about 825 to 950 VHN, in the annealed condition. The peak hardening temperature (360 °C) also corresponds with the precipitation temperature range.

### ***1.5.2 Internal stress***

Internal stress in electroless nickel coatings is primarily a function of coating composition. For example, stress in coatings used on steel containing more than 10 w% phosphorus is neutral or compressive. With lower phosphorus deposits, however, tensile stresses of 15 to 45 MPa develop because of the difference in thermal expansion between the deposits and substrate. The high level of stress in these coatings promotes cracking and porosity and heat treatment at temperatures above 220 °C causes the EN deposits to shrink 4-6 % in volume. This increases tensile stress and reduces compressive stress in the coating. The presence of excess complexing agents in the plating solution as well as codeposition of orthophosphates or heavy metals increase the stress in deposit. Finally, as might be expected, high levels of internal stress reduce the ductility of the coating and increase cracking [38, 42, 55-57].

### ***1.5.3 Uniformity and adhesion***

With electroless nickel, the plating rate and coating thickness are the same on any section of the part exposed to fresh plating solution. Grooves

and blind holes have the same amount of coating as the outside of a part [38, 55].

Adhesion of electroless nickel coatings to most metals is excellent. The initial replacement reaction, which occurs with catalytic metals, together with the associated ability of the baths to remove submicroscopic material, allows the deposit to establish metallic as well as mechanical bonds with the substrate [38]. With noncatalytic or passive metals, such as stainless steel, an initial replacement reaction does not occur, and adhesion is reduced [38, 42, 55, 58]. With proper pretreatment, however, the bond strength of the coating usually is improved. With metals such as aluminum, parts are baked after plating to increase the adhesion of the coating. These treatments relieve hydrogen from both part and deposit and provide a very minor amount of co-diffusion between coating and substrate [38, 42, 55, 59].

#### ***1.5.4 Physical properties***

The density of an EN coating is inversely proportional to the phosphorus content. Density varies from about  $8.5 \text{ g/cm}^3$  for low-phosphorus deposits to  $7.75 \text{ g/cm}^3$  for a coating containing 10 to 11w% phosphorus [38, 42, 58-62]. The thermal and electrical properties of these coatings also vary with composition. These coatings are significantly less conductive than conventional conductors such as copper or silver [38].

Heat treatments often precipitate phosphorus from the alloy and can increase conductivity by three to four times [63]. The formulation of the plating solution can also affect conductivity. Finally, the phosphorus content also has a strong effect on the thermal expansion of electroless nickel.

As deposited, coatings containing more than 10% phosphorus are completely nonmagnetic. Lower phosphorus coatings, however, have some magnetic susceptibility, although heat treatment at temperatures above 300 °C may improve the magnetic response of electroless nickel [38, 64, 65].

### ***1.5.5 Mechanical properties***

Electroless nickel deposits have high strength, limited ductility, and a high modulus of elasticity. The ductility of EN coatings also varies with composition [38, 66] . Thin films of deposit can be bent completely around themselves without fracture. With lower phosphorus deposits or with deposits containing metallic or sulfur impurities, ductility is greatly reduced and may approach zero. As might be expected, hardening heat treatments reduce both the strength and ductility of EN deposits [66].

As deposited the microhardness of EN coatings is about 500 to 600 HV<sub>100</sub> (HV<sub>100</sub> is the Vickers Hardness at 100 mg load). Heat treatment causes these alloys to age harden and can produce hardness values as high as 1100 HV<sub>100</sub>, equal to most commercial hard chromium coatings [38, 42, 55]. For some applications, high temperature treatments cannot be used because parts may warp, or the strength of the substrate may be reduced. For these

applications, longer times and lower temperatures are sometimes used to obtain the desired hardness. EN coatings have excellent resistance to wear and abrasion, both in the as-deposited and hardened conditions. After heat treatment, high phosphorus deposits provide the best wear resistance [38, 42, 55, 59, 67-69].

#### ***1.5.6 Frictional properties***

Frictional properties of electroless nickel coatings are excellent and are similar to those of chromium because the phosphorus content provides a natural lubricity. The frictional properties of these coatings vary little with either phosphorus content or heat treatment [38, 42, 69, 70].

#### ***1.5.7 Solderability***

Electroless nickel coatings can be easily soldered, and are used in electronic applications to facilitate soldering light metals such as aluminum. For most components, rosin mildly activated (RMA) flux is specified along with conventional tin-lead solder. Preheating the component to 100 – 110 °C improves the ease and speed of joining. With moderately oxidized surfaces, activated rosin (RA) flux is usually required to obtain wetting of the coating [38, 42, 71].

#### ***1.5.8 Corrosion resistance***

Electroless nickel is a barrier coating, protecting the substrate by sealing it off from the environment. Because of its amorphous nature and

passivity, the corrosion resistance of the coating is excellent and in many environments is superior to that of pure nickel or chromium alloys. Amorphous alloys have better resistance to attack than equivalent polycrystalline materials, because of the absence of grain or phase boundaries, and because of the glassy films which form on and passivate their surfaces [38, 42, 57, 72-74].

#### *1.5.8.1 Effect of coating composition*

The corrosion resistance of an electroless nickel coating is a function of its composition, in particular, the P content. Interestingly, high phosphorus EN coatings have poorer corrosion resistance in hot concentrated sodium hydroxide than either low phosphorus or medium phosphorus coatings; these in turn have a corrosion resistance comparable to Ni [38, 57, 60, 75, 76].

In acidic environments, the higher P EN (10-12 w%) coatings are more resistant. Often the minor constituents present in an EN coating are even more influential in corrosion resistance than the phosphorus content. Some coatings are applied from baths that contain lead, tin, cadmium, or sulfur as inhibitors. Codeposition of these elements in greater amounts causes the corrosion resistance of the coating to be increased by 5 to 40 times [57].

#### *1.5.8.2 Effect of heat treatment*

When nickel-phosphorus deposits are heated to temperatures above 220 °C, nickel phosphide particles begin to form, reducing the P content of the remaining material. This reduces the corrosion resistance of the coating. The particles also create small active/passive corrosion cells, further contributing to the destruction of the deposit. The deposit also shrinks as it hardens, which can crack the coating and expose the substrate to attack [38, 57, 77].

#### *1.5.8.3 Effect of coating porosity*

It is obvious that increasing porosity decreases the corrosion resistance of the coating. The important factors that determine coating porosity and ultimate resistance to corrosion attack are substrate condition, pre-treatment, and electroless nickel process selection [38, 78].

### 1.6 PROPERTIES OF ELECTROLESS NICKEL-BORON COATINGS

In order to deposit boron, there is a need for a bath which is stabilized by thallium [38]. Some of this thallium is codeposited with boron.

The properties of nickel-boron deposits produced from borohydride or aminoborane - containing baths are similar to those of electroless nickel-phosphorus [38]. The hardness of Ni-B alloys is very high, and these alloys can be heat treated to levels greater than that of hard chromium [38]. Ni-B coatings also have outstanding abrasion and wear resistance [38]. However,

unlike high-phosphorus electroless alloys, nickel-boron deposits are not completely amorphous in the as-plated condition [38]. Rather, the deposit consists of a mixture of nickel-boron glass and a small amount of crystalline nickel. Some x-ray diffraction studies have in fact suggested the alloy is in a state of transition between amorphous and very finely crystalline states. These coatings typically have a columnar structure [38, 42, 44].

The composition of these coatings also varies throughout thickness. The boron content of the deposit is very low immediately adjacent to the substrate and increases with depth. However, the distribution of thallium which is used to stabilize the solution is the reverse. Its concentration is highest near the interface with the substrate then declines slowly as thickness increases [79]. During heating, EN-B hardens in the same manner as the Ni-P coatings. At temperatures above 200 °C distinct particles of nickel boride begin to form, and at 310 °C the coating crystallizes. The type of boride formed depends upon heat treatment temperature and the boron content of the deposit. At lower temperatures, Ni<sub>3</sub>B typically forms, whereas at temperatures higher than 400 °C, Ni<sub>2</sub>B and Ni<sub>7</sub>B<sub>3</sub> may also be present. The boride, Ni<sub>7</sub>B<sub>3</sub>, is unstable, however, and dissociates to Ni<sub>2</sub>B and Ni<sub>3</sub>B at temperatures higher than 450 °C. The final structure of most hardened nickel boron coatings typically consists of Ni<sub>3</sub>B and about 10% crystalline nickel and thallium [80, 81].

The internal stress of nickel-boron deposits is highly tensile. The boron content of the coatings which were produced by borohydride-reduction is

known to significantly affect the internal stress of these deposits. Although the effect has not been quantified, it may be similar to that measured with coatings reduced with dimethyl aminoborane (DMAB). With DMAB-reduced deposits, stress decreases with increasing boron concentration [82].

The density of EN-B ( $8.25 \text{ g/cm}^3$  for commercial borohydride-reduced coatings) is very similar to that of Ni-P coatings of equal metalloid content [83]. However, unlike the nickel-phosphorus alloys, these coatings do not shrink during heat treatment and their density is the same in the as-deposited and hardened conditions. The melting point of Ni-B coatings is  $1080 \text{ }^\circ\text{C}$ , which is significantly higher than that of EN-P coatings ( $890 \text{ }^\circ\text{C}$ , Table 1.1 [38]).



**Table 1.1 Physical and mechanical properties of electroless nickel-boron and Nickel-phosphorus deposits<sup>a</sup> [38].**

Property	Electroless nickel-boron (5 w% boron)	Electroless nickel-phosphorus (10.5 w% phosphorus)
Density, g/cm <sup>3</sup> (lb/in. <sup>3</sup> )	8.25 (2.98)	7.75 (2.8)
Melting point, °C (°F)	1080 (1980)	890 (1630)
Electrical resistivity, μΩ.cm	89	90
Thermal conductivity, W/m.K (cal/cm.s. °C)	...	4 (0.01)
Coefficient of thermal expansion 22-100°C (72-212°F), μm/m. °C (μin./in. °F)	12.6 (7.1)	12 (6.7)
Magnetic properties	Very weakly ferromagnetic	Non-magnetic
Internal stress, MPa (ksi)	110 (16)	Nil
Tensile strength, MPa (ksi)	110 (16)	700 (100)
Ductility, % elongation	0.2	1.0
Modulus of elasticity, GPa (10 <sup>6</sup> psi)	120 (17)	200 (29)
As-deposited hardness, HVN <sub>100</sub> <sup>b</sup>	700	500
Heat treated hardness, 400°C (750°F) for 1h, HVN <sub>100</sub>	1200	1100
Coefficient of friction versus steel, lubricated	0.12	0.13
Wear resistance, as-deposited, Taber <sup>c</sup> mg/1000 cycles	9	18
Wear resistance, heat treated 400°C (750°F) for 1h, Taber <sup>c</sup> mg/1000 cycles	3	9

<sup>a</sup>Properties are for coatings in the as-deposited condition, unless noted.

<sup>b</sup>HVN<sub>100</sub> is the Vickers Hardness at 100mg load.

<sup>c</sup>Taber Wear Index is the weight loss in mg per 1000 cycles in a Taber Abraser.

The electrical resistivity of a Ni-B coating ranges from 89  $\mu\text{Ohm-cm}$  (Table 1.1 [39]) in the as-deposited condition to 43  $\mu\text{Ohm-cm}$  after heating to 1100  $^{\circ}\text{C}$ . The coefficient of thermal expansion for coatings containing 5 w% boron ranges from 12.1  $\mu\text{m}/\text{m}^{\circ}\text{C}$  in the as-deposited condition to 10.8  $\mu\text{m}/\text{m}^{\circ}\text{C}$  after heat treating for 2 h at 350  $^{\circ}\text{C}$  [38, 83] and in the as-deposited condition, Ni-B coatings are weakly ferromagnetic. The magnetic susceptibility, however, is increased by heat treatment [38, 83].

Finally, the maximum elongation of EN produced by borohydride-reduction is only about 0.2%. By comparison, the ductility of high-phosphorus deposits is about 1% (Table 1.1). Unlike a coating produced by hypophosphite-reduction, however, heat treatment appears to have little effect upon the ductility of Ni-B [38, 83].

### ***1.6.1 Hardness and wear resistance***

The principal advantages of EN produced by borohydride-reduction are hardness and superior wear resistance [38, 42, 46]. In the as-deposited condition, microhardness values of 650 to 750  $\text{VHN}_{100}$  are typical for coatings containing 5% boron. After heat treatment for 1 h at 350 to 400  $^{\circ}\text{C}$  hardness values of 1200  $\text{VHN}_{100}$  can be produced [38, 42, 84].

Very long-term (30 to 40 weeks) treatments at 200 to 300  $^{\circ}\text{C}$  can produce hardness values of 1700 to 2000  $\text{VHN}_{100}$ . These low temperatures cause a finer dispersion of nickel boride as compared with higher temperatures. The wear resistance of EN produced by borohydride-reduction is reported to be

outstanding and after heat treatment equals or exceeds that of hard chromium coatings. EN produced by borohydride-reduction coatings are naturally lubricious [38, 42].

### ***1.6.2 Corrosion resistance***

In general the corrosion resistance of borohydride-reduced EN is less than that of coatings reduced with sodium hypophosphite [38]. In environments that cause little corrosion of high phosphorus coatings (eg. alkalis and solvents), EN-B is very resistant. However, in environments that cause moderate attack of Ni-P (eg., acids, and ammonia solutions), Ni-B coatings can be severely corroded. In strongly anodizing media neither coating is satisfactory [38].

Because borohydride-reduced EN is not totally amorphous, the passivation films that form on its surface are not as glassy or protective as those that form on high phosphorus coatings. The phase boundaries present in these deposits also produce passivation film discontinuities, which are preferred sites for corrosion to begin. Also, because boron and thallium are not homogeneously distributed throughout the coating, areas of different corrosion potential are produced on the surfaces leading to the formation of small active/passive corrosion cells; thus, accelerated attack occurs [83].

### ***1.6.2.1 Laboratory corrosion testing techniques***

Polarization methods such as potentiodynamic polarization, potentiostaircase, and cyclic voltammetry are often used for laboratory corrosion testing [85, 86]. Useful information about the mechanisms of corrosion, corrosion rate and susceptibility of specific materials to corrosion in various environments can be provided by using these techniques [87-89].

In polarization, the potential of the working electrode is changed with respect to the reference electrode and the resultant current is measured as a function of time or voltage. There are three types of polarization [90]:

- Anodic polarization where the potential is varied in the anodic (or more positive direction) causing the working electrode to become the anode.
- Cathodic polarization where the working electrode becomes more negative and electrons are added to the surface, in some cases causing electrodeposition.
- Cyclic polarization where both anodic and cathodic polarization are performed in a cyclic manner.

In potentiodynamic techniques, the potential of the electrode is varied at a selected rate by passing of a current through the electrolyte. It is probably the most commonly used polarization testing method for measuring corrosion resistance [91]. Electrochemical techniques have been used for the assessment of porosity in EN deposits, investigation of the formation of anodic oxide films on EN surfaces in acidic, neutral, and basic solution,

investigation of the effect of phosphorus content on anodic dissolution and passivation of EN coatings [92]. Among the electrochemical methods, cyclic voltammetry has been used extensively by many researchers to investigate the passive film formed on nickel and nickel-phosphorus alloys [92].

Cyclic voltammetry (CV), one of the most commonly used electroanalytical techniques, is an excellent development tool, but is not usually a good technique for quantitative analysis. Its main advantage in electroanalysis is its ability to characterize an electrochemical system [93, 94].

In a CV experiment, the potentiostat applies a potential ramp to the working electrode to gradually change the potential and then reverses the scan, returning to the initial potential (see the triangular waveform in Figure 1.4) where  $E$  and  $t$  are applied voltage and measured current, respectively [94].

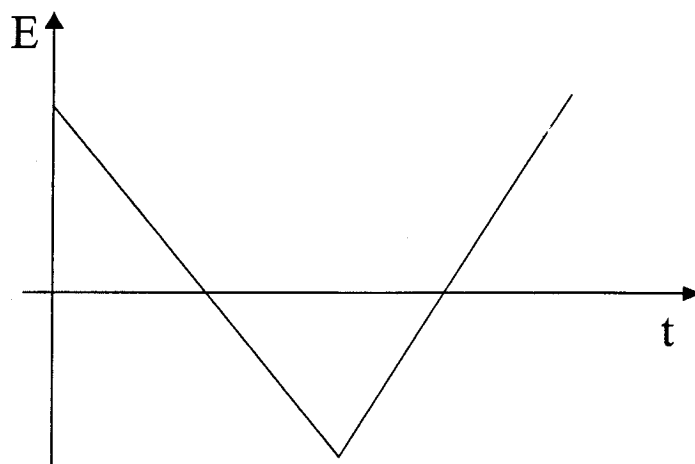


**Figure 1.4 Triangular waveform of potential ramp [94]**

During the potential sweep, the potentiostat measures the current resulting from the applied potential. These values are then used to plot the CV graphs of current versus applied potential. Either single-cycle or multiple cyclic CV experiments can be run. The repetition of the potential waveform allows the system to come to a steady-state or allows the build up of  $i_p$  of reaction products on the electrode surface. Figure 1.5, a typical CV plot, shows the four important pieces of information obtained from a CV experiment – the cathodic peak height ( $I_{pc}$ ), the anodic peak height ( $I_{pa}$ ), the cathodic peak potential ( $E_{pc}$ ), and the anodic peak potential ( $E_{pa}$ ) [94].

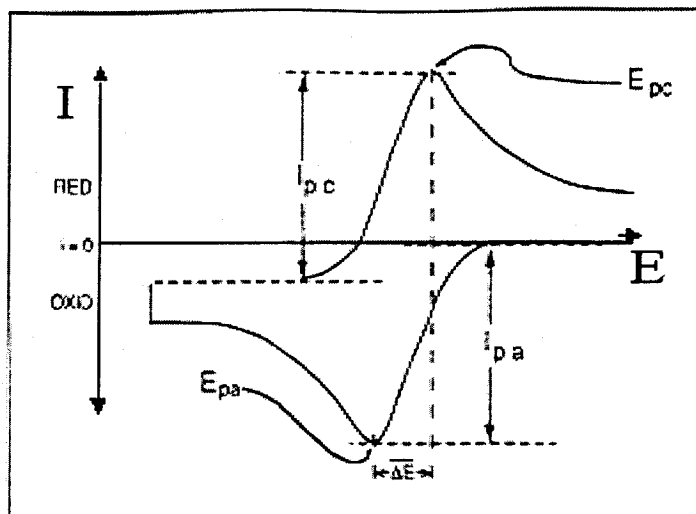


Figure 1.5 A typical cyclic voltammogram [94]

Note that Figure 1.5 uses the American convention for plotting electrochemical data – that is, negative potential to the right and cathodic (reductive) current positive (upward). A single CV is useful for determining whether or not a species is electroactive. A peak current response within a given potential range indicates whether or not a material has been involved in a reaction [94].

Unfortunately, only limited conclusions can be drawn from a single CV plot about the reversibility of a redox couple. One criterion for reversibility is that the  $I_{pc}$  should equal the  $I_{pa}$ , so it may seem that if a single CV shows  $I_{pc}$  equal to  $I_{pa}$  that the system is reversible. However, if the scan rate is increased the  $I_{pc}$  may no longer equal the  $I_{pa}$  and the system would appear irreversible. The same can be true of other variables in the experiment. A change of electrolyte concentration could also affect the results of the

experiment. Thus, a single CV is only useful to define reversibility for a very specific set of experimental conditions [94].

Cyclic voltammetry has been used extensively by many researchers to investigate the voltammetric behaviour of nickel and nickel hydroxide electrodes in acidic, neutral, and basic solutions [94]. The study of the nickel (II) hydroxide / nickel (III) oxyhydroxide (commonly referred to as the nickel oxide) electrode is of considerable interest in the battery development field and the potential cyclic technique is a useful method for generating films for investigation in this area [95-98]. In this application potential cycling can convert the nickel to hydrated oxide in basic environments [95]. It is well established that the reduced form of nickel hydroxide is  $\text{Ni(OH)}_2$  and the oxidized form is generally believed to be  $\text{NiO(OH)}$  [95]. Both these structures have been shown to exist in two modifications called  $\alpha$  and  $\beta$  for the reduced structure and  $\gamma$  and  $\beta$  for the corresponding oxidized structure. The reduced  $\alpha$  form has further been shown to have the formula  $3\text{Ni(OH)}_2 \cdot 2\text{H}_2\text{O}$ . These structures and their modifications are probably hydrated to a greater or lesser extent [99, 100].

Although phases  $\alpha$ ,  $\beta$ , and  $\gamma$  have layered structures [101], the  $\beta$ -phase is an anhydrous phase whereas  $\alpha$ , and  $\gamma$  are hydrated. Thus in the  $\alpha$ -phase the planar metal hydroxide layers are separated from each other by planes of water molecules whereas in the  $\gamma$ -phase the layers are separated by electrolyte [101]. Two peaks  $\beta(\text{II})$  to  $\beta(\text{III})$  and  $\alpha(\text{II})$  to  $\gamma(\text{III})$  may be



expected on the anodic sweep and two further peaks on the subsequent cathodic sweep [101].

On the basis of Barke and Twomey's work [99] at  $\text{pH} < 14$ , two cathodic and one anodic peaks appear, and the anodic  $\beta(\text{II})$  to  $\beta(\text{III})$  transition was absent. This could be due either to the poor conductivity of  $\alpha(\text{II})$  surrounding the  $\beta(\text{II})$  or to the absence of  $\beta(\text{II})$  material during the anodic sweep at  $\text{pH} < 14$  [99].

According to Burke and Whelan's work [102], electron transfer in the oxidized hydrous form occurs more easily because of the existence of mixed oxidation states in the oxidized form. This may explain the higher conductivity of the oxidized form relative to the reduced form, and thus the appearance of two cathodic peaks compared to only one anodic peak in 1M NaOH [102]. At high base concentration, the second anodic peak appears, possibly because the reduced hydrous form becomes more conductive. As a result the peak for the oxidation of the anhydrous hydroxide is observed [102].

Smith and collaborators [103] showed that in 0.15 N  $\text{Na}_2\text{SO}_4$  solution, the anodic film observed on pure Ni was primarily  $\text{Ni}(\text{OH})_2$  and that at different pH levels and potentials NiO forms simultaneously with  $\text{Ni}(\text{OH})_2$ . They also determined that at  $\text{pH} > 8$ , the  $\text{Ni}(\text{OH})_2$  film is oxidized to  $\text{NiOOH}$  at potentials near those required for oxygen evolution. A deprotonation reaction to convert the  $\text{Ni}(\text{OH})_2$  to  $\text{NiOOH}$  was suggested as explanation for the findings [103].

Visscher and Barendrecht [104] studied the cyclic voltammetry of nickel metal in basic solutions. They observed two peaks in the positive sweep, one at about +0.27 V vs. SHE and the other at 1.4 V vs. SHE. The intensity for the upper peak increased on cycling and split into a doublet due to the presence of hydrous and anhydrous components. The interpretation of the voltammetric behaviour in the lower region was complicated by the inability to distinguish between the surface metal atom and adsorbed hydrogen oxidation processes. This was due to the presence of a variety of reactions, e.g. adsorbed hydrogen oxidation, formation of chemisorbed OH or O species, compound formation resulting in NiO or Ni(OH)<sub>2</sub> layers [104].

A further complication mentioned by Visscher and Barendrecht [104] is that, after pre-anodizing at 1.2 V vs. SHE, hydrogen can penetrate into the nickel on cycling between 1.2 and -0.8 V vs. SHE; this absorbed hydrogen gives rise to an additional anodic peak at about 0.1 V vs. SHE on a subsequent slow (2 mV/s) anodic scan.

Shumilova and Bagotsky [105, 106] have demonstrated that the amount of oxide or hydroxide produced on the surface at constant potential in the lower region increases with time, as does the strength of the metal to oxygen bond.

Typical examples of cyclic voltammograms recorded for nickel in basic solutions are shown in Figures 1.6 and 1.7. The presence of a hysteresis effect in the peaks observed at low potentials (Figure 1.6) is

indicative of alternating metal surface oxidation and reduction (or metal/hydroxide formation and removal) reactions [95]. Since the thermodynamic data [107] indicate that the reversible potential for NiO formation is in the region of 0.1 V vs. Hg/Hg<sub>2</sub>Cl<sub>2</sub>, it is assumed here that the anodic peak at low potentials (Figure 1.6 ) is due to the production of a Ni(II) species at the nickel surface [95]. The main peak in the lower region appears to be superimposed on a background current which is probably due to a combination of adsorbed hydrogen oxidation and formation of a layer of OH<sub>ads</sub> species [108, 109]. In certain cases this lower peak on the positive sweep appeared to split to form a doublet e.g., Figure 1.4 [95].

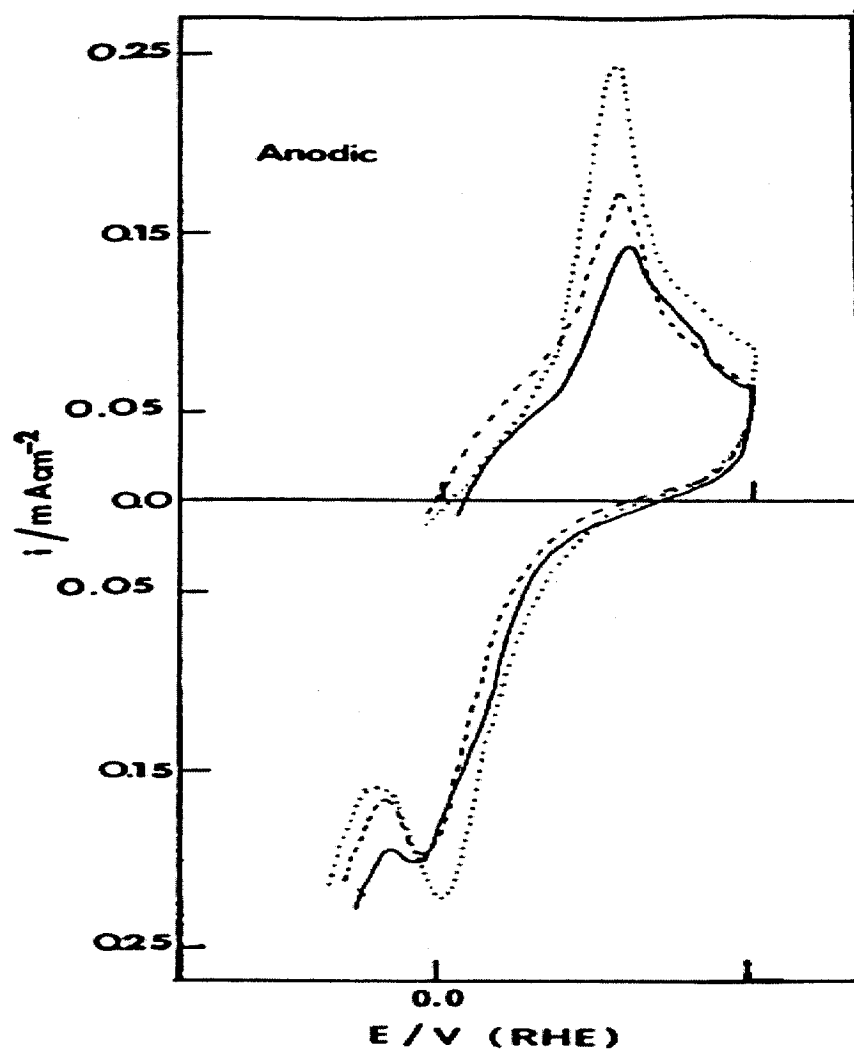
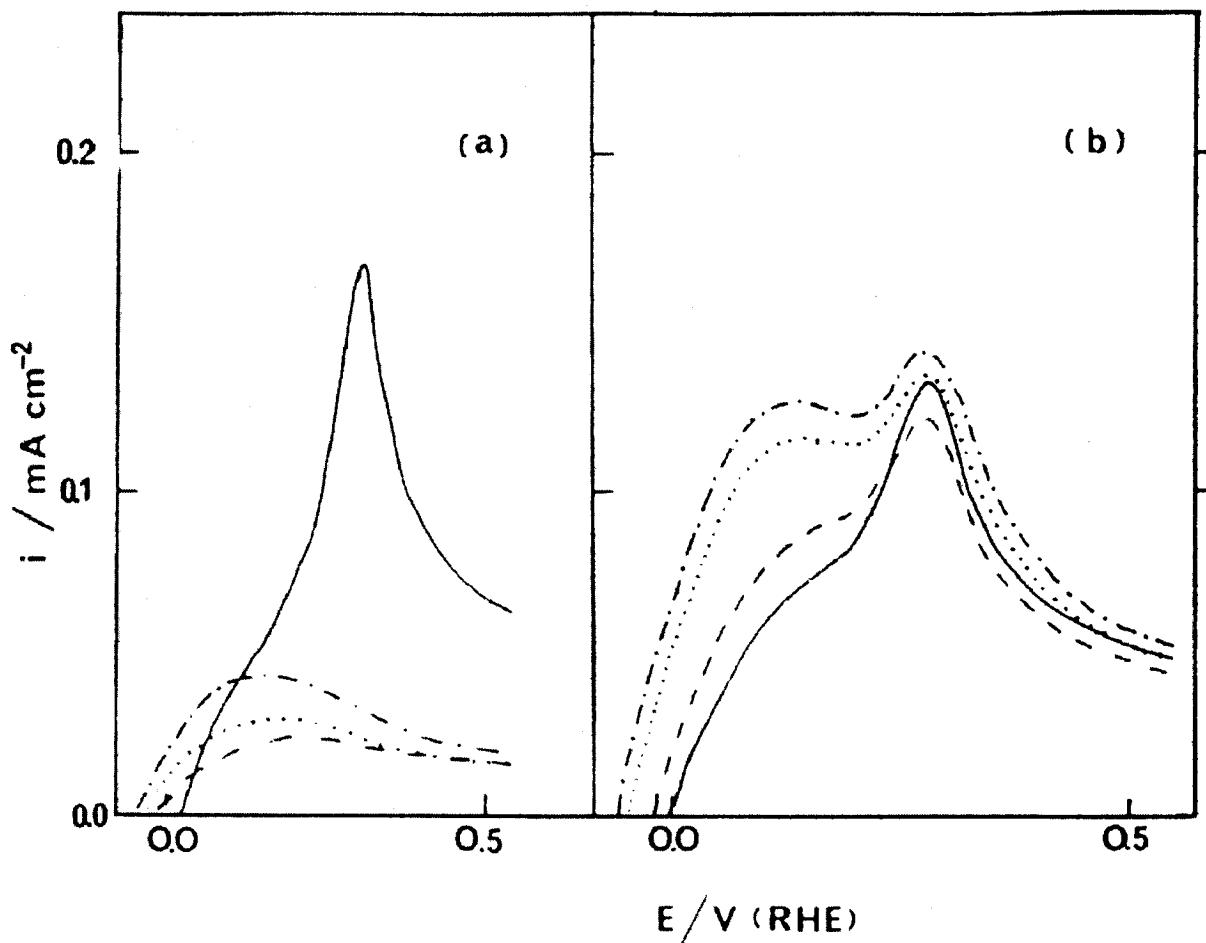
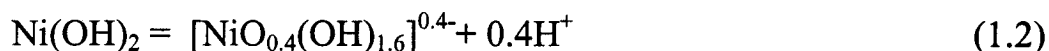


Figure 1.6 Cyclic voltammograms recorded for a clean nickel electrode (first cycle in each case) in  $1.0 \text{ mol dm}^{-3} \text{ NaOH}$  at  $25^\circ \text{C}$ . Values for lower limit: (—)  $-0.15 \text{ V}$ ; (---)  $-0.3 \text{ V}$ ; (.....)  $-0.50 \text{ V}$ . The upper limit was constant in each case at  $0.5 \text{ V}$ ; Sweep rate was  $0.041 \text{ V/s}$  [95].

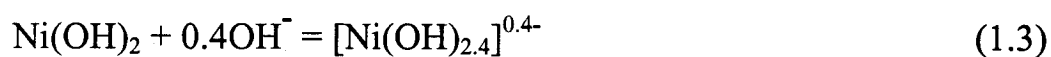


**Figure 1.7** Effect of lower limit on the anodic peaks observed at low potentials in the case of cyclic voltammograms recorded for an initially clean nickel electrode in  $1.0 \text{ mol dm}^{-3} \text{ NaOH}$  at  $25^\circ \text{C}$ . Upper limit,  $1.55 \text{ V}$ ; sweep rate,  $0.041 \text{ V s}^{-1}$ . (a) Lower limit  $-0.2 \text{ V}$ ; (—) 1<sup>st</sup> cycle; (----) 2<sup>nd</sup>; (.....) 3<sup>rd</sup>; (·-·-·-·) 10<sup>th</sup>. (b) Lower limit  $-0.3 \text{ V}$ ; (—) 1<sup>st</sup> cycle; (----) 2<sup>nd</sup>; (.....) 6<sup>th</sup>; (·-·-·-·) 10<sup>th</sup> [95].

However, this splitting usually occurred only when traces of an outer charge storage film were present [95]. Thus whereas the origin of the lower peak of the doublet is uncertain, it does not appear to be an intrinsic feature of the initial film formed on elemental nickel under positive sweep conditions [95]. The decrease in redox potential for the anodic reaction, about 0.013 V per unit increase in pH, with respect to a pH-independent reference electrode, is indicative of the simultaneous occurrence of oxidation and hydrolysis processes. Here there may be two partial reactions involved as follows [95]:

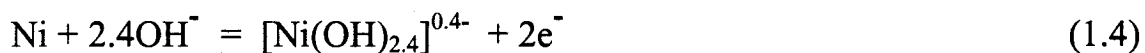


As an alternative in this case, since the investigation was confined to alkaline solutions, the latter reaction may be represented as an hydroxide ion adsorption step [95]



The formulae for the anionic species in equations (1.2) and (1.3) are given solely to rationalize the observed pH dependence on potential. The real identity of the rather transient species involved is difficult to establish. All that is claimed is that the layer formed in the initial stages of metal oxidation

is anionic in character [110]. In very simple terms the net anodic reaction may be represented as [95]



To derive an expression for the variation of the peak potential with pH, the electrode is considered to be as a metal/metal ion electrode as follows [95]:



Applying the Nernst equation to equation (1.1) yields [95]:

$$E = E^0 + (RT/2F)\ln(a_{\text{Ni}^{2+}}) \quad (1.6)$$

and substituting for  $a_{\text{Ni}^{2+}}$  in terms of a stability constant for the anionic complex [95]:

$$K_s = a_{[\text{Ni}(\text{OH})_{2.4}]^{0.4-}} / (a_{\text{Ni}^{2+}})(a_{\text{OH}^-})^{2.4} \quad (1.7)$$

results in a final equation [95]

$$E = E^0 + (RT/2F)\ln[a_{[\text{Ni}(\text{OH})_{2.4}]^{0.4-}} / (K_s)(K_w)^{2.4}] - 1.2(2.303RT/F)(\text{pH}) \quad (1.8)$$

According to this treatment a response in excess of the usual 0.059 V/pH unit can still be regarded as Nernstian in character [95, 111]. Such high values may also be rationalized in terms of additional stabilization of the oxidized form of the couple, i.e.  $\text{Ni}^{2+}$  or  $\text{Ni}(\text{OH})_2$  [95] with increasing hydroxide ion activity in solution due to anionic complex formation. As well the latter process may be regarded in forms of either hydrolysis or a hydroxide ion adsorption reaction [95].

The peak for the oxide reduction shows the more usual type of behaviour, i.e., a zero shift in redox potential with respect to pH. On going from the positive to the negative sweep the initially produced hydrous species alters to a more anhydrous form, e.g. NiO, so that the predominant reduction step is as follows [95]:



This interpretation of the difference in potential/pH behaviour between the formation and reduction of the initial anodic layer has been discussed in detail recently for the case of platinum [110]. The post-electrochemical reactions involved result in conversion of terminal oxygen ( $\text{O}^-$ , OH and  $\text{OH}_2$ ) to bridging oxygen (Ni-O-Ni) species. Consequently a decrease in the level of ionizable protons in the surface layer has also been suggested [112] as the origin of the hysteresis effects observed in oxide layer formation/removal processes.



In the earlier work [103] on the charge storage reactions of hydrous nickel oxide grown on cycling, one anodic and two cathodic peaks were observed at base concentrations lower than about  $4.0 \text{ mol/dm}^3$ . The fact that at quite slow sweep-rates or after an extended number of cycles, two anodic peaks were also observed in the positive sweep may be due to slow restructuring of the initial layer with partial conversion of the hydrous to anhydrous material.

Similar conclusions with regard to rearrangement of material within the surface layer have been arrived at by Arvia and coworkers [113, 114]. It may also be noted that this reaction, the conversion of hydrous ( $\alpha$ ) to anhydrous ( $\beta$ ) nickel hydroxide, is a standard procedure [115] in the battery field for the preparation of crystalline  $\beta\text{-Ni(OH)}_2$ . Evidently it is a slow process as in the case of bulk material a typical period of 18h at  $100^\circ\text{C}$  is allowed for the conversion. While time (or sweep rate) is obviously important in the case of thin films, film thickness also is important. However, in the latter case time could also be the major factor, i.e. the material formed during the early (e.g. the first twenty) cycles may require a significant time (up to the 60<sup>th</sup> cycle) in order to attain a significant formation of  $\beta\text{-Ni(OH)}_2$ . Whereas the above account assumes a slow conversion of hydrous to anhydrous material on the positive sweep, the reverse occurs on the negative sweep, since reducing the sweep-rate gives a more pronounced hydrous film reduction response. Possibly at the upper positive limit, 1.55 V, oxygen gas evolution results in significant dehydration of the  $\gamma\text{-NiOOH}$ . Reduction at slower sweep rate

may give the resulting  $\beta$ -Ni(III) material more time to hydrate, hence the more distinct hydrous oxide reduction peak [95].

As the base concentration is increased, there is less tendency for the pH of the solution at the electrode surface to decrease as the layer is oxidized [95]:



On the positive sweep, oxide formation, rather than dissolution, is thereby assumed to be favoured. It was also pointed out [116] that increasing the base concentration may significantly raise the level of Ni(IV) species in the surface layer at the upper end of the sweep. Furthermore, the high base concentration, along with increased  $\text{OH}^-$  ion adsorption, probably also favours the formation of nikelite and nikelate species in the layer [95].

It is quite difficult to obtain direct information concerning the structure of species, especially surface oxycations, involved in reactions at the electrode-solution interface. This was illustrated [117, 118], by the fact that two sets of data, obtained by the same technique, on the composition of the passive oxide film on iron were quite contradictory. Although cyclic voltammetry provides no direct structural data, it does provide information from which it is possible to arrive at a new viewpoint on some of these systems [114]. One of the most interesting ideas from that work is the

suggestion that initial monolayer anodic film growth involves not simply uncharged hydroxyl groups at the surface but anionic species. Whereas this suggestion may not be totally novel, direct evidence for the state of charge of such species is quite difficult to obtain and its implication with regard to repulsion effects at the electrode surface, obviously requires further consideration [95]. The restructuring of the initial layer, in particular its apparent conversion from an anionic to a neutral form, is an important aspect of the hysteresis effect in the oxide electrochemistry of both non-noble and noble metals [95].

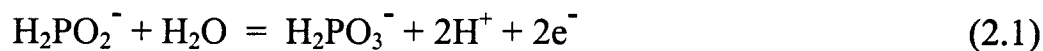
## 2. THEORETICAL CONSIDERATIONS

The characteristics of an EN coating depend upon the type and concentration of components of the chemical bath used to deposit these coatings, as well as temperature and plating duration. Therefore, the electroless deposition process is important from both theoretical and practical points of view. However, such a study is rather complicated due to the process being autocatalytic and because of the presence of parallel reactions of nickel (II) reduction.

### 2.1 ELECTROLESS NICKEL PHOSPHORUS PRODUCTION MECHANISMS

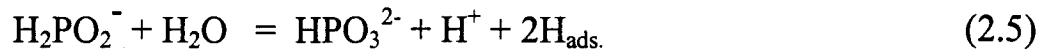
Several mechanisms have been proposed for the chemical reactions which occur in the electroless nickel plating produced by hypophosphite reduction plating from solutions [38, 41]:

- 1) The electrochemical mechanism where catalytic oxidation of the hypophosphite yields electrons at the catalytic surface which in turn reduce nickel and hydrogen ions [119], is:



- 2) The atomic hydrogen mechanism where atomic hydrogen is released

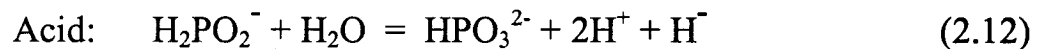
as a result of the catalytic dehydrogenation of hypophosphite molecule adsorbed at the surface [41]. The adsorbed atomic hydrogen reduces nickel ions and also forms, by combination, hydrogen gas:

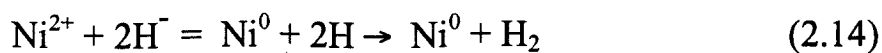


- 3) The atomic hydrogen theory as proposed by Gutzeit [43] was based on the mechanism of catalytic dehydrogenation of hypophosphorous acid. According to this mechanism the electroless deposition reaction can be written as:



- 4) Hersch [120] introduced the hydride theory which was developed further by Lukes [121]. According to the hydride mechanism the nickel ion reducing action is due to hydride ions released by the reaction of hypophosphite with water [120]:





Each of the theories accounts for the simultaneous deposition of nickel and evolution of hydrogen [41]. The most recent proposed theory considers the adsorption of hypophosphite and homolysis of the hydrogen bond with the production of hydrogen radicals (Figure 2.1) [122, 123].

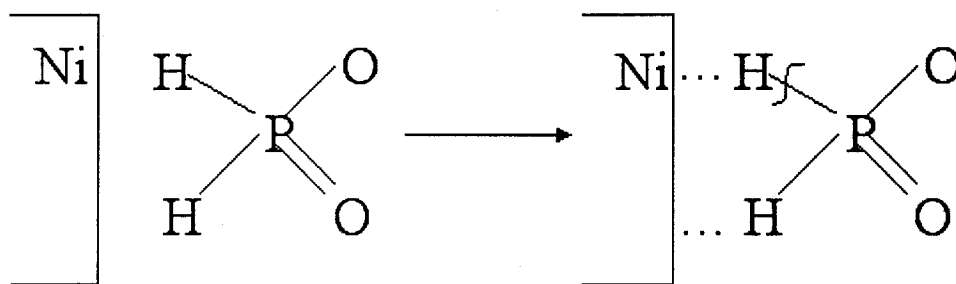


**Figure 2.1 Schematic of the initial steps of the electroless nickel deposition over a catalytic surface [122].**

This step takes place spontaneously over a catalytic material or over an electrolessly inactive substrate. The main reactions can be expressed by the following equations [122].



The combination of two adsorbed hydrogen atoms will be responsible for part of the observed gas evolution [122]. Thus,



and if nickel ion reduction occurs then equation (2.19) takes place to some degree

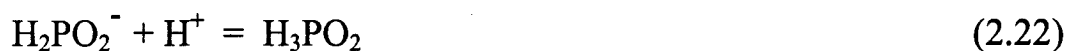


The reduced metal mainly results from the direct reaction among the nickel ions and the reductant radicals rather than from the consumption of the electrons produced by the anodic oxidation of the reducing agent. The latter is the main reason for the failure of the mixed potential theory [122]. The other radical,  $\text{HPO}_2^-$ , will oxidize with the formation of atomic hydrogen or, depending on the experimental conditions, give rise to an anodic current. The resultant electrons from the oxidation of the  $\text{HPO}_2^-$  radical, are responsible to some extent for the reduction of the metal and the hydrogen ions [122] according to



In an electroless experiment using the hypophosphite ion as the reducing agent, there is always phosphorus codeposition simultaneous with the nickel reduction which produces a Ni-P film. Typically the amount of nonmetallic element in the alloy can vary between 3 and 35 atomic percent, depending on experimental conditions [124]. This quantity is strongly dependent on solution pH, and is usually reported as increasing with acidity [125].

Phosphorus formation is a result of the reaction between the hypophosphorous acid with a hydrogen radical as follows [122]

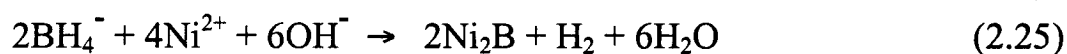


Equations (2.22) and (2.23) explain the decrease of phosphorus content with alkalinity by means of the equilibrium displacement of reaction (2.22) to the left, but this cannot explain the change in this behaviour after a particular pH value. Early electroless nickel formulations were ammoniacal and operated at high pH. Later, acidic solutions were found to have several advantages over the alkaline solutions such as higher plating rate, better stability and improved deposit corrosion resistance [122]. Accordingly, most electroless hypophosphite reduction nickel solutions are operated between pH 4 - 5.5 [126].



## 2.2 ELECTROLESS NICKEL-BORON COATING PRODUCTION MECHANISMS

Borohydride ions hydrolyze readily in acid or neutral solutions and if nickel ions are present nickel boride will form spontaneously. If the pH of the plating solution is maintained above 12, however, decomposition can be prevented and an alloy of nickel and boron will be produced. The commonly accepted reactions for this deposition can be written as follows [44, 127, 128]:



These equations are incomplete, however, because they overlook the complex dehydrogenation and oxidation reactions that occur during borohydride reduction and assume that hydrogen is not evolved during nickel deposition [44, 127, 128]. In addition, they inaccurately imply that crystalline nickel boride ( $\text{Ni}_2\text{B}$ ) is produced as part of the coating and ignore the codeposition of thallium and other metals used to stabilize the solution [44, 127, 128]. A more likely mechanism for these reactions is described in the following section.

### 2.2.1 *Anodic and cathodic reactions*

All electroless deposition is due to electrochemical reactions occurring under mixed-potential control. This means that competing anodic

(oxidation) and cathodic (reduction) reactions occur simultaneously on plated surfaces [127].

In the anodic reaction the reducing agent,  $\text{NaBH}_4$ , is oxidized, releasing electrons, which then are used in the cathodic reaction to reduce the metals (Ni and Ti) to be deposited. The anodic reaction with borohydride occurs in a series of steps as shown below. The first reaction is the dehydrogenation of borohydride at catalytic surfaces [127]:

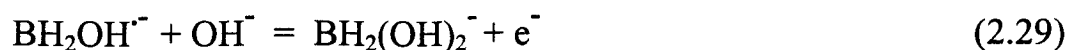


This reaction can only begin on metals that are a dehydrogenation catalyst; iron is an example. A metal that cannot survive this step will be non-catalytic to electroless deposition. Next, the electrons needed for the reduction of nickel are produced by the oxidation of the dehydrogenated borohydride ion [127]:

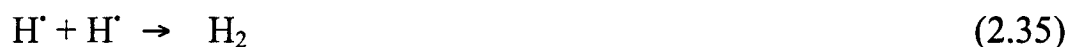


Because borane hydroxides can also be dehydrogenated, this is only the first of a chain of reactions yielding more hydrogen molecules and electrons until the final product, a borate, is reached [127]:

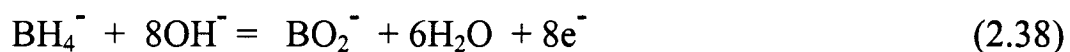
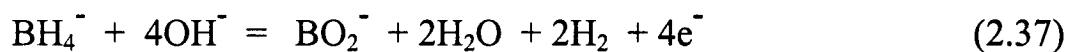




Two reactions in which hydrogen ions are produced by dehydrogenation are possible, i.e., recombination to produce hydrogen gas or further oxidation producing water and additional electrons [127]:



Accordingly, the overall anodic reaction can be either of the following two reactions given as equations (2.37) and (2.38) [127]:



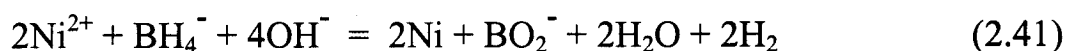
The extent to which these competing reactions occur depends on pH, potential and especially the metal being plated [127]. With metals such as copper and nickel only hydrogen recombination is possible, whereas with

platinum and palladium only oxidation can occur [127]. Thus the efficiency of borohydride reduction of nickel is about half that possible with more noble metals. Both types of reactions can occur with metals such as gold and thallium [127-129]. It is probably for this reason that the addition of thallium (and some other metals) to solutions used for the production of nickel by borohydride reduction increases their efficiency from about 20 to almost 50 percent [127].

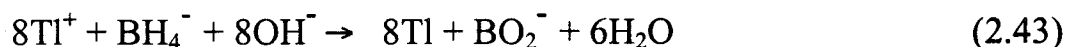
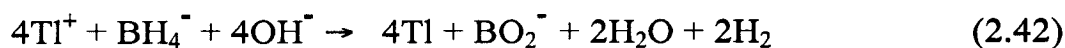
The cathodic reactions that occur in solutions containing borohydride are more straightforward. Nickel and stabilizers like thallium are deposited by direct reduction [127]



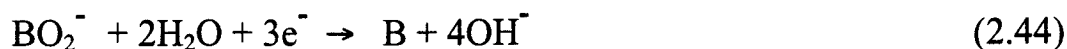
Thus the overall reaction for nickel deposition is [127]



The reactions for the deposition of thallium are as follows [127]



The deposition of boron is similar. Amorphous boron (and not nickel boride) is deposited by the reduction of borate [127]



The overall reaction is



A third cathodic reaction can also occur in alkaline environments, i.e., the reduction of water at the metal surface [127, 128]



The following reaction is the source of much of the inefficiency of electroless plating because it consumes reducing agent without depositing any coating [127]



This reaction is similar to the hydrolysis of borohydride in acidic solutions [127, 128]. Because of the high operating pH of borohydride-containing baths, strong complexing agents must be added to prevent the precipitation of nickel hydroxide. Many different complexers have been tried with these solutions, including ammonia, amine and imino compounds,

acetates, citrates and tartrates. However, ethylene diamine has proved to be most effective and is now used for most solutions. Continuous additions of an alkali, usually caustic, are also required to maintain alkalinity and a high pH. However, again borohydride baths are not normally used for aluminum substrates. Finally, most of the heavy metals and sulfide and thio compounds used to stabilize EN-P baths are also effective with borohydride-containing solutions [127, 128]. Thallium nitrate or sulfate is commonly used to stabilize the bath. Thallium not only increases the efficiency of borohydride reducing power, but also its codeposition improves the quality of the coating. Unfortunately, thallium compounds are highly toxic and require careful handling and protective clothing [127].

With borohydride baths, concentrations of nickel, borohydride, ethylene diamine and thallium as well as level of alkalinity are critical and must be carefully monitored and adjusted. Bath chemicals are usually added continuously in small amounts during operation, rather than by batch replenishment. Either automatic or frequent analysis of the components of the solution are needed to ensure optimum deposit properties [44, 127, 128].

### 2.3 RESEARCH OBJECTIVES

The purpose of this research was to produce a hard and wear resistant coating primarily for automotive applications and investigate the corrosion behaviour of these coatings. To accomplish this, the deposition of a hard and wear resistant nickel-boron coating on AA6061, preceded by a protective zincating/electroless nickel-phosphorous pretreatment was attempted. The

amount of constituents in each alloy and their distribution in the substrate, i.e. whether they are in solid solution or present as discrete intermetallic segregations, that create microstructures with different chemical or electrochemical reactivities. Therefore, to achieve the desired coating on the aluminum alloy, the experimental parameters for Ni-P and Ni-B baths need to be optimized, and the effect of various experimental parameters on the plating rate was examined. Electron probe microanalysis (EPMA) and atomic absorption spectroscopy (AAS) were chosen to measure the phosphorous and boron contents of each deposit, respectively; the surface morphology of each coating was examined using scanning electron microscopy (SEM).

Finally, as the intended application for the coated aluminum alloy was automotive – related, the corrosion behaviour of electroless nickel-phosphorus (EN) with various phosphorus content and nickel-boron coatings was investigated. Potentiodynamic (PT) and cyclic voltammetry (CV) techniques in 0.5 M sodium hydroxide were chosen as the means of investigation. A schematic of the proposed coating technique and characterization is shown in Figure 2.2. In this Figure, the treatments developed for each of EN-B and EN-P are summarized and the general techniques used in the work to characterize the final products are given.





### 3. EXPERIMENTAL PROCEDURES

The following sections detail the materials, instrumentation, and experimental procedures employed in this research work.

#### 3.1 MATERIALS

As a basis for all experiments, AA6061 commercial alloy (main composition: Al-1.0Mg-0.6Si-Cu-Cr) alloy and brass 70:30 (main composition: 0.7Cu-0.3Zn) were used. Disks of AA6061 and brass 70:30 (1.2 cm diameter, 0.3 cm thick) were cut from AA6061 and brass 70:30 stocks, respectively. Their surfaces were polished through 240, 320, 400, 600 grit SiC followed by 1 and 0.05 micron alumina.

The chemicals used in this work are listed below:

Acetic acid ( $\text{CH}_3\text{COOH}$ , Glacial, Reagent A.C.S., 99.7% Assay, Fisher Scientific Company)

2-Butyl-1,4-diol ( $\text{HOCH}_2\text{C}\equiv\text{CCH}_2\text{OH}$ , 99% Assay, Aldrich Chemical Company Inc.)

Ethylenediamine ( $\text{H}_2\text{NCH}_2\text{CH}_2\text{NH}_2$ , 99% Assay, Alfa Aesar Company)

Glycine ( $\text{H}_2\text{NCH}_2\text{COOH}$ , 99.5% Assay, Alfa Aesar Company)

Nickel (II) chloride ( $\text{NiCl}_2 \cdot 6\text{H}_2\text{O}$ , AnalaR analytical reagent, BDH Chemicals Ltd Poole England)

Zinc Oxide (ZnO, Certified A.C.S., Fisher Scientific Company)

Nickel (II) sulfate ( $\text{NiSO}_4 \cdot 6\text{H}_2\text{O}$ , Certified A.C.S., Fisher Scientific Company)

Nitric acid ( $\text{HNO}_3$ , 69-70.0% Assay, J. T. Baker Company)

Sodium hydroxide (NaOH, anhydrous, 97.0% min assay, Alfa Aesar Company)

Sodium hypophosphite ( $\text{NaH}_2\text{PO}_2 \cdot \text{H}_2\text{O}$ , Alfa Aesar Company)

Sodium tetrahydridoborate ( $\text{NaBH}_4$ , 98% Assay, Alfa Aesar Company)

Sulfuric acid ( $\text{H}_2\text{SO}_4$ , Reagent A.C.S.)

Thallium (-ous) acetate ( $\text{TlC}_2\text{H}_3\text{O}_2$ , Fisher Scientific Company)

### 3.2 INSTRUMENTATION

A potentiostat/galvanostat Model 273A EG&G Princeton Applied Research Group was used for cyclic voltammetry and potentiodynamic experiments. For the potentiodynamic experiments, software controlled by Labview<sup>TM</sup> was used.

A JEOL JSM 840 scanning electron microscope (SEM) operating at 25 kV and a current of 0.3 nA was used to study the surface morphology of each deposit.

A JEOL 733 electron microprobe using appropriate standards for quantitative evaluation (EPMA) was used to measure the P content of the EN-P deposits. The instrument was equipped with four wavelength spectrometers and an Oxford Link pentafet 131eV energy dispersive detector. The microprobe was fully computer controlled by a Link EXL system. This facility provided rapid, non-destructive, and quantitative chemical analyses of the samples.

Atomic absorption spectroscopy (AAS) using a model VIDEO 12E (nitrous oxide–acetylene flame) was used to measure the B content of the EN-B deposits. The absorption was measured at wavelength  $\lambda=247.9$  nm. To prepare the sample solutions, the electroless nickel-boron coated samples were dipped into 25 cm<sup>3</sup> nitric acid (50% v/v) for 1h to dissolve all of the coating. The samples were then removed from the solution followed by rinsing with distilled water into the solution to make sure all the coating has been left in the solution. The solution was then transferred into a volumetric flask (50 cm<sup>3</sup>) and by adding distilled water, the total volume was made up to 50 cm<sup>3</sup>. Finally, 5 cm<sup>3</sup> of the solution was aspirated with nitrogen into a nebulizing/mixing chamber to form small droplets before entering the flame. Concentration measurements were determined from a working curve after calibrating the instrument with standards of known concentration.

An x-ray diffractometer was used for identifying the phases present in EN-B and EN-P deposits before and after heat treatment. All specimens were

examined under Cu K $\alpha$  radiation using a Rigaku<sup>TM</sup> XRD unit with operating parameters of 40 KV, 40 mA, and scan speed of 4 deg/min.

To measure the pH of the EN solution, an Accumet 910 (Fisher Scientific) pH-meter was used. A vacuum oven (VWR 1410 Scientific Inc.) was used for heat treatment experiments. All experiments were performed at controlled temperature using a water bath (Immersion C10 Analog Circulator, Accuracy 0.01, VWR Canlab).

### 3.3 PRETREATMENT PROCESSES

#### ***3.3.1 Pretreatment process for electroless nickel-phosphorus coating on aluminum alloy AA6061***

Aluminum is very reactive and when exposed to air, a thin oxide layer is formed on the surface. This oxide layer can prevent the formation of a metallic bond between the coating and the substrate leading to poor adhesion, blistering and coating failure and thus must be removed. The treatment chosen in this work included degreasing, deoxidizing (removing oxide layer) and zincating.

##### ***3.3.1.1 Deoxidising and zincating the surface of AA6061 aluminum alloy***

Following the degreasing of the surface of AA6061 alloy samples by acetone, the surface was deoxidized by dipping into sulfuric acid 15% (v/v) at 85-90 °C for 3 min. This was followed by zincating, which

involved coating the surface with a thin layer of zinc following deoxidizing, to prevent reoxidation prior to electroless coating. The procedure for deoxidizing and zincating was modelled after that described in reference [131] and is shown in Figure 3.1.

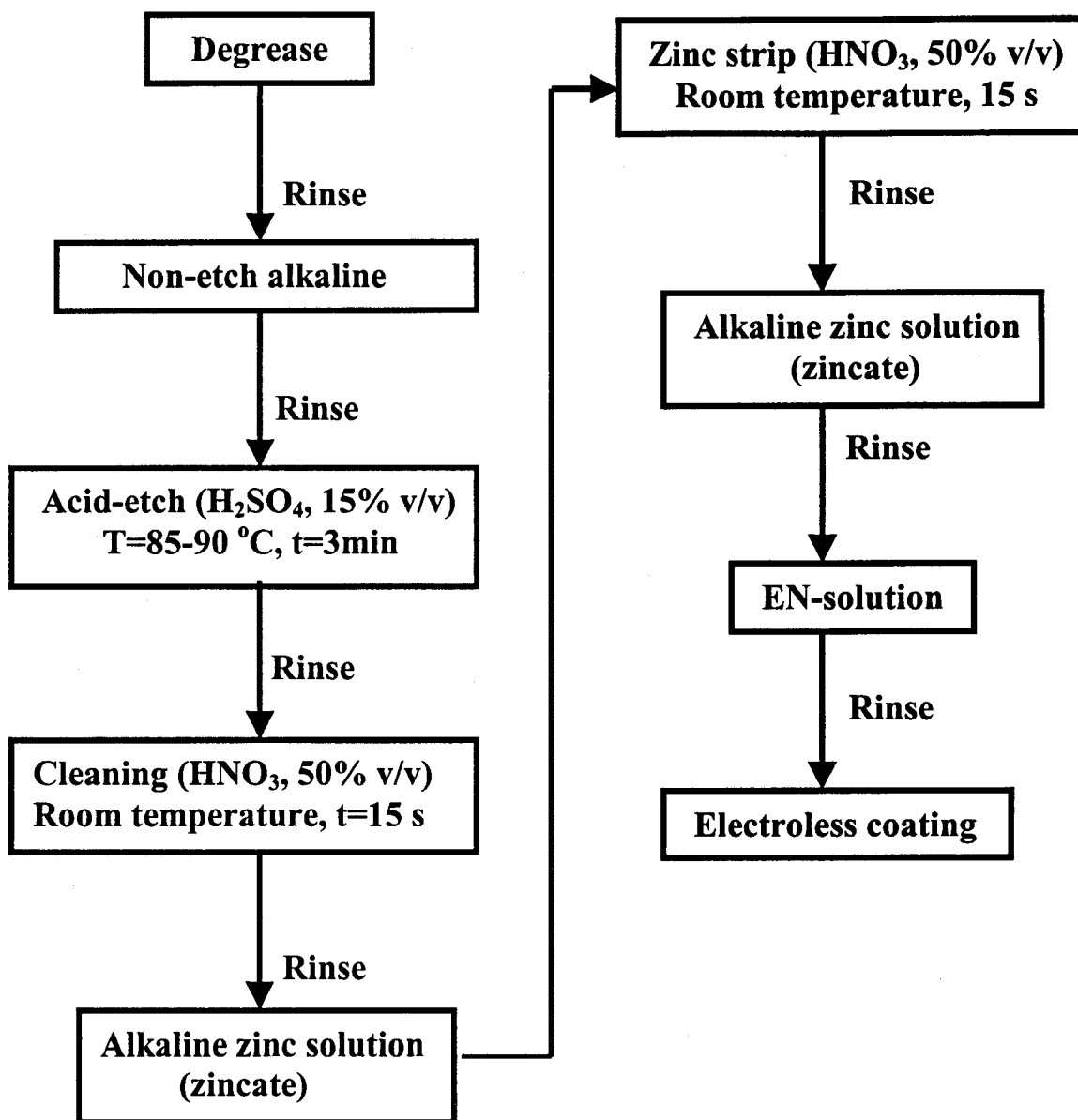


Figure 3.1 Flow chart of deoxidizing and zincating treatment of AA6061.

The purpose of the zincating process is to obtain a thin zinc layer as a barrier coating against reoxidation of the cleaned aluminum surface prior to EN plating. Aluminum alloy substrates require two immersion treatments in the zincating solution to obtain consistently adherent deposits of EN without heat treatment. This process is called double zincating [139]. The first treatment further etches the surface and aluminum is displaced by zinc. The zinc is subsequently removed in nitric acid (50% v/v), to dissolve microconstituents exposed by the dissolution of the substrate in the first zincate solution and again developing aluminum-rich surface. The second zincate treatment produces thinner deposits of zinc because of the passivity of the aluminum surface. The thinner deposits of zinc are essential for EN plating of aluminum because, unlike electrolytic deposition, the zinc film dissolves in the EN plating solution and deposition is on the conditioned aluminum surface rather than zinc.

### ***3.3.2 Pretreatment process for electroless nickel-boron coating on aluminum alloy AA6061***

After degreasing, deoxidising, and double zincating of the aluminum alloy substrate, as explained in section 3.3.1, prior using the EN-B bath, the surface was coated electrolessly with a thin layer (5  $\mu\text{m}$ ) of nickel-phosphorus which was followed by a suitable heat treatment process (220  $^{\circ}\text{C}$ , 9h in a vacuum oven). This intermediate electroless nickel-phosphorus deposition was necessary because of the high operating pH of the EN-B bath (pH>11) which can vigorously dissolve the aluminum.

### 3.4 ELECTROLESS NICKEL-PHOSPHORUS DEPOSITION

To electrolessly coat the pretreated surface of AA6061 the samples were dipped into the EN-P bath. The EN-P bath was contained in a Pyrex™ cylindrical container (70 cm<sup>2</sup> cross section area x 10 cm) immersed in a temperature-controlled water-bath. The container was filled with the EN-P plating solution, and the samples to be coated were dipped into the solution. The solution was agitated by bubbling argon gas through it. To prevent evaporation of the solution, the container was covered with a lid containing six holes (0.2 cm in diameter) to hang six samples into the solution, and two holes (0.5 cm in diameter) for bubbling the argon gas.

#### 3.4.1 Preparation of EN-P bath

To prepare an EN-P bath, the following stock solutions were made by weighing the chemicals and dissolving them in de-ionised water: nickel sulfate (281.25 g/L), sodium hypophosphite (200 g/L) as a reducing agent, glycine (100 g/L) as a complexing agent, sodium hydroxide (400 g/L), thallium acetate (2.5 g/L) as an inhibitor, and acetic acid (250 g/L). The optimum bath temperature, plating time, and concentration of bath constituents were determined by varying the concentration of each compound while maintaining the concentration of others constant and investigating the effect of each composition on P content of the deposit, surface morphology, deposition rate and coating thickness.

### 3.5 ELECTROLESS NICKEL-BORON DEPOSITION

To electroless coat the pretreated surface of AA6061 samples, they were dipped into the EN-B bath. The same bath setup explained in section 3.4 was used here, except that the bath was filled with the EN-B solution. Again, argon gas was bubbled through the solution for agitation and deaeration.

#### *3.5.1 Preparation of EN-B bath*

To prepare an EN-B bath, the following stock solutions were made by weighing the chemicals and dissolving into de-ionised water: nickel chloride (300 g/L), sodium borohydride (1.8 g/L) as a reducing agent, ethylenediamine (850 g/L) as a complexing agent, sodium hydroxide (400 g/L), thallium acetate (2.5 g/L) as an inhibitor, and 2-butyl-1,4-diol (2.5 g/L) as a brightener.

The optimum concentrations of bath constituents were again determined by varying the concentration of each compound while maintaining the concentration of others constant and investigating the effect of each composition on B content of the deposit, surface morphology, deposition rate and coating thickness. All electroless nickel coated samples were heated in an evacuated oven at 220 °C for times ranging from 9 to 144 h.



### 3.6 HARDNESS TESTING

A Knoop hardness tester (Leitz Wet Zlar, Germany) was used to measure hardness. In each hardness measurement, a diamond pyramid indenter was forced into the surface using an applied load of 0.0981 N. To produce a single data point, the overall process was repeated 7 times and the results averaged.

### 3.7 CORROSION TESTING

#### *3.7.1 Preparation of working electrode for corrosion testing of EN-P coatings*

Disks of AA6061 (1.2 cm in section x 0.3 cm thick) were surface polished through 240, 320, 400, 600 grit SiC, 1 and 0.05 micron alumina. After deoxidizing and double zincating pretreatments, the surfaces of aluminum alloys were coated with a 5  $\mu\text{m}$  intermediate EN-P coating using bath 1, Table 3.1. The pH of the bath was adjusted to 4.87 using sodium hydroxide solution and the plating was performed at  $85 \pm 0.01^\circ\text{C}$  for 20 min. In order to investigate the effect of phosphorus content on corrosion resistance, deposits were prepared using EN baths at four different pH levels. The following compositions of the deposits were achieved: Ni 2 w% P, Ni 6.5 w% P, Ni 8 w% P, and Ni 12.5 w% P. In order to obtain these compositions for the deposits on an AA6061 substrate both very low pH (pH 3.5) and very high pH (pH 10.5) environments were used. The aluminum surface was covered by an intermediate layer which offered protection from the bath. The thickness of the intermediate layer was 5  $\mu\text{m}$  for all samples as

determined by gravimetric measurements. These intermediary Ni-P coated samples were heated in a vacuum oven at 220 °C for 9 h. The surface of each intermediate Ni-P coated sample was coated with nickel-phosphorus using the four baths given in Table 3.1.

**Table 3.1 The composition of EN-P plating baths**

*Bath	Nickel sulfate (M)	Sodium hypophosphite (M)	Glycine (M)	Acetic acid (M)	Thallium acetate (M)	pH
1	0.171	0.29	0.53	0.16	$9.35 \times 10^{-4}$	3.5
2	0.171	0.29	0.53	0.16	$9.35 \times 10^{-4}$	5.5
3	0.171	0.29	0.53	0.16	$9.35 \times 10^{-4}$	7.5
4	0.171	0.29	0.53	0.16	$9.35 \times 10^{-4}$	10.5

\* Baths 1, 2, 3, and 4 produce EN-P coatings containing 12.5, 8, 6.5 and 2 W% P, respectively.

Baths 1, 2, 3, and 4 (Table 3.1) were used for samples 1, 2, 3, and 4, respectively. All baths differed only in pH. The coating took place at  $85 \pm 0.01$  °C for 1h. The thickness of the Ni-P coatings was 15 µm for all samples as determined by gravimetric measurements. The percentage of phosphorus in each sample was obtained using a nomograph developed in this work and shown in Figure 4.15. The results showed the following phosphorus contents for the samples: sample 1 (12.5 w% P), sample 2 (8 w% P), sample 3 (6.5 w% P), and sample 4 (2 w% P). Figure 3.2 gives a schematic representation of the AA6061 substrate after final treatment.

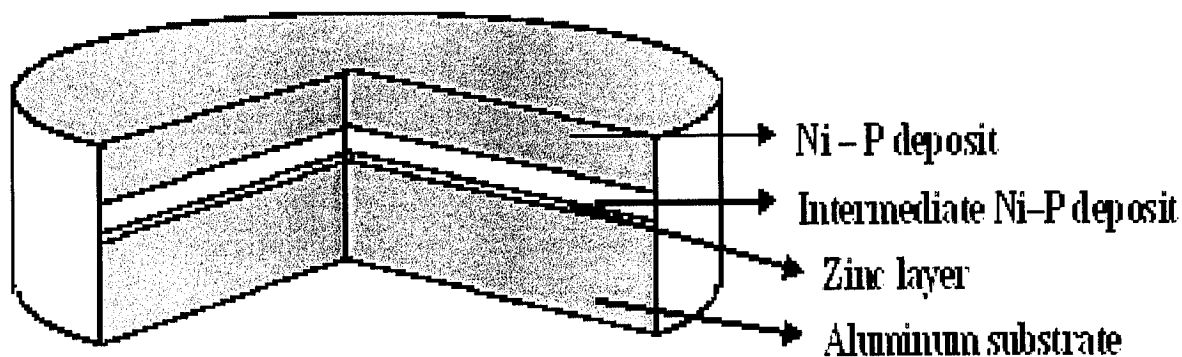


**Figure 3.2** Schematic diagram of the AA6061 substrate coated with EN-P.

### ***3.7.2 Preparation of working electrode for corrosion testing of EN-B coatings***

Disks of brass 70:30 (1.2 cm in section x 0.3 cm thick) were surface polished as described earlier followed by deposition of an intermediate electroless nickel – phosphorus coating using bath 1, Table 3.1. The intermediary Ni-P coating (5  $\mu\text{m}$ ) was followed by electroless nickel-boron coating using a bath with the following composition: nickel chloride (0.126 M), ethylenediamine (1.42 M), sodium borohydride (0.095 M), thallium acetate ( $9.35 \times 10^{-4}$  M), 2-butyl-1,4-diol ( $1.2 \times 10^{-3}$  M), NaOH (1 M). The EN-B plating was performed at  $85 \pm 0.01^\circ\text{C}$  for 1h at pH 12. The electroless nickel – boron coated samples were heat treated in a vacuum oven at  $220^\circ\text{C}$  for times of 0, 9, 12, 24, 36, 48, 60, 72, 84, 96, 108, 120, 132, and 144 h.

The thickness of the Ni-B coatings was 15  $\mu\text{m}$  for all samples as determined by gravimetric measurements. The percentage of boron in electroless nickel – boron was measured using atomic absorption spectroscopy.

### **3.7.3 *Electrolysis cell***

The electrolysis cell (Figure 3.3) of 700  $\text{cm}^3$  capacity used for corrosion testing consisted of a four-necked glass container to hold the solution and associated electrodes. The working electrode was a disk shape (1.2 cm in cross section x 0.3 cm thick) of the coated sample held by a plexiglass rod and the surface of sample was connected to a potentiostat through a thin platinum wire. The reference electrode was Ag/AgCl (in 1 M KCl) and the counter electrode was platinum wire (of 0.785  $\text{mm}^2$  surface area). Finally, the electrolyte was 0.5 M NaOH (pH 11.6) prepared using sodium hydroxide (anhydrous, ACS, 97.0% min assay) in distilled water.

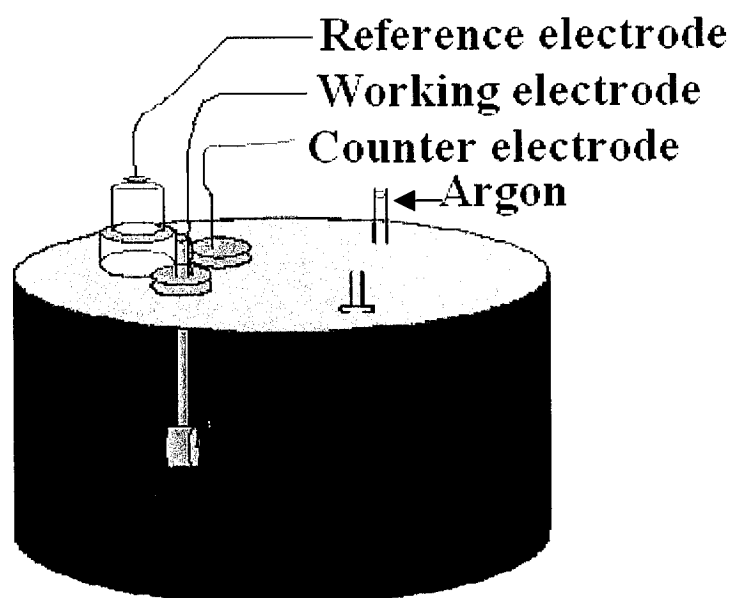


**Figure 3.3 The electrolysis cell used for corrosion testing**

The working, reference and counter electrodes were connected to the potentiostat/galvanostat (Model 273A EG&G Princeton Applied Research Group). The solution (sodium hydroxide 0.5 M) was deaerated by bubbling pure argon gas prior to the experiment. An argon blanket was then maintained over the surface of the quiescent solution to prevent the diffusion of air into solution. The potentiodynamic experiment was performed first. A potential ramp (5 mV/s) starting from -0.96 V vs. Ag/AgCl and ending at 0.74 V vs. Ag/AgCl was applied to the working electrode by the potentiostat. For each sample, the potentiodynamic run was repeated several times and potentiodynamic curves were recorded. Following potentiodynamic experiments, cyclic voltammograms (CV) of each sample were obtained using the same electrolysis cell and electrolyte. In a CV experiment, the potentiostat applied a potential ramp to the working electrode to gradually

change the potential and then reversed the scan, returning to the initial potential (the initial potential was -0.96 V vs. Ag/AgCl and the potential where the scan reversed was 0.74 V vs. Ag/AgCl). The scan rates used for experiments were 0.010, 0.050, 0.100, 0.200, 0.300, 0.400, and 0.500 V/s. All experiments were performed at room temperature (25 °C).

## 4. RESULTS AND DISCUSSION

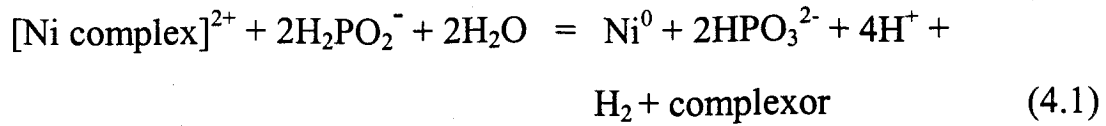
### 4.1 ELECTROLESS NICKEL-BORON PLATING ON AA6061

Electroless nickel-boron (EN-B) plating was preceded by a protective zincating/electroless nickel-phosphorus (EN-P) pretreatment. The experimental parameters for EN-P and EN-B baths were optimized, and the effect of various experimental parameters on the plating rate were examined. The phosphorus and boron contents of each deposit were measured using electron probe microanalysis (EPMA) and atomic absorption spectroscopy (AAS), respectively; the surface morphology of each coating was examined using scanning electron microscopy (SEM). Results showed that the surface morphology of the Ni-B coating varies with that of the intermediate EN-P coating. In turn, the surface morphology of intermediate Ni-P coating depends on the thickness of the coating and the EN-P plating bath condition.

#### *4.1.1 Pretreatment process before EN-B coating*

##### *4.1.1.1 Intermediate electroless nickel-phosphorus deposition*

Because of the necessity for a high pH bath, the surface of AA6061 aluminum alloy was covered with a thin layer of EN-P. This was followed by the heat treatment process. To determine the optimum bath composition, the influence of temperature, plating time, and concentration of bath constituents on P content of the deposit, surface morphology, deposition rate and coating thickness were investigated. For EN-P plating, the overall chemical reaction can be written as follows [135]:



As well, the general form of the rate of deposition can be written as follows:

$$U = d\text{Ni}^0 / dt = k[\text{H}_2\text{PO}_2^-]^\alpha [\text{Ni}^{2+}]^\beta [\text{L}]^\delta [\text{H}^+]^\gamma [\text{HPO}_3^{2-}]^\varepsilon \exp(-E_a/RT) \quad (4.2)$$

where  $U$  is deposition rate ( $\mu\text{m/h}$ ),  $T$  is the temperature (K),  $E_a$  is activation energy, and  $[L]$  is the concentration of complexing agent.

From equation (4.2),

$$\text{Log}U = K_1 + \alpha \text{Log}[\text{H}_2\text{PO}_2^-] + \beta \text{Log}[\text{Ni}^{2+}] + \delta \text{Log}[L] - \gamma \text{pH} + \varepsilon \text{Log}[\text{HPO}_3^{2-}] - E_a/RT \quad (4.3)$$

where

$$K_1 = \log K$$

$$(\text{dlog}U / \text{dlog}[\text{H}_2\text{PO}_2^-])_a = \alpha$$

$$(\text{dlog}U / \text{dlog}[\text{Ni}^{2+}])_b = \beta$$

$$(\text{dlog}U / \text{dlog}[L])_c = \delta$$

$$(\text{dlog}U / \text{pH})_d = -\gamma$$



$$(\text{dlog}U / \text{dlog}[\text{HPO}_3^{2-}])_e = \varepsilon$$

$$(\text{dlog}U / (1/T)) = -E_a/2.3RT$$

The subscripts a, b, c, d and e show each set of variables which were held constant for the particular partial derivative.

To determine the reaction orders  $\alpha$ ,  $\beta$ ,  $\delta$ , and  $\gamma$  the logarithm of deposition rate was plotted versus the logarithm of concentration of sodium hypophosphite, nickel sulfate, glycine (the complexing agent), and hydrogen ion, respectively. The reaction order can then be determined from the slope. The  $\text{HPO}_3^{2-}$  ion is the principal byproduct of the electroless nickel-phosphorus plating reaction which accumulates in the solution and thus its effect on deposition rate may be ignored. Therefore,  $\varepsilon$  may be set a value of 0 and the term  $[\text{HPO}_3^{2-}]$  in equation (4.2) ignored [135]:

$$U = K_1 [\text{HPO}_2^-]^\alpha [\text{L}]^\delta [\text{Ni}^{2+}]^\beta [\text{H}^+]^\gamma \exp(-E_a/RT) \quad (4.4)$$

$$\begin{aligned} \text{Log } U = \text{log}K_1 + \alpha \text{log}[\text{HPO}_2^-] + \delta \text{log}[\text{L}] + \beta \text{log}[\text{Ni}^{2+}] + \\ \gamma \text{log}[\text{H}^+] - E_a/RT \end{aligned} \quad (4.5)$$

First, the effect of time on the thickness of the deposit was investigated in the range of 0 to 200 min and the results are given in Figure 4.1 whereas the actual data are presented in Table A1, Appendix A. The plating bath consisted of nickel sulfate (0.171 M), sodium hypophosphite

(0.29 M), glycine (0.53 M), thallium acetate ( $9.35 \times 10^{-4}$  M), and acetic acid (0.16 M). The pH was adjusted at 4.87 using sodium hydroxide solution. The temperature of the bath was fixed at  $85 \pm 0.01$  °C.

As may be expected the thickness of deposit can be increased provided the bath condition can be kept constant by replenishment and filtering. The deposition rate was relatively constant for an immersion up to 4 h. For longer times the deposition rate decreased. For all subsequent experiments the time of 2 h was adopted.

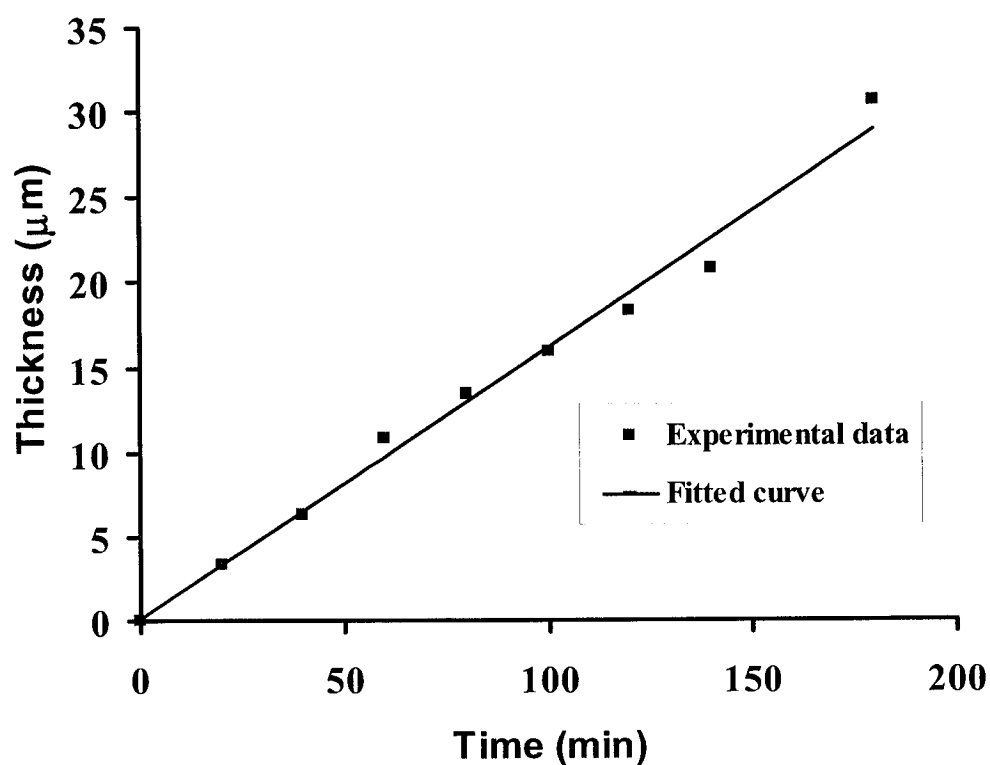


**Figure 4.1** Effect of time on the thickness of coating deposited. The bath contained nickel sulfate (0.171 M), sodium hypophosphite (0.29 M), glycine (0.53 M), thallium acetate ( $9.35 \times 10^{-4}$  M), and acetic acid (0.16 M). The pH was adjusted at 4.87 using sodium hydroxide solution. The temperature of the bath was fixed at  $85 \pm 0.01$  °C.

Figures 4.2 and 4.3 show the effects of nickel sulfate, and sodium hypophosphite concentrations on the rate of deposition, respectively. The data for Figures 4.2 and 4.3 are shown in Tables A.2 and A.3, Appendix A, respectively. The error for these calculations is due to the relative uncertainty in the weight and area determination of the samples and of the chemicals to prepare the bath. The error is estimated to be 1 percent. An increase in concentration of nickel sulfate and sodium hypophosphite in the bath results

in an initial increase in deposition rate followed by a plateau. The initial increase of deposition rate with concentration of nickel sulfate and sodium hypophosphite is expected. An increase in nickel sulfate concentration increases the free nickel ions available for reduction, therefore, the deposition rate increases. Sodium hypophosphite supplies the hypophosphite anions in solution needed to reduce nickel ions. Therefore, the deposition rate is expected to increase with an increase in concentration of reducing agent i.e. sodium hypophosphite. The occurrence of the plateau indicates that the reduction process may be mass-transport controlled. Therefore, the deposition rate does not change with further increase in sodium hypophosphite and nickel sulfate concentrations. From Figure 4.2, the data below the value where the deposition rate becomes independent of the concentration of nickel sulfate are used to plot the logarithm of deposition rate as a function of logarithm of nickel sulfate concentration in Figure 4.4. The slope of this plot is the  $\beta$  value.

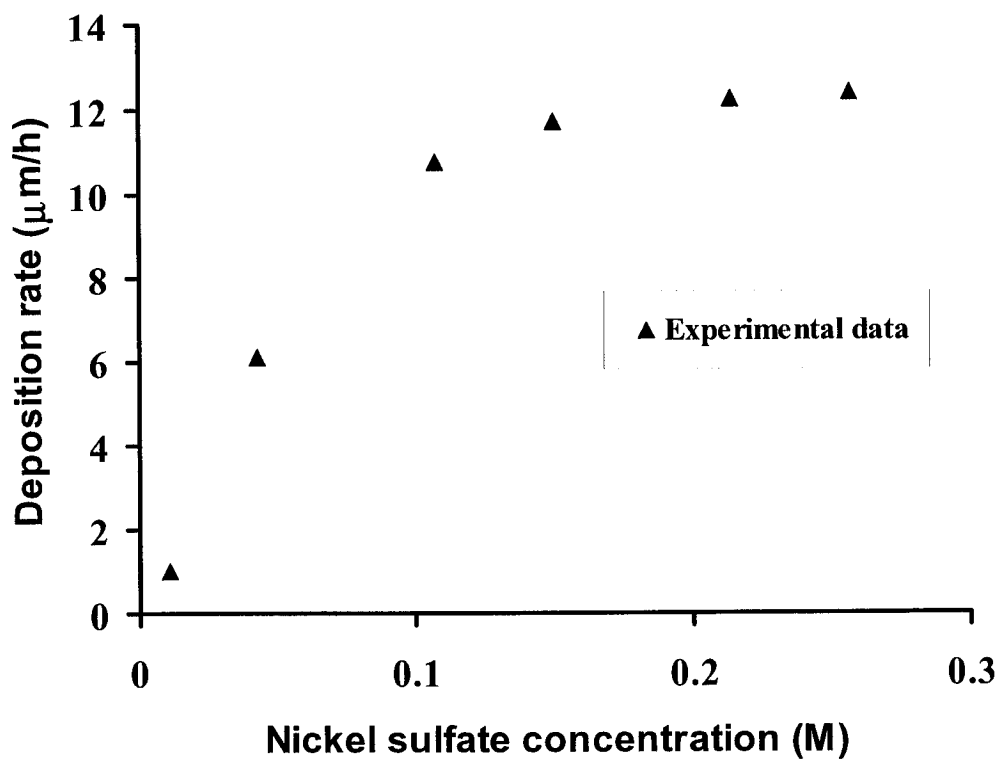


**Figure 4.2** Effect of nickel sulfate concentration on deposition rate of EN-P coating. The bath contained sodium hypophosphite (0.29 M), glycine (0.53 M), thallium acetate ( $9.35 \times 10^{-4}$  M), and acetic acid (0.16 M). The pH was adjusted at 4.87 using sodium hydroxide solution. The plating was performed at bath temperature of  $85 \pm 0.01$  °C for 2 h.

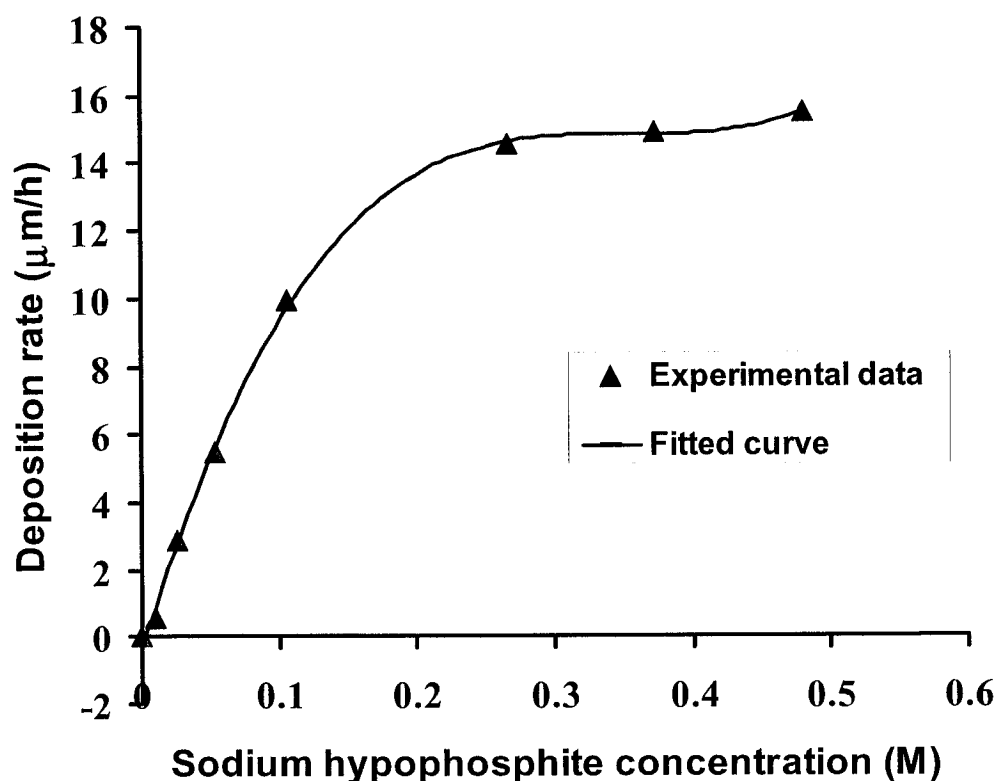


**Figure 4.3** Effect of sodium hypophosphite concentration on deposition rate of EN-P coating. The bath contained nickel sulfate (0.171 M), glycine (0.53 M), thallium acetate ( $9.35 \times 10^{-4}$  M), and acetic acid (0.16 M). The pH was adjusted at 4.87 using sodium hydroxide. The plating was performed for 2 h at bath temperature of  $85 \pm 0.01$  °C.

The data for Figure 4.4 are given in Table A.4, Appendix A. Similarly, to determine the  $\alpha$  value, in Figure 4.3 the data below the value where the deposition rate becomes independent of the concentration of sodium hypophosphite are used to plot the logarithm of deposition rate versus logarithm of sodium hypophosphite concentration. The slope of this

plot, Figure 4.5, is the  $\alpha$  value. The data for Figure 4.5 are given in Table A.5, Appendix A.

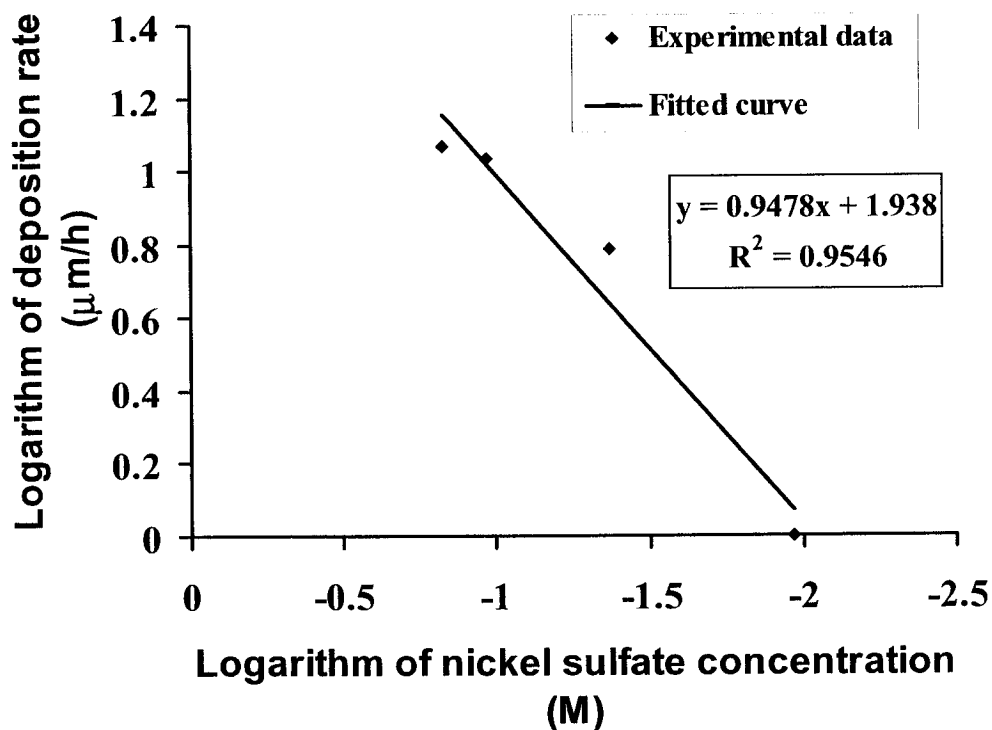


**Figure 4.4** Plot of logarithm of deposition rate versus logarithm of nickel sulfate concentration. The slope of the line is approximately 0.95. Therefore,  $\beta$  is 0.95. The bath contained sodium hypophosphite (0.29 M), glycine (0.53 M), thallium acetate ( $9.35 \times 10^{-4}$  M), and acetic acid (0.16 M). The pH was adjusted at 4.87 using sodium hydroxide. The plating was performed for 2 h at bath temperature of  $85 \pm 0.01$  °C.

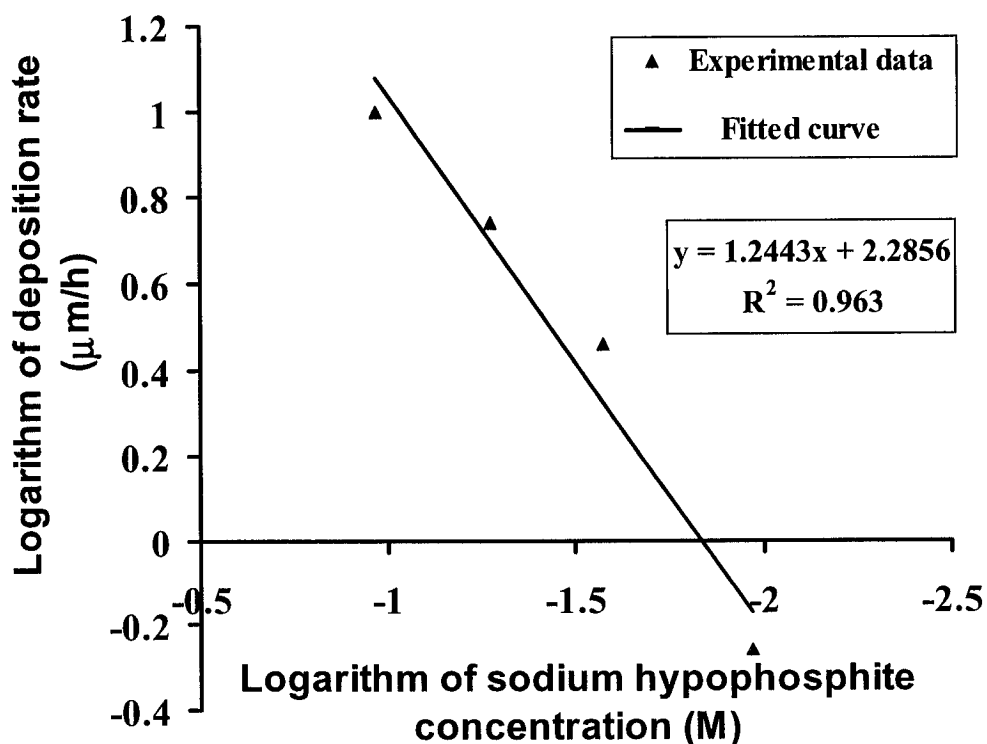


**Figure 4.5** Plot of logarithm of deposition rate versus logarithm of sodium hypophosphite concentration. The slope of the line is approximately 1.24. Therefore,  $\alpha$  is 1.24. The bath contained nickel sulfate (0.171 M), glycine (0.53 M), thallium acetate ( $9.35 \times 10^{-4}$  M), and acetic acid (0.16 M). The pH was adjusted at 4.87 using sodium hydroxide. The plating was performed for 2 h at bath temperature of  $85 \pm 0.01$  °C.

Nickel ions in solution are bound to specific numbers of water molecules which can be 4 or 6. These are called coordination numbers. A schematic representation of a 6-coordinate nickel ion in aqueous solution is shown in Figure 4.6.



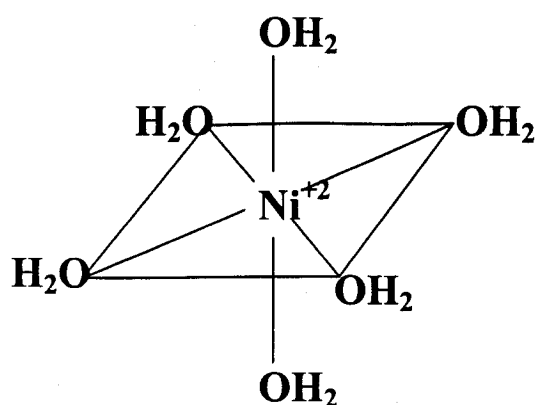


**Figure 4.6** Schematic diagram of a 6-coordinated nickel ion in a given solution.

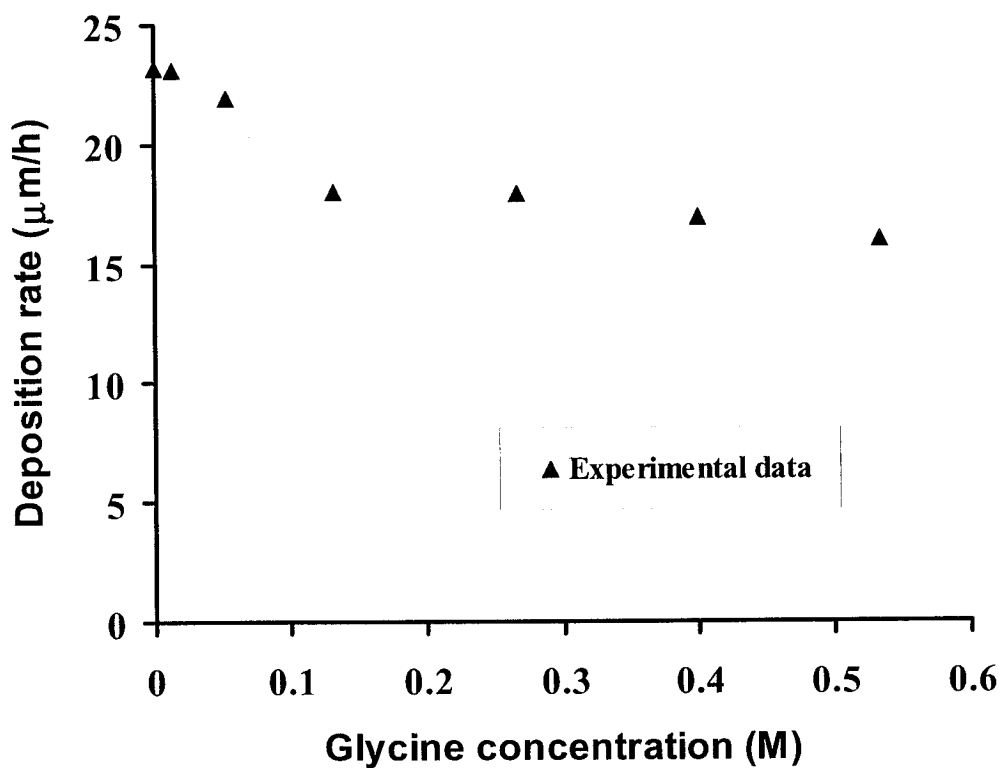
When water molecules coordinated to the nickel ion are replaced by other ions or molecules, a nickel complex forms and the combining or donor group is called complexing agent. If the complexing agent does not have a sufficient number of donor atoms to satisfy the coordination number (sites) of the metal ion, the remaining sites may be occupied by water molecules. In aqueous solution, chemical reactions with metal ions take place at free coordination sites where the sites are weakly bonded to coordinated water molecules. Therefore, a complexing agent has an important role in the regulation and maintenance of the free metal ion concentration within a specific pH range.

In an electroless nickel plating bath, the deposition rate is a function of free nickel ion concentration. This was shown in Figure 4.2 which corresponds to the conclusion obtained by Mallory [76].

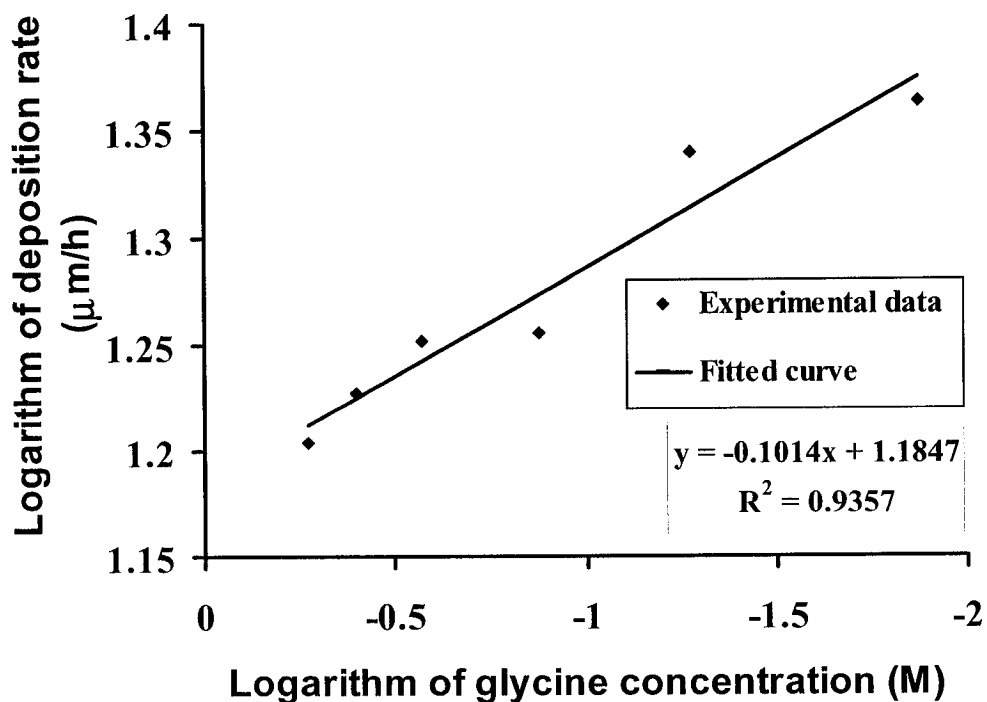
In the present work, glycine was used as a complexing agent to control the free nickel available to the reduction reaction. The complex formation here involves coordination of the complexing agent, glycin, with the nickel ion through oxygen and nitrogen atoms. The effect of glycin concentration on the rate of deposition, all other parameters remaining constant, was investigated in the range 0 to 0.6 M and the results are shown in Table A.6, Appendix A.

Figure 4.7 shows the effects of glycine concentration on the rate of deposition. The deposition rate decreases with an increase in glycine concentration. This was expected as by increasing the glycine concentration, the free coordination sites in nickel ion decreases.

In order to determine the  $\delta$  value, all the data are used to plot the logarithm of deposition rate versus glycine concentration. The slope of this plot, Figure 4.8, is  $\delta$ . The data for Figure 4.8 are shown in Table A.7, Appendix A.



**Figure 4.7** Effect of glycine concentration on deposition rate of EN-P coating. The bath contained nickel sulfate (0.171 M), sodium hypophosphite (0.29 M), acetic acid (0.16 M), and thallium acetate ( $9.35 \times 10^{-4}$  M). The pH was adjusted at 4.87 using sodium hydroxide solution. The plating was performed for 2 h at a bath temperature of  $85 \pm 0.01$  °C.



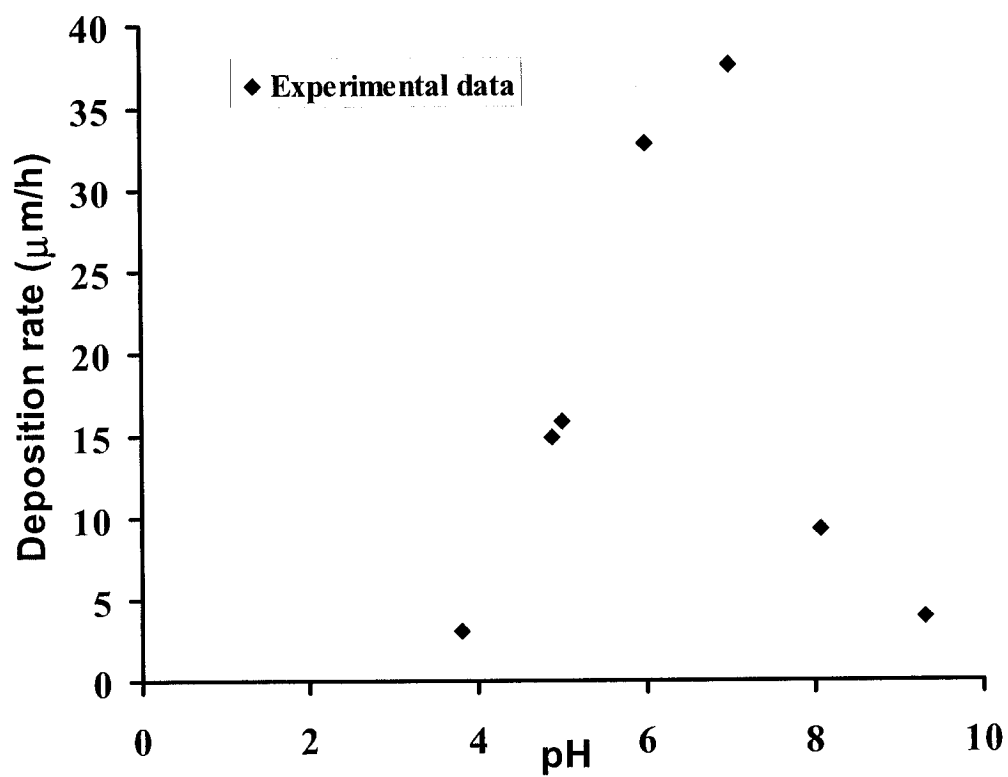
**Figure 4.8** Plot of logarithm of deposition rate versus logarithm of glycine concentration. The slope of the line is approximately  $-0.10$ . Therefore,  $\delta$  is  $-0.1$ . The bath contained nickel sulfate ( $0.171$  M), sodium hypophosphite ( $0.29$  M), acetic acid ( $0.16$  M), and thallium acetate ( $9.35 \times 10^{-4}$  M). The pH was adjusted at  $4.87$  using sodium hydroxide solution. The plating was performed for  $2$  h at a bath temperature of  $85 \pm 0.01$  °C.

The effect of pH on the rate of deposition of EN-P coatings was investigated in the pH range 3 to 11 for a bath containing nickel sulfate ( $0.171$  M), sodium hypophosphite ( $0.29$  M), glycine ( $0.53$  M), acetic acid ( $0.16$  M), and thallium acetate ( $9.35 \times 10^{-4}$  M). The plating was

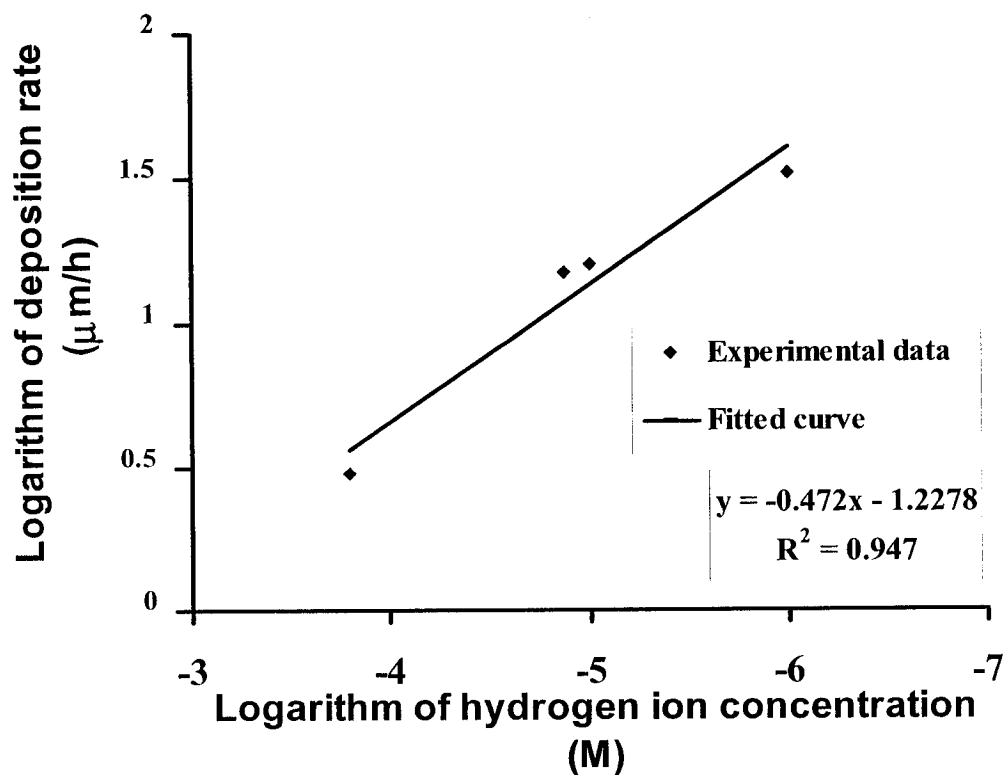
performed for 2 h at bath temperature of  $85 \pm 0.01$  °C. The results are presented in Table A.8, Appendix A.

Figure 4.9 shows the effects of pH on the rate of deposition. The rate is seen to reach a maximum at a pH of 7. Baldwin and Such [64] studied the effect of solution pH on deposition rate of EN-P at pH range 3 to 7. Their results are in agreement with the results obtained in this research work for  $\text{pH} < 7$ .

In order to determine the reaction order for  $[\text{H}^+]$ , the data in Figure 4.9 were divided into two groups: one group of data before the maximum rate is reached ( $\text{pH} < 7$ ), and one group of data after the maximum rate ( $\text{pH} > 7$ ). The first and second groups were then used to plot of logarithm of deposition rate versus logarithm of  $[\text{H}^+]$  for  $\text{pH} < 7$  and  $\text{pH} > 7$ , Figures 4.10 and 4.11, respectively. Therefore, there are two different reaction orders for  $[\text{H}^+]$  depending on the pH: For  $\text{pH} < 7$ , the reaction order is given by slope of Figure 4.10, whereas for  $\text{pH} > 7$ , the reaction order is given by the slope of Figure 4.11. The data for Figures 4.10 and 4.11 are presented in Tables A.9 and A.10, Appendix A, respectively.



**Figure 4.9** Effect of pH on deposition rate of EN-P. The bath contained nickel sulfate (0.171 M), sodium hypophosphite (0.29 M), glycine (0.53 M), acetic acid (0.16 M), and thallium acetate ( $9.35 \times 10^{-4}$  M). The plating was performed for 2 h at bath temperature of  $85 \pm 0.01$  °C.



**Figure 4.10** Plot of logarithm of deposition rate versus logarithm of hydrogen ion concentration. The slope of the line is approximately -0.47. Therefore,  $\gamma$  is -0.47. The bath contained nickel sulfate (0.171 M), sodium hypophosphite (0.29 M), glycine (0.53 M), acetic acid (0.16 M), and thallium acetate ( $9.35 \times 10^{-4}$  M). The plating was performed for 2 h at a bath temperature of  $85 \pm 0.01$  °C.

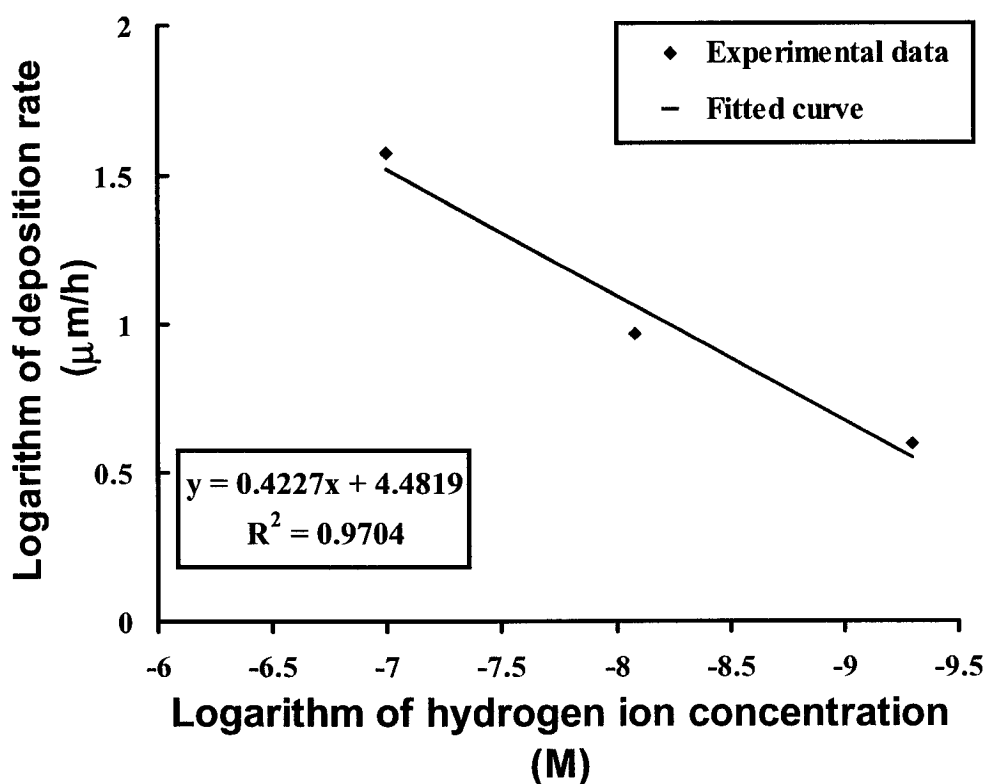


**Figure 4.11** Plot of logarithm of deposition rate versus logarithm of hydrogen ion concentration. The slope of the line is approximately  $-0.054$ . Therefore,  $\gamma$  is  $-0.054$ . The bath contained nickel sulfate ( $0.171$  M), sodium hypophosphite ( $0.29$  M), glycine ( $0.53$  M), acetic acid ( $0.16$  M), and thallium acetate ( $9.35 \times 10^{-4}$  M). The plating was performed for 2 h at bath temperature of  $85 \pm 0.01$  °C.

In summary, the reaction orders are as follows:

$$\alpha = 1.24, \beta = 0.95, \delta = -0.10, \text{ and for } \text{pH} < 7, \gamma = -0.47 \text{ or for } \text{pH} > 7, \gamma = 0.42$$

Therefore,

$$\text{For } \text{pH} < 7: v = K_2 [\text{HPO}_2^-]^{1.24} [\text{L}]^{-0.10} [\text{Ni}^{2+}]^{0.95} [\text{H}^+]^{-0.47} \exp(-E_a/RT) \quad (4.6)$$



$$\text{And for pH} > 7: \quad v = K_2 [\text{HPO}_2^-]^{1.24} [\text{L}]^{-0.10} [\text{Ni}^{2+}]^{0.95} [\text{H}^+]^{0.42} \exp(-E_a/RT) \quad (4.7)$$

Temperature also had an effect on the deposition process. The temperature was varied from 40 to 87 °C for a bath containing nickel sulfate (0.171 M), acetic acid (0.16 M), sodium hypophosphite (0.29 M), glycine (0.53 M), and thallium acetate ( $9.35 \times 10^{-4}$  M). The pH of the bath was adjusted at 4.87 using sodium hydroxide solution and the plating was performed for 2 h. The results are presented in Table A.11, Appendix A.

Figure 4.12 shows the effect of temperature on the rate of deposition using the data from Table A.11. It can be seen that temperature has a strong effect upon the deposition rate of acid hypophosphite-reduced solutions. The rate of deposition is very low at temperatures below about 323 K but increases rapidly with increasing temperature. At temperatures above 373 K the bath for electroless nickel plating decomposes. The data for Figure 4.13 are presented in Table A.12, Appendix A. Using the Arrhenius relationship [43, 135] the activation energy,  $E_a$ , may be obtained from the slope of the rate of deposition vs. reciprocal temperature plot. The data plotted in Figure 4.13 are representative of the activation energy curves, and from this plot:

$$d \log v / d(1/T) = -E_a/2.3R, \quad \text{and } E_a = 18.8 \text{ kcal/mol} \quad (4.8)$$

The activation energy has been calculated for several electroless nickel-phosphorus plating solutions previously using the slope of the deposition rate versus reciprocal temperature plot. It has been reported that

the values ranged from 13 to 23 kcal/g.mol depending on the bath formulation [135].

For the bath formulation that was used in this research work, the activation energy  $E_a = 18.8$  kcal/mol was calculated as shown above.

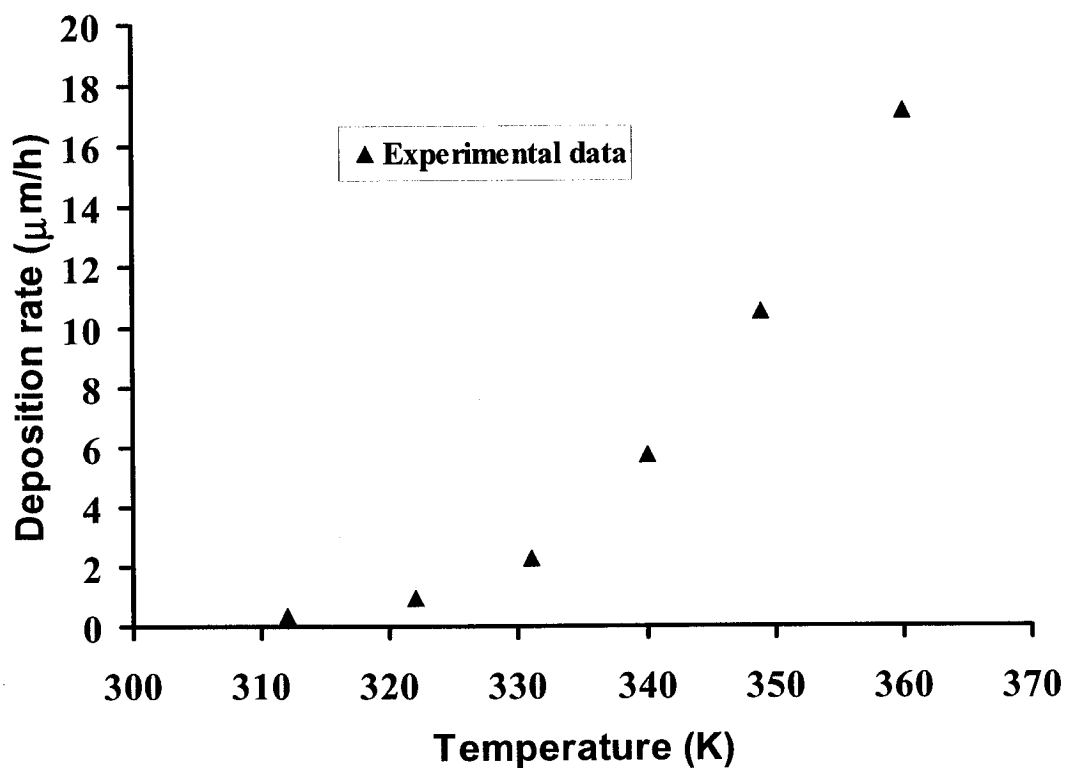


**Figure 4.12** Effect of temperature on rate of deposition of nickel-phosphorus coating. The bath contained nickel sulfate (0.171 M), acetic acid (0.16 M), sodium hypophosphite (0.29 M), glycine (0.53 M), and thallium acetate ( $9.35 \times 10^{-4}$  M). The pH of the bath was adjusted at 4.87 using sodium hydroxide solution and the plating was performed for 2 h.

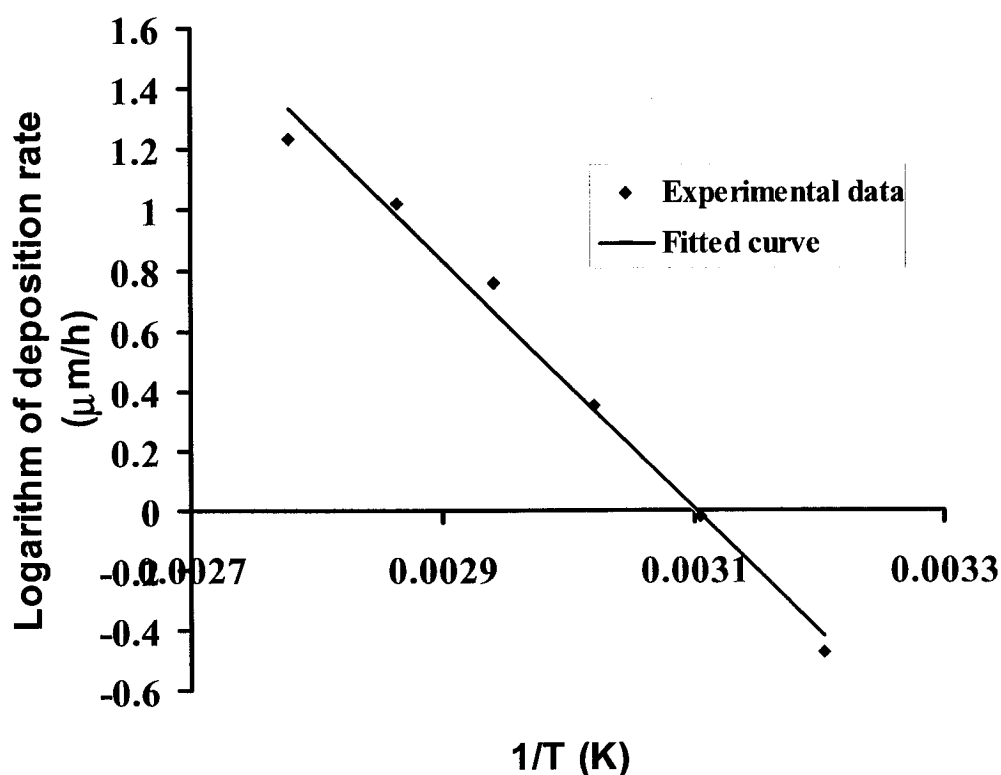


**Figure 4.13** Temperature dependence plot of logarithm of deposition rate of nickel-phosphorus versus reciprocal of temperature (K). The bath contained nickel sulfate (0.171 M), acetic acid (0.16 M), sodium hypophosphite (0.29 M), glycine (0.53 M), and thallium acetate ( $9.35 \times 10^{-4}$  M). The pH of the bath was adjusted at 4.87 using sodium hydroxide solution and the plating was performed for 2 h.

Figures 4.14, and 4.15 show the effects of temperature and pH on the P content of an EN-P deposit, respectively. The experimental data are shown in Tables A13 and A14, Appendix A, respectively. It seems that the temperature has only a slight effect on the P content of deposit.

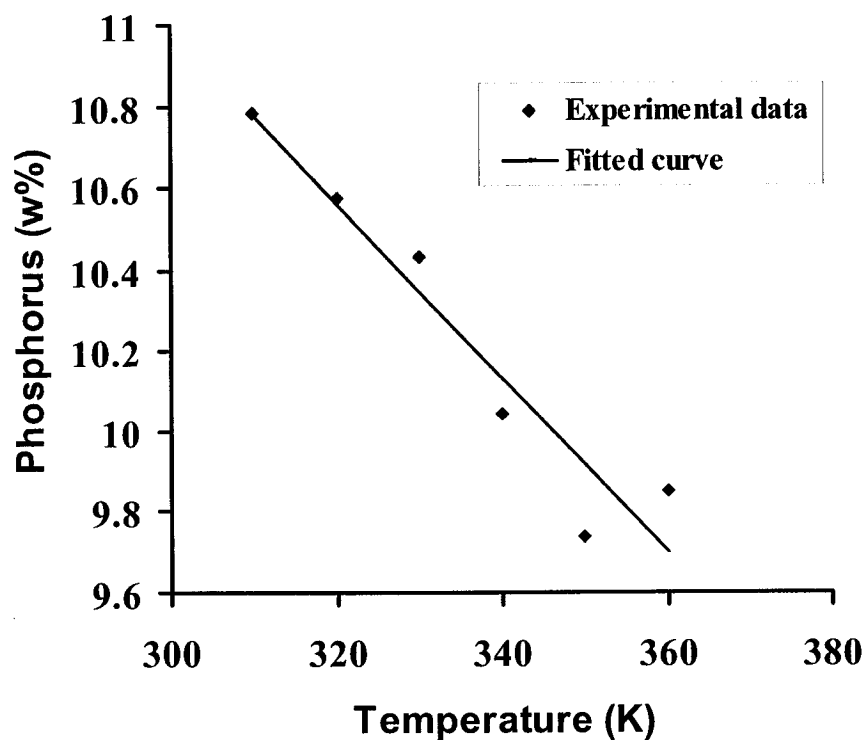


**Figure 4.14** Effect of temperature on the phosphorus content of an EN-P deposit. The bath contained nickel sulfate (0.171 M), acetic acid (0.16 M), sodium hypophosphite (0.29 M), glycine (0.53 M), and thallium acetate ( $9.35 \times 10^{-4}$  M). The pH of the bath was adjusted at 4.87 using sodium hydroxide solution and the plating was performed for 2 h.

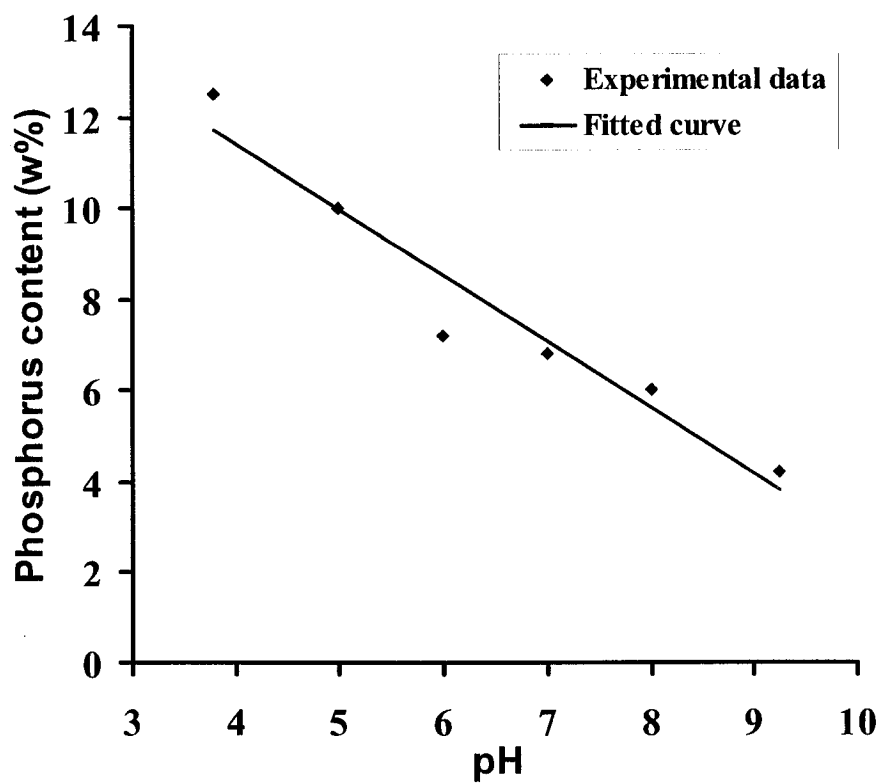


**Figure 4.15** Effect of pH on the phosphorus content of an EN-P deposit. The bath contained nickel sulfate (0.171 M), sodium hypophosphite (0.29 M), glycine (0.53 M), thallium acetate ( $9.35 \times 10^{-4}$  M), and acetic acid (0.16 M). The plating was performed for 2h at bath temperature of  $85 \pm 0.01$  °C.

#### ***4.1.2 Electroless nickel-boron plating***

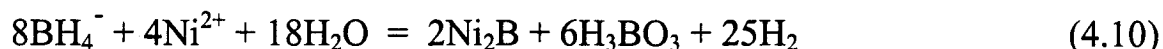
The intermediate EN-P plating process was followed by a heat treatment process to improve the adhesion of the intermediate electroless nickel-phosphorus coating on AA6061 thereby preventing blistering of the final EN-B coating. After heat treatment, samples were coated with EN-B using the solution with following composition: nickel chloride (0.126 M), sodium borohydride (0.095 M), ethylenediamine (1.42 M), thallium acetate ( $9.35 \times 10^{-4}$  M), 2-butyl-1,4-diol ( $1.2 \times 10^{-3}$  M), sodium hydroxide (1 M) at pH 12, and temperature  $85 \pm 0.01$  °C for 1 h. Nickel chloride provides nickel ions in solution, sodium borohydride acts as reducing agent, ethylenediamine is the complexing agent which controls free nickel ions available for reduction reaction, 2-butyl-1,4-diol is a brightener, thallium acetate acts as inhibitor preventing the decomposition of bath solution and sodium hydroxide maintains the pH above 12.

To prevent precipitation of nickel hydroxide, complexing agents such as ethylenediamine, that are effective between pH 12 to 14 must be used. Such strong complexing agents, however, decrease the free nickel ions present thereby decreasing the rate of deposition. To avoid this, thallium acetate, was used instead as stabilizer in both solutions. Thallium not only increases the efficiency of borohydride reduction, but its codeposition improves the quality of the coating [83].

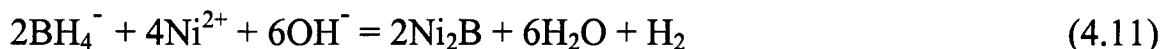
The hydrolysis of borohydride ions in acid or neutral solutions is very rapid and the reaction may be written as follows [83]:



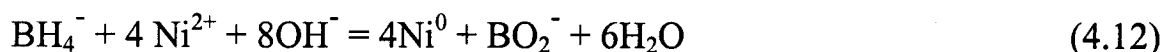
However, in the presence of nickel ions, nickel boride is formed as follows:



In a basic solution the reduction reaction can be written as follows:



However, if the solution pH is adjusted between 12 and 14 the formation of nickel boride is suppressed and the reaction product is principally elemental nickel:



Parameters such as nickel, borohydride, ethylenediamine and thallium as well as alkalinity are critical and must be carefully monitored and adjusted.

The deposition process was investigated in the range of sodium borohydride concentration 0 to 0.2 M for a bath containing nickel chloride (0.126 M), ethylenediamine (1.42 M), thallium acetate ( $9.35 \times 10^{-4}$  M) and sodium hydroxide (1 M). The pH of the bath was 12, and the plating was performed for 2 h at a bath temperature of  $85 \pm 0.01$  °C. The deposits produced contained between 6 and 9 w% boron and 2 to 5 w% thallium as measured using atomic absorption spectrometry (AAS).



Figures 4.16 and 4.17 show the effect of the concentration of sodium borohydride in solution on the rate of deposition and boron content of the coating, respectively. Sodium borohydride was used as reducing agent. The data for Figures 4.16 and 4.17 are given in Tables A.15 and A.16, respectively.

Examination of a cross section of the Ni-B deposit over the Ni-P layer, showed that the deposit was uniformly distributed over the substrate, with a uniform thickness and appeared to be well-bonded to the substrate (Figure 4.18).

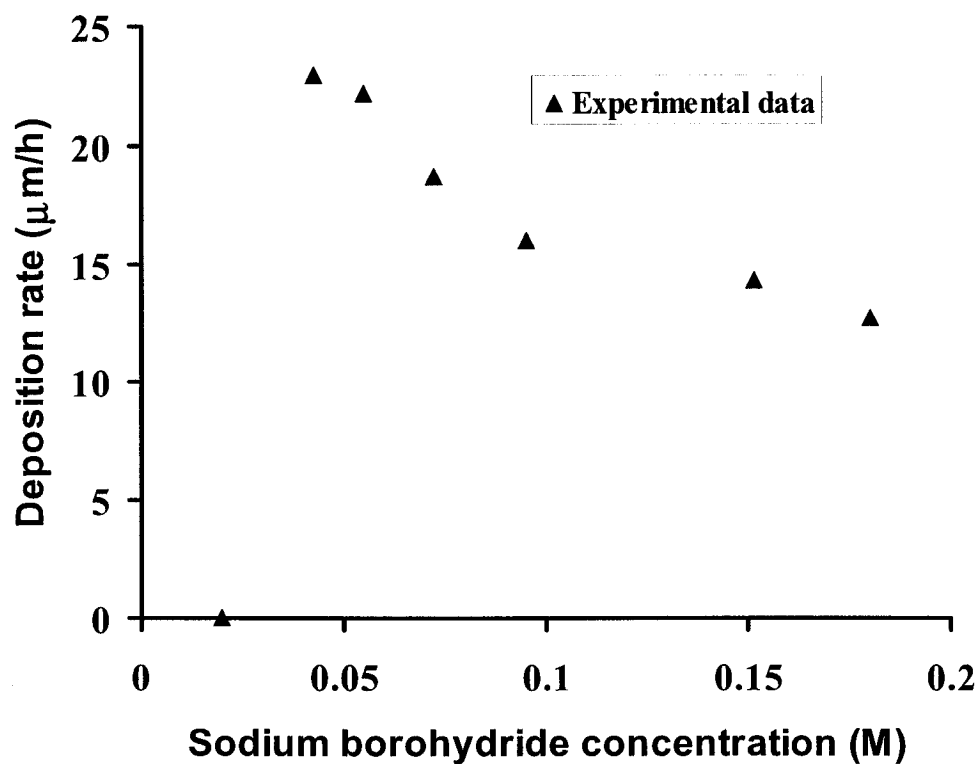


**Figure 4.16** Effect of sodium borohydride concentration on deposition rate of EN-B. The bath contained nickel chloride (0.126 M), ethylenediamine (1.42 M), thallium acetate ( $9.35 \times 10^{-4}$  M), 2-butyl-1,4-diol ( $1.2 \times 10^{-3}$  M), and sodium hydroxide (1 M). Bath pH was 12, and the plating was performed for 2 h at a bath temperature of  $85 \pm 0.01$  °C.

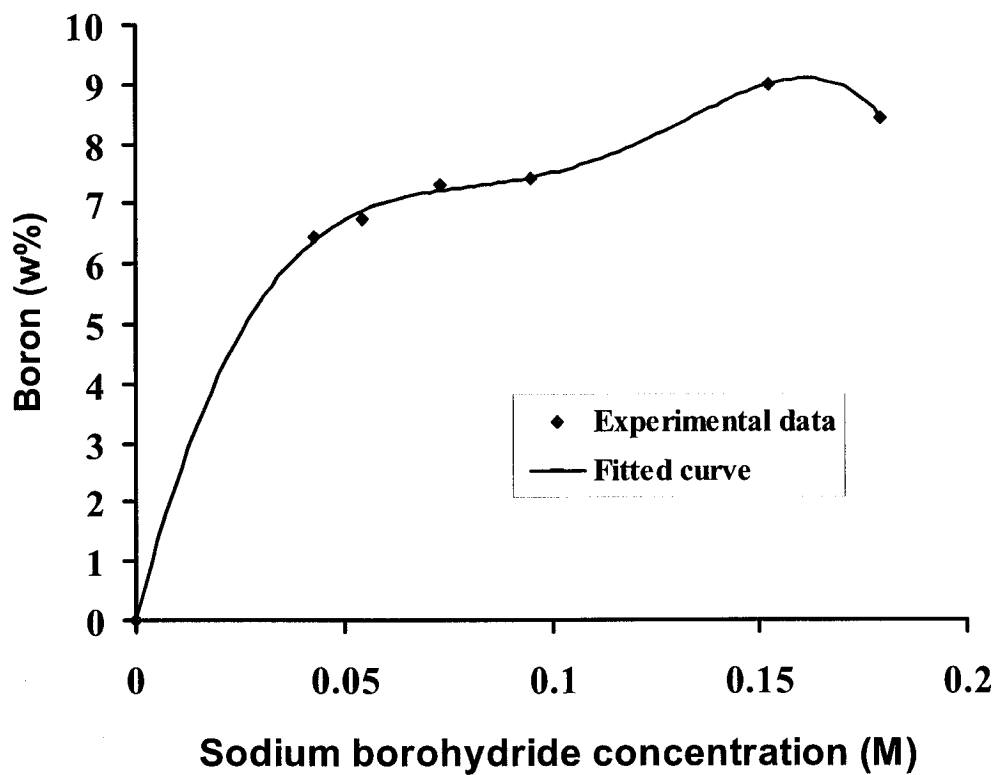


**Figure 4.17** Effect of sodium borohydride concentration on boron content of EN-B coating. The bath contained nickel chloride (0.126 M), ethylenediamine (1.42 M), thallium acetate ( $9.35 \times 10^{-4}$  M), 2-butyl-1,4-diol ( $1.2 \times 10^{-3}$  M), and sodium hydroxide (1 M). Bath pH was 12, and the plating was performed for 2 h at a bath temperature of  $85 \pm 0.01$  °C.

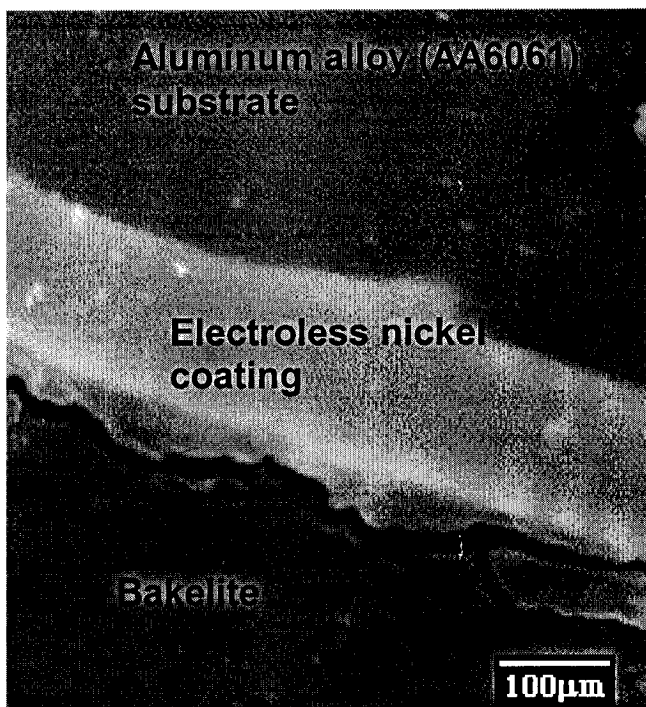


**Figure 4.18** Cross section of EN-B coating over intermediate EN-P coated aluminum alloy (AA6061).

The surface morphology of the Ni-P coatings was studied using SEM and found to be dependent on coating thickness. Figure 4.18 shows a micrograph of the interface between the AA6061 substrate and the electroless nickel coating. The adherence appears to be very good. Figures 4.19a, 4.19b, 4.19c, and 4.19d show the SEM micrographs of Ni-P coatings with different thicknesses. It can be seen that for the very low thickness, the surface morphology of the Ni-P coating duplicates the surface morphology of uncoated surface of double zincated aluminum alloy. By increasing the thickness, the surface morphology changes and the substrate surface is masked.

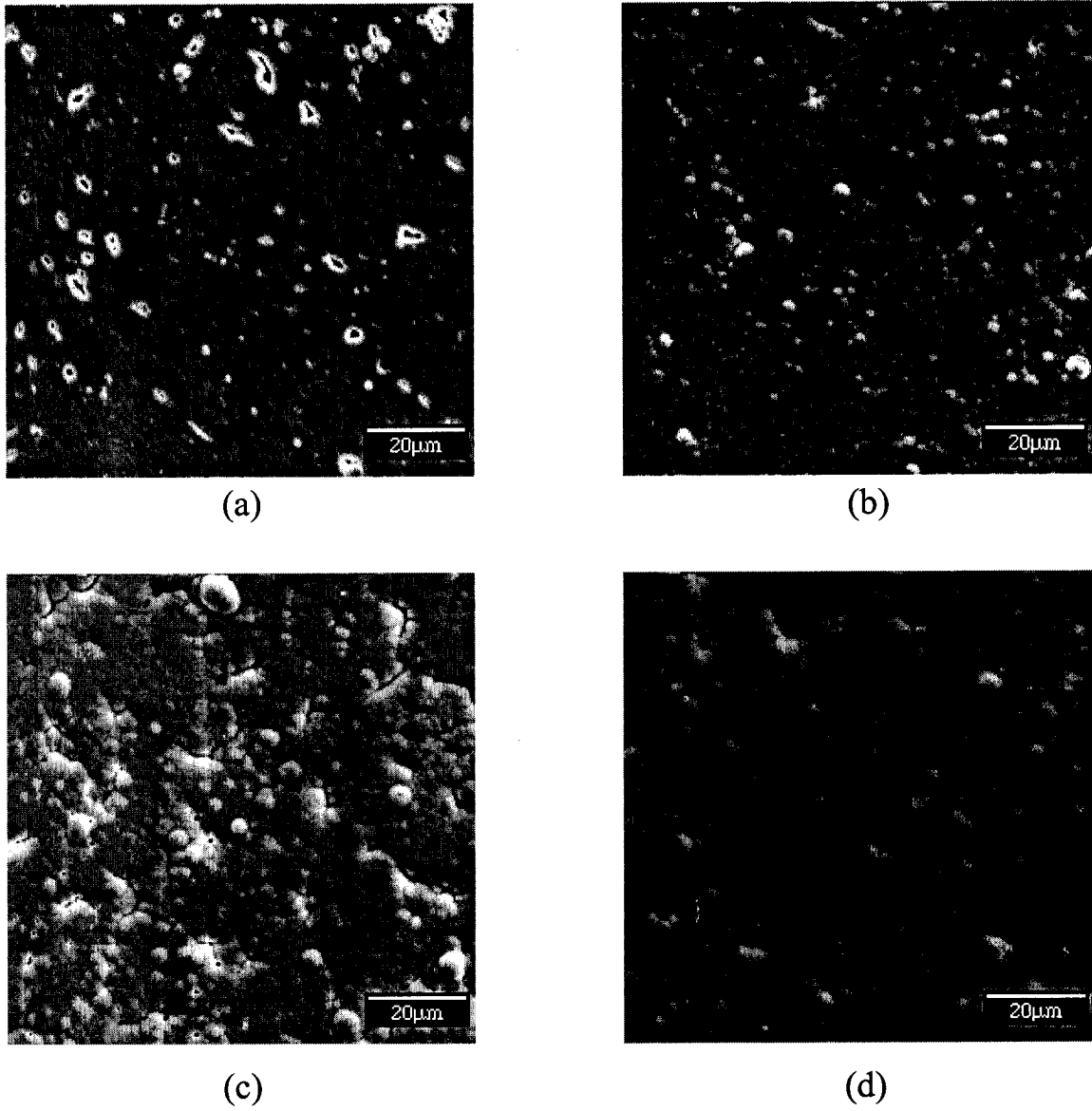


**Figure 4.19** SEM micrographs of Ni-P coatings with different thicknesses: (a) 1.4 μm, (b) 3.5 μm, (c) 7.5 μm, and (d) 9 μm.

Figures 4.20 and 4.21 show the surface morphology of the Ni-B coating over the EN-P coated aluminum alloy. It can be seen that the surface morphology of the Ni-B coating depends upon the surface morphology of Ni-P coated AA6061.

The method developed for producing the Ni-B coating produces a hard, uniform deposition of nickel-boron that should provide increased wear resistance (see section 4.1.3). The process deposits evenly on all surfaces and therefore should not require machining after coating. The coating has a columnar structure composed of uniformly deposited nodules. These nodules are expected to provide a low friction surface by greatly reducing the contact surface; as well the columnar nodule structure should also contribute to the enhanced toughness of the coating. The bond between the nodules and the substrate appears to be substantial. Figure 4.22 is a micrograph of the Ni-B coated aluminum alloy prepared under optimized conditions. The nodular structure is evident in Figure 4.22a.

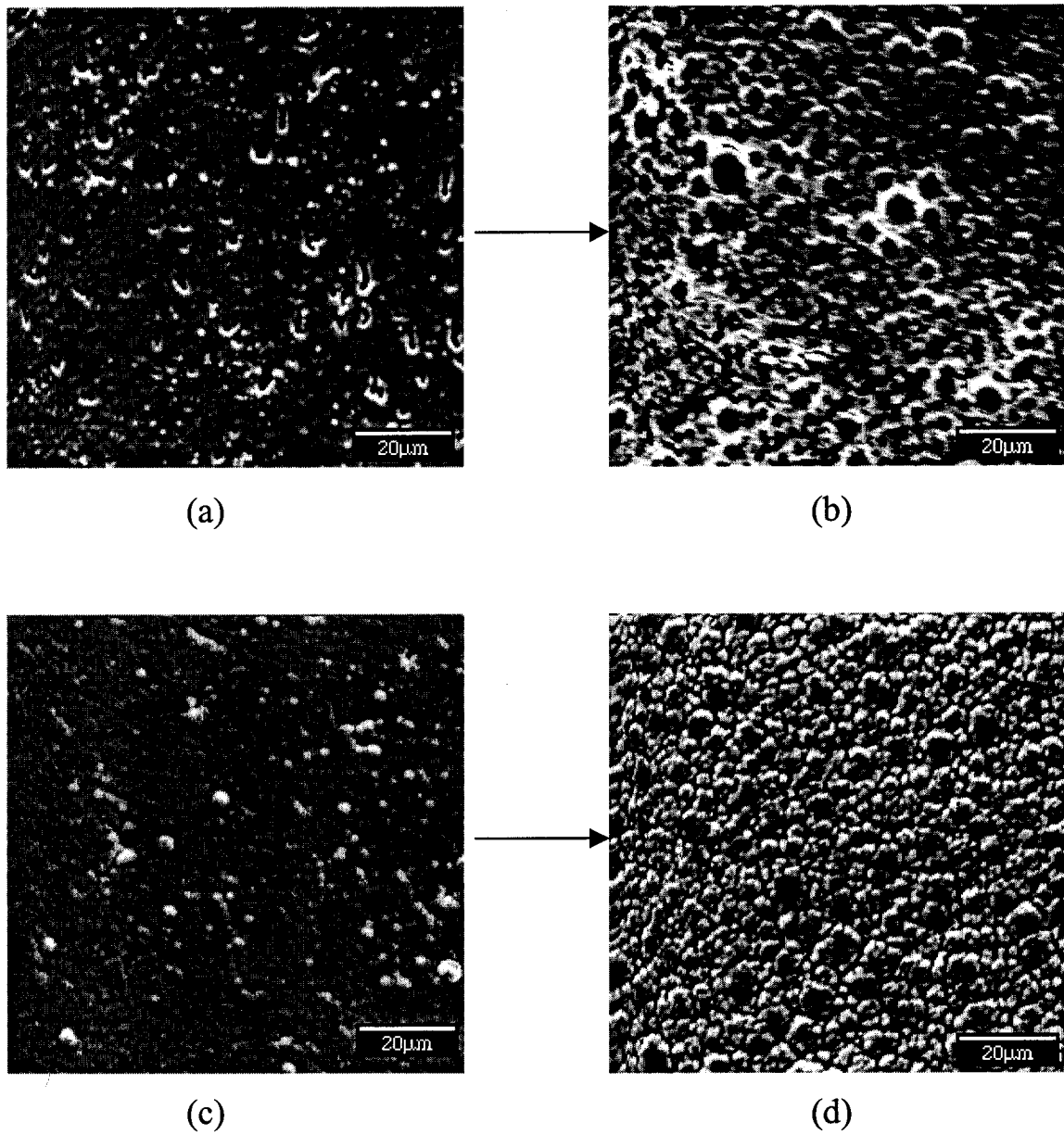


**Figure 4.20** SEM micrographs of Ni-P and Ni-B coatings on Ni-P with different thicknesses: (a) Ni-P coating; 1.1 μm thickness, (b) Ni-B coating; 8.7 μm, (c) Ni-P coating; 2.3 μm, and (d) Ni-B coating; 13.5 μm.

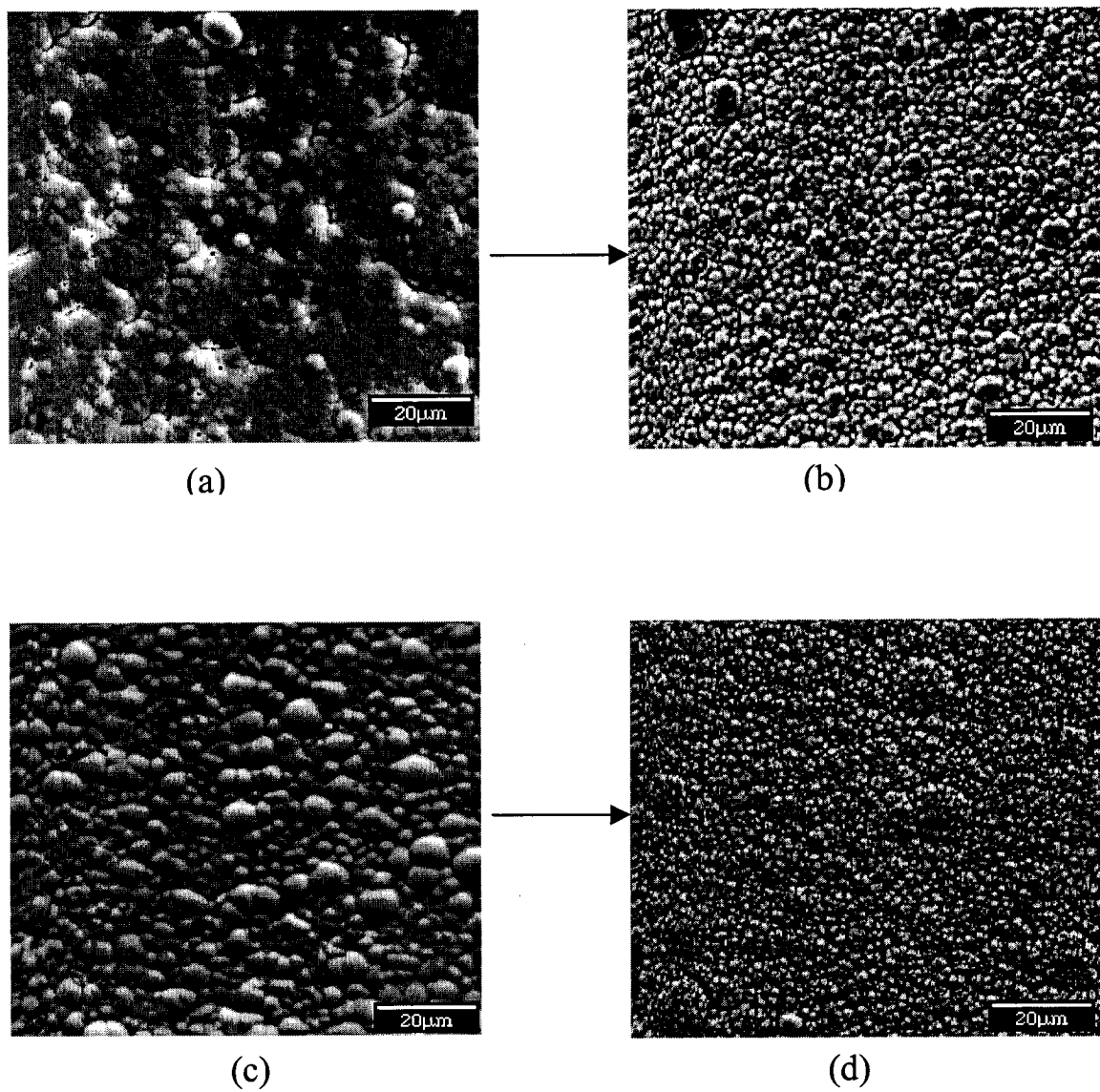


**Figure 4.21** SEM micrographs of Ni-P and Ni-B coatings on Ni-P with different thicknesses: (a) Ni-P coating; 7.5  $\mu\text{m}$ , (b) Ni-B coating; 9.2  $\mu\text{m}$ , (c) Ni-P coating; 24  $\mu\text{m}$ , and (d) Ni-B coating; 11.8  $\mu\text{m}$ .



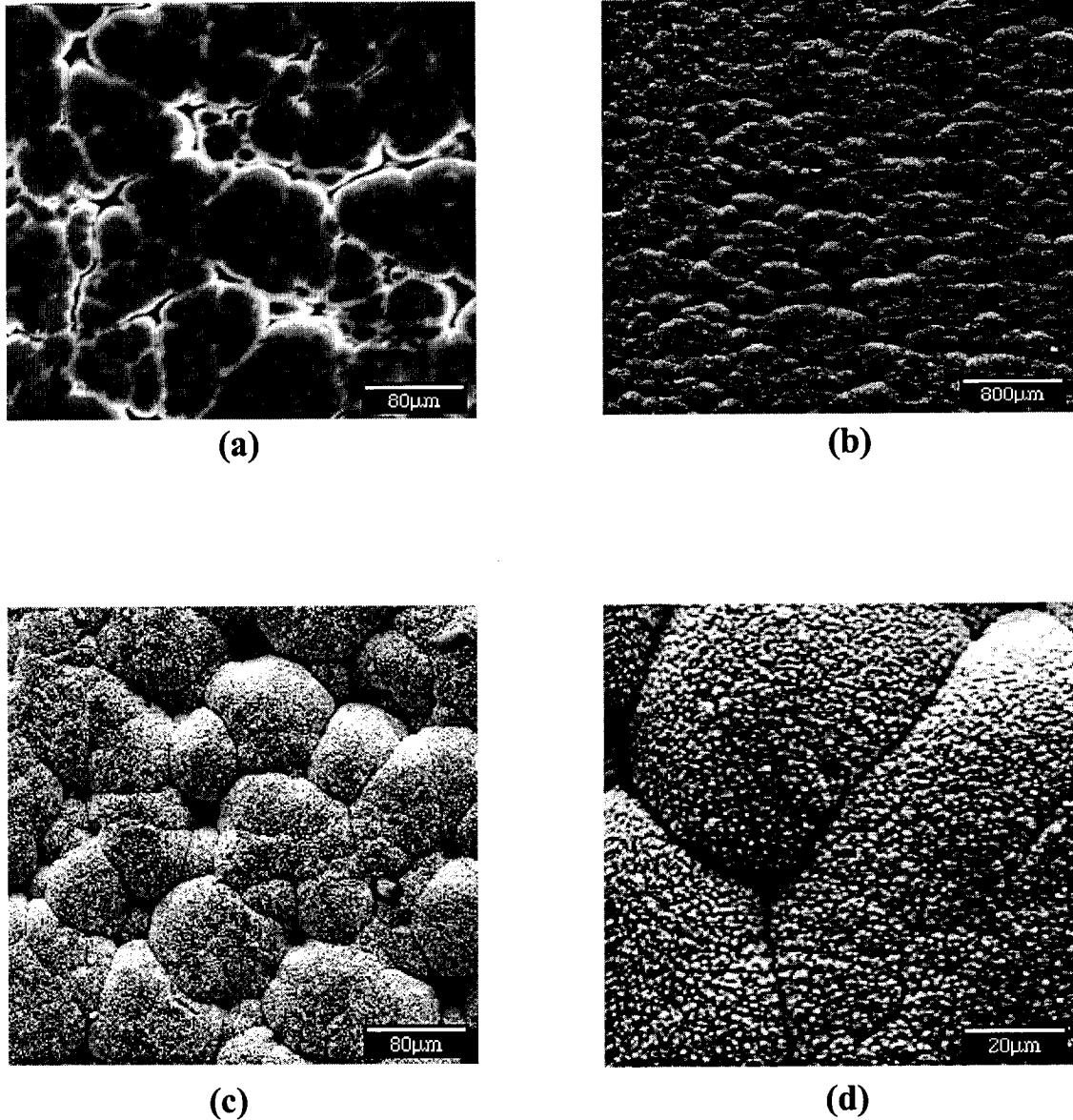


**Figure 4.22** SEM micrographs of Ni-B coatings (on Ni-P) with different thicknesses and magnifications: (a) 20  $\mu\text{m}$ ; 249X, (b) 9.4  $\mu\text{m}$ ; 25X, (c) 9.4  $\mu\text{m}$ ; 249X, and (d) 9.4  $\mu\text{m}$ ; 996X. The EN-B bath contained nickel chloride (0.126 M), ethylenediamine (1.42 M), sodium borohydride (0.095 M), thallium acetate ( $9.35 \times 10^{-4}$  M), 2-butyl-1,4-diol ( $1.2 \times 10^{-3}$  M), and sodium hydroxide (1 M). Bath pH was 12, and the plating was performed for 2 h at a bath temperature of  $85 \pm 0.01$   $^{\circ}\text{C}$ . The thickness of the intermediate EN-P coating was 5  $\mu\text{m}$ . The intermediate EN-P coated AA6061 was heat treated in vacuum at  $220$   $^{\circ}\text{C}$  for 9 h.

### 4.1.3 Hardness testing

The hardness of the substrate and of the coatings was measured using a Vickers diamond pyramid indenter at a load of 0.0981 N. The results are presented in Table B.1, Appendix B. Figure 4.23 gives the corresponding plot of the results presented in Table B.1.

The following formula was used to calculate the Vickers hardness:

$$HV = (189 \times F \times 10^3) / I^2 \quad (4.13)$$

where HV is Vickers hardness, F is test force in Newtons, and I is the length of the longer diagonal in micrometers. By substituting  $F = 0.0981$  and I as measured by a microscope using (4.13), Vickers hardness values for the uncoated aluminum alloy substrate and the nickel-boron coated aluminum alloy (39  $\mu\text{m}$  thickness of coating containing 6.8 w% B) were calculated as  $111.76 \pm 2.43$  and  $384.96 \pm 8.75$ , respectively. The value for the aluminum substrate compares favourably with literature value of about 100 HV. The Ni-B coated aluminum alloy sample was subjected to heat-treatment at 220 °C for 9 h in vacuum. After heat-treatment the Vickers hardness was increased to  $857.48 \pm 19.97$ . In order to investigate the effect of time of heat treatment at 220 °C on hardness, Ni-B coated AA6061 samples were subjected to heat treatments in vacuum at 220 °C for 9, 12, 24, 36, 48, 60, 72, 84, 96, 108, 120, 132, and 144 h. The results show that the hardness increases slightly as heat-treatment time increases, Figure 4.23.

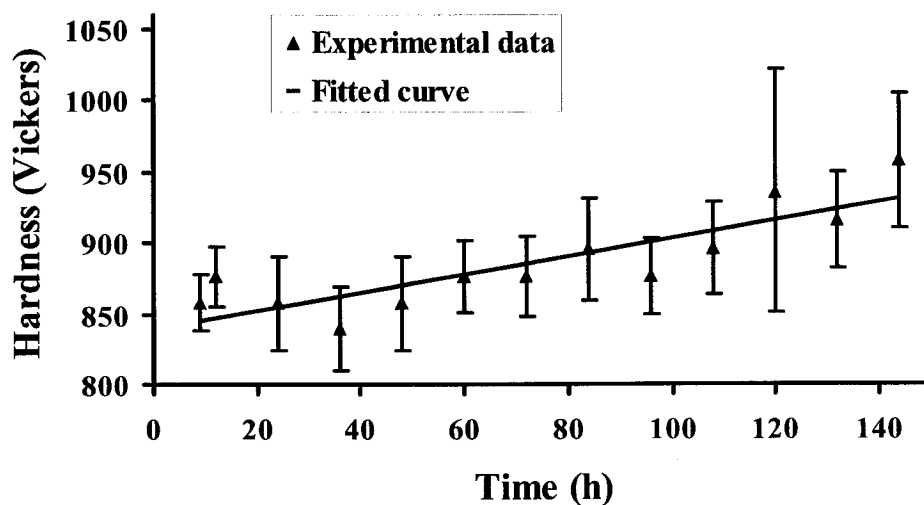


**Figure 4.23** Effect of heat treatment time on Vickers hardness of Ni-B coated AA6061 aluminum alloy. The coating was 39  $\mu\text{m}$  thick and contained 6.8 w% B. The heat treatment was performed at 220  $^{\circ}\text{C}$  in vacuum.

#### 4.2 INVESTIGATION OF THE CORROSION BEHAVIOUR OF ELECTROLESS NICKEL-PHOSPHORUS COATINGS ON AA6061 IN BASIC SOLUTIONS

The corrosion behaviour of electroless nickel-phosphorus (EN) coatings with phosphorus contents ranging from 2 to 12.5 w% was investigated using potentiodynamic and cyclic voltammetry techniques in 0.5 M sodium hydroxide for samples which were not heat treated.

#### ***4.2.1 Potentiodynamic study of the electroless nickel-phosphorus coated AA6061 samples***

Figures 4.24, 4.25, 4.26 and 4.27 show the polarization curves of EN-P coated samples in 0.5M NaOH solution for 12.5, 8, 6.5, and 2 w% P compositions, respectively. For each sample, the polarization experiment was repeated four times.

Figures 4.24a, 4.24b, 4.24c, and 4.24d show first, second, third, and fourth runs of EN-P coated sample 1, (12.5 w% P, bath 1, Table 3.1) in 0.5 M NaOH solution. It can be seen that in the first run in the anodic polarization region, there is one small peak 1 at  $-0.744$  V vs. Ag/AgCl, a sharp peak 2 at  $-0.523$  V vs. Ag/AgCl, and a very broad, small peak 3 at  $-0.102$  V vs. Ag/AgCl. In the cathodic polarization region a broad peak 4 appears at  $0.411$  V vs. Ag/AgCl with a very small shoulder, peak 5 at about  $0.431$  V vs. Ag/AgCl.

After the second run (which immediately followed the first run), the height and the position of peak 1 does not change, but the position of peak 2 changes towards a more positive potential ( $-0.322$  V vs. Ag/AgCl). Also in the anodic polarization region, a new minor peak 6, at  $-0.445$  V vs. Ag/AgCl, appears, and in the cathodic polarization area, the position of peak 4 changes towards a more negative potential ( $0.375$  V vs. Ag/AgCl) and the shoulder peak 5 also appears.

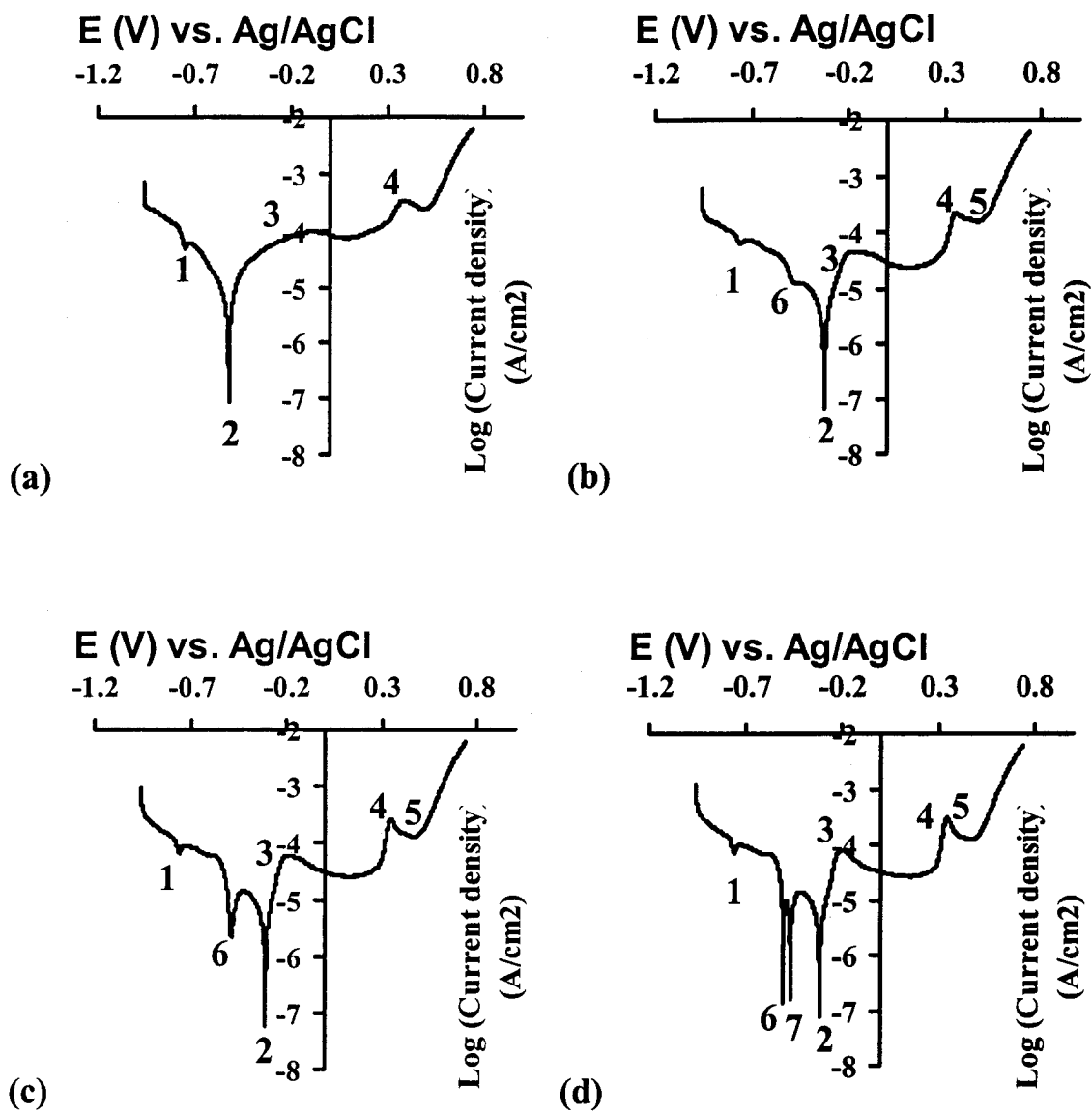


Figure 4.24 Polarization curves of EN-P coated sample 1 in 0.5 M NaOH at 5 mV/s scan rate; (a) first run, (b) second run, (c) third run (d) fourth run.

After the third run, in the anodic polarization region, the height and the position of peak 1 does not change but peak 6 grows in height and shifts towards a more negative potential (-0.485 V vs. Ag/AgCl), peak 2 shifts slightly towards a less negative potential (-0.309 V vs. Ag/AgCl) and peak 3 becomes larger and shifts towards a more negative potential (-0.181 V vs. Ag/AgCl). Finally, in the cathodic area, peak 4 shifts towards a more negative potential (0.359 V vs. Ag/AgCl).

In the final run for the anodic polarization area, the height and position of peak 1 again does not change. Rather, peak 6 splits into two sharp peaks at -0.503 V vs. Ag/AgCl and -0.465 V vs. Ag/AgCl, peak 2 remains constant and peak 3 grows slightly and shifts towards a more negative potential (-0.192 V vs. Ag/AgCl). In the cathodic region, the position and the height of peak 4 remains constant.

Figures 4.25a, 4.25b, 4.25c, and 4.25d show first, second, third, and fourth runs of EN-P coated sample 2 (8 w% P, bath 2, Table 3.1) in 0.5 M NaOH. It can be seen that in the first run, in the anodic polarization region, a sharp peak 1 does appear at -0.645 V vs. Ag/AgCl and in the cathodic region a broad peak 2 appears at 0.405 V vs. Ag/AgCl. In the second run (immediately following the first run), the position of peak 1 shifts towards more positive potential (-0.255 V vs. Ag/AgCl) and peak 2 grows slightly and shifts towards a more negative potential (0.367 V vs. Ag/AgCl). In the third and fourth runs of sample 2, peaks 1 and 2 retain their position, and peak 2 does not grow further.

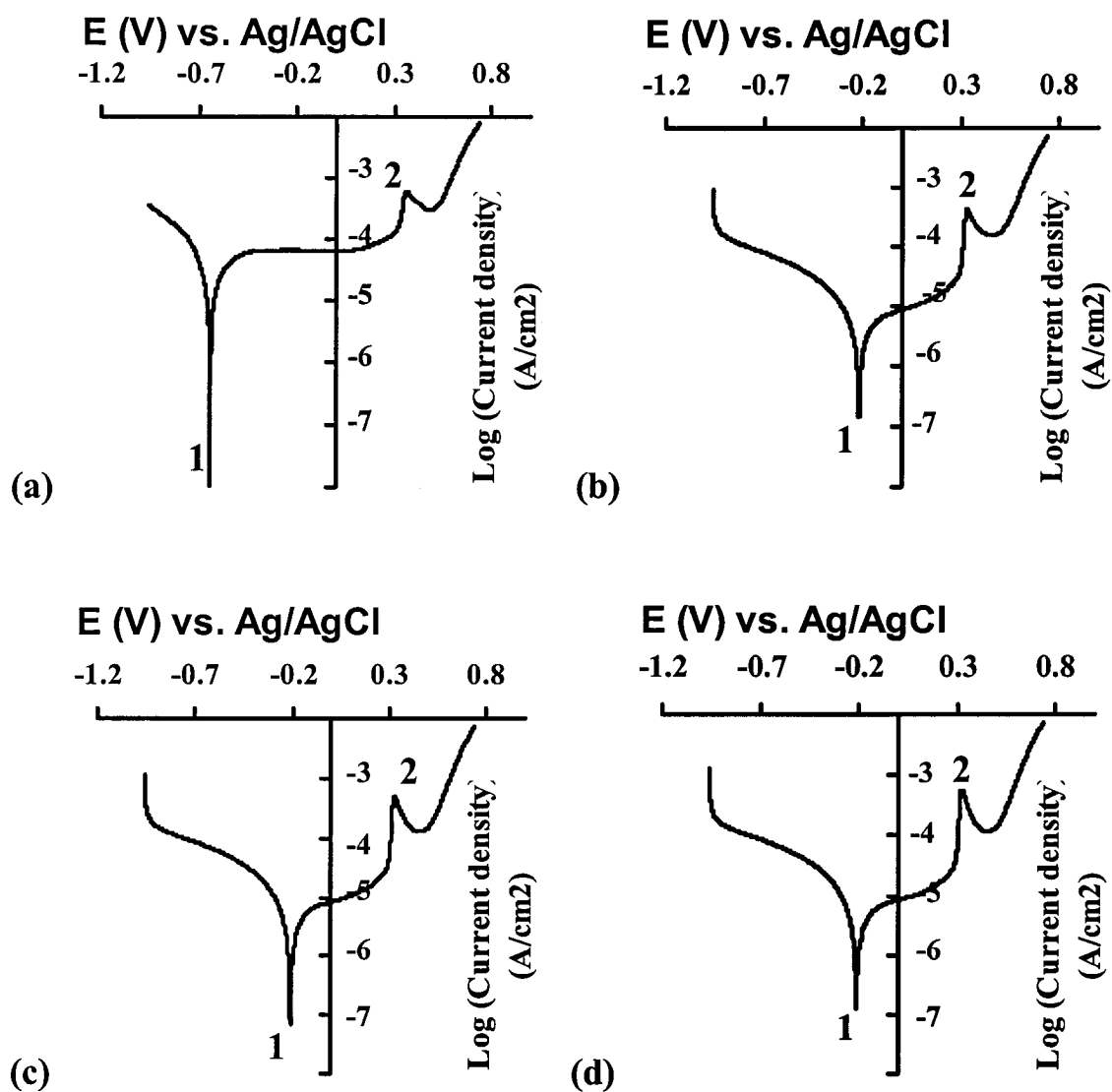


Figure 4.25 Polarization curves of EN-P coated sample 2 (8w% P) in 0.5 M NaOH at 5 mV/s scan rate; (a) first run, (b) second run, (c) third run, (d) fourth run.

Figures 4.26a, 4.26b, 4.26c, and 4.26d show first, second, third, and fourth run, respectively, of EN-P coated sample 3 (8 w% P, bath 3, Table 3.1) in 0.5 M NaOH. For this sample, in the first run peak 1 appears at  $-0.642$  V vs. Ag/AgCl in the anodic polarization region and peak 2 appears at  $0.405$  V in the cathodic polarization region. In the second run, the position of peak 1 shifts towards more positive potentials ( $-0.215$  V vs. Ag/AgCl) and in the cathodic polarization area, peak 2 grows slightly and shifts towards more negative ( $0.335$  V vs. Ag/AgCl) potential. In the third, and fourth runs, the positions of peaks 1 and 2 remain constant and peak 2 does not grow further.

Finally, Figures 4.27a, 4.27b, 4.27c, and 4.27d show first, second, third, and fourth runs, respectively, of EN-P coated sample 4 (2 w% P) in 0.5M NaOH. It can be seen that in the first run peak 1 appears at  $-0.174$  V vs. Ag/AgCl in the anodic polarization region, and a very small peak 2 appears at  $0.415$  V vs. Ag/AgCl in the cathodic polarization region. In the second, third, and fourth runs the positions of peaks 1, and 2 remain constant and peak 2 does not grow.



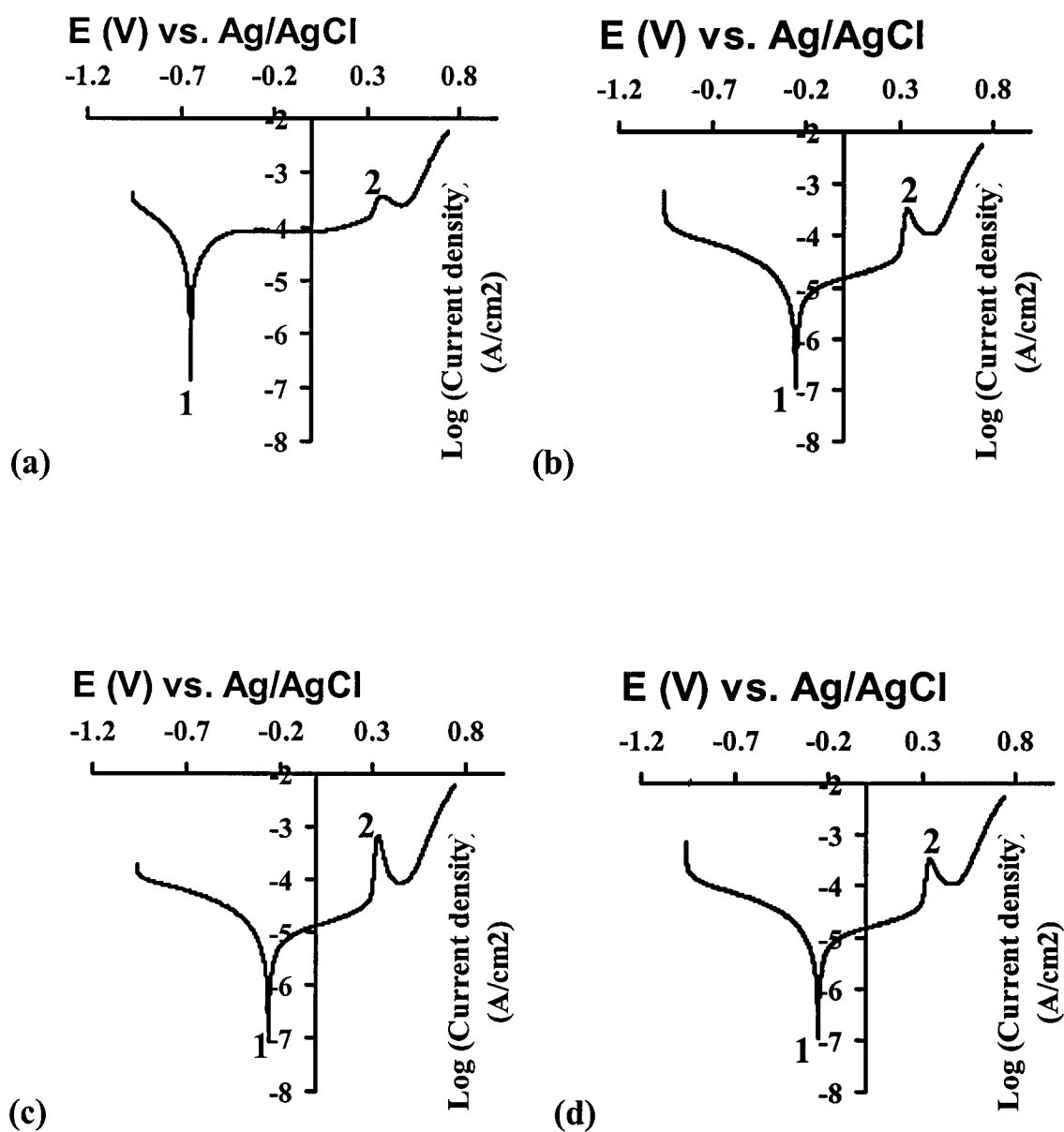


Figure 4.26 Polarization curves of EN-P coated sample 3 (6 w% P) in 0.5 M NaOH at 5 mV/s scan rate; (a) first run, (b) second run, (c) third run, (d) fourth run.

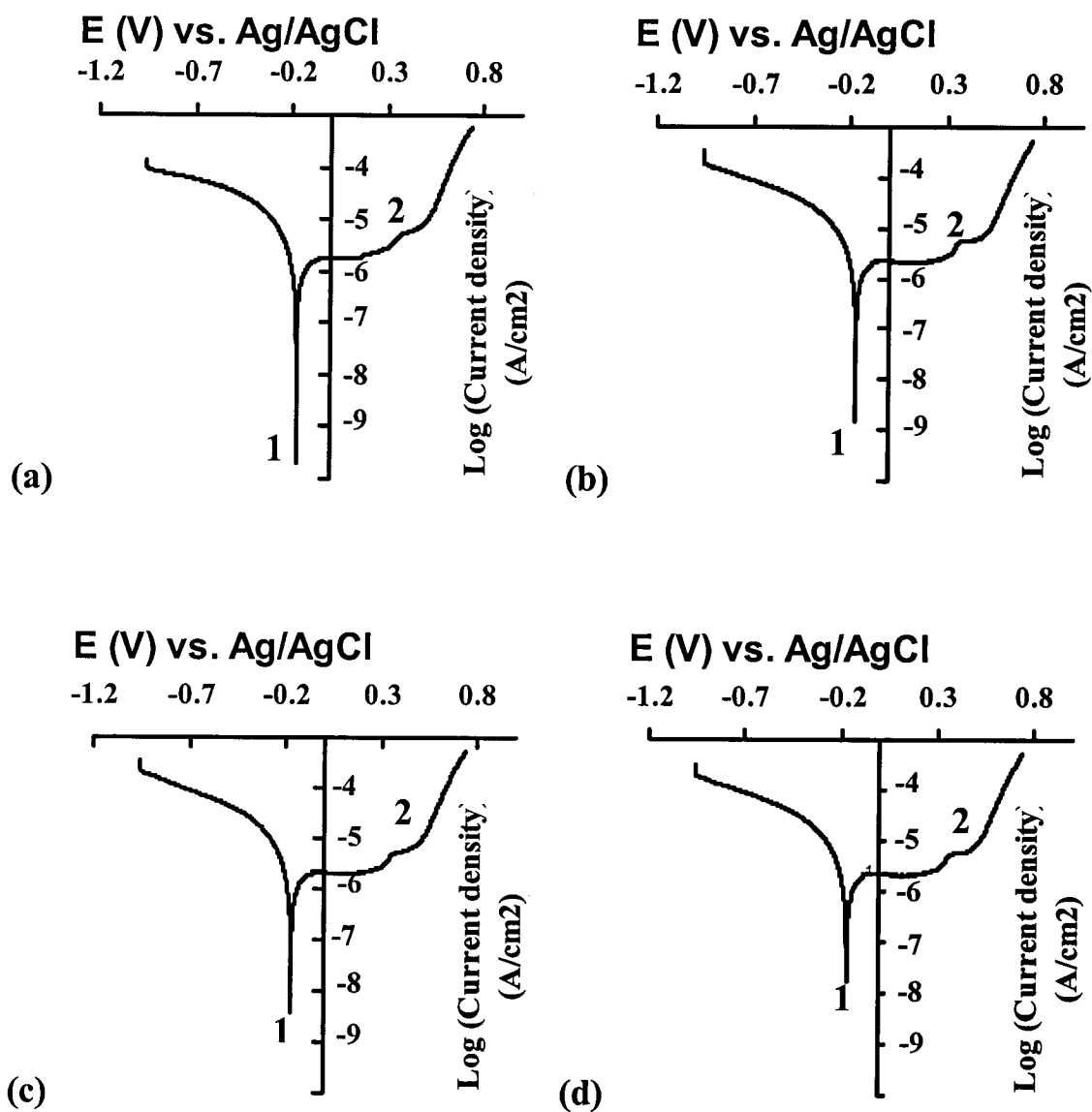
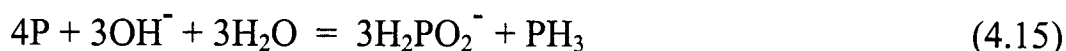


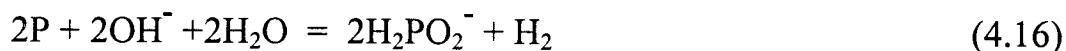
Figure 4.27 Polarization curves of EN-P coated sample 4 (2w% P) in 0.5 M NaOH at 5 mV/s scan rate; (a) first run, (b) second run, (c) third run, (d) fourth run.

To determine the possible reactions happening during anodic and cathodic polarization, the possible reactions are first considered from a thermodynamic viewpoint. The relationship between the various phosphorus oxidation states in basic solutions has been discussed by Latimer [136]. Phosphorus is unstable with respect to its partitioning into the +1 and -3 states as shown in equations (4.14) and (4.15)



for which the standard Gibbs free energies are  $\Delta G_1^0 = -30.1$  kcal/mole and  $\Delta G_2^0 = -80.0$  kcal/mole at 25 °C, respectively.

The negative free energy,  $\Delta G_2^0$ , for the reaction (4.15) in alkaline solution is large and the reaction is expected to proceed favourably. Because of the high reducing power of phosphorus in basic solution  $\text{H}_2$  is also produced, according to reaction (4.16):



for which the standard Gibbs free energy,  $\Delta G_3^0$ , is -56.25 kcal/mole at 25 °C.

Hypophosphorous acid is unstable with respect to its decomposition into phosphorus acid and phosphine as follows:



for which the standard Gibbs free energy,  $\Delta G_4^0$ , is -29.9 kcal/mole at 25 °C. This reaction is expected to occur easily, and because of the strong reducing potential of the acid, water will also be reduced according to reaction (4.18):



for which the standard Gibbs free energy  $\Delta G_5^0$  is -23.0 kcal/mole at 25 °C. The decomposition of phosphorous acid into phosphine and phosphoric acid, equation (4.19), has a small positive Gibbs free energy,  $\Delta G_6^0 = 0.9$  kcal/mole at 25 °C, and should not proceed.



Therefore it seems likely that the phosphorus on the surface of the EN coated samples exists mostly as elemental phosphorus and phosphate species.

Sample 1 [bath 1, Table 3.1] has a high phosphorus content (12.5 w% P) relative to the other samples. Thus, the appearance of any peaks related to any phosphorus species should be favoured relative to other samples. Comparing the first run of sample 1 (Figure 4.24a) with that of the other samples, it can be seen that the small peak 1 in Figure 4.24a does not appear in the other samples. Also the position and the height of the peak remains constant in subsequent runs for sample 1, Figures 4.24b, 4.24c, 4.24d. It seems that this peak is related to oxidation of a phosphorus species. Peak 1

appears at  $-0.744$  V vs. Ag/AgCl, which is very close to the equilibrium potential of  $\text{HPO}_3^{-2}/\text{HPO}_4^{-2}$  at pH 11.6 ( $-0.81$  V vs. Ag/AgCl [136]).

Anodic oxidation of nickel in alkaline solutions has been investigated by many researchers and it has been reported [146] that the following compounds are found on nickel depending on experimental conditions: NiO or  $\text{Ni}(\text{OH})_2$ ,  $\text{Ni}_3\text{O}_4$  or  $\text{Ni}_3\text{O}_2(\text{OH})_4$ ,  $\text{Ni}_2\text{O}_3$  or  $\beta$ -NiOOH,  $\text{NiO}_2$ .

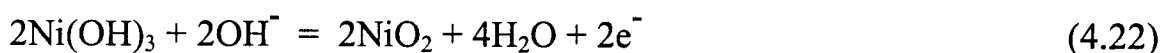
Possible oxidation reactions producing these compounds can be written as follows [136]:



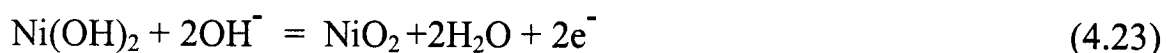
for which  $E^0_{25^\circ\text{C}} = -0.72$  V and  $E_{\text{eq}, 25^\circ\text{C}} = -0.58$  V



for which  $E^0_{25^\circ\text{C}} = -0.24$  V and  $E_{\text{eq}, 25^\circ\text{C}} = -0.098$  V



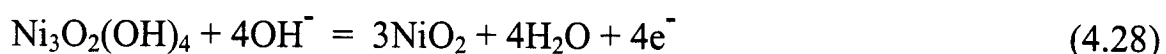
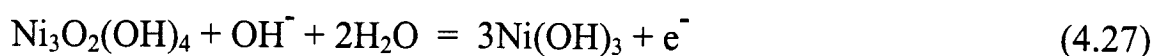
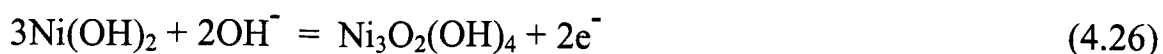
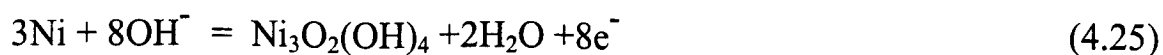
for which  $E^0_{25^\circ\text{C}} = +0.27$  V and  $E_{\text{eq}, 25^\circ\text{C}} = +0.41$  V



for which  $E^0_{25^\circ\text{C}} = +0.49$  V and  $E_{\text{eq}, 25^\circ\text{C}} = +0.63$  V



for which  $E^0_{25^\circ\text{C}} = +0.71$  V and  $E_{\text{eq}, 25^\circ\text{C}} = +0.85$  V



In the above equations, the  $E^0$  value for each reaction was calculated from the free energy of formation of the components at the same temperature whereas  $E_{\text{eq}}$  values were calculated from  $E^0$  and using the Nernst equation for a pH 11.6 (Appendix C). There is no standard free Gibbs energy of formation for the intermediate compound,  $\text{Ni}_3\text{O}_2(\text{OH})_4$ , reported in literature. However, it is predicted that for reaction (4.25) the  $E_{\text{eq}, 25^\circ\text{C}}$  value may lie between  $-0.58$  and  $-0.098$  V and for reaction (4.28) the  $E_{\text{eq}, 25^\circ\text{C}}$  value may lie between  $0.41$  and  $0.63$  V. Therefore, thermodynamically, the possible oxidation reactions in the anodic region ( $-0.96 - 0$  V vs. Ag/AgCl), are reactions (4.20), (4.21), and (4.25). In the oxidation of  $\beta\text{-Ni}(\text{OH})_2$  to  $\beta\text{-NiOOH}$ , compounds such as  $\text{Ni}_3\text{O}_2(\text{OH})_4$  or  $\text{Ni}_3\text{O}_4 \cdot x\text{H}_2\text{O}$  have been considered as intermediates, which shows the existence of a nickel oxidation state of about 2.7 [138]. According to Briggs and co-workers [139], this  $\text{Ni}_3\text{O}_2(\text{OH})_4$  can be accounted for by a mixture of  $\beta\text{-Ni}(\text{OH})_2$  and  $\beta\text{-NiOOH}$ . Reaction (4.22), which shows the formation of this intermediate species,  $\text{Ni}_3\text{O}_2(\text{OH})_4$ , can be considered as a possible reaction in the anodic polarization region, for which  $E_{\text{eq}, 25^\circ\text{C}}$  may lie between  $-0.098$  and  $-0.58$  V.

The position of peak 2 is also seen to change towards a more positive potential (-0.322 V vs. Ag/AgCl). It seems that this peak may be related to the oxidation of elemental nickel, which becomes more difficult after the first run resulting from the formation of a surface oxide layer. This may explain the shift of peak 2 towards the more positive potentials. Peak 2 in Figure 4.24 and peak 1 in Figures 4.25, 4.26, and 4.27 may be the result of reaction (4.20), and peak 3 in Figure 4.24 may be related to reaction (4.21) for which the calculated  $E_{\text{eq}, 25^{\circ}\text{C}}$  is -0.098 V.

In the cathodic region (0 – 0.74 V vs. Ag/AgCl), the reaction



is the most favorable from a thermodynamic viewpoint. Thus it appears that peak 4 in Figure 4.24 and peak 2 in Figures 4.25, 4.26 and 4.27, are due to reaction (4.29). The reduced form is  $\text{Ni(OH)}_2$  and the oxidized form is generally believed to be  $\text{NiO(OH)}$ . Both these structures have been shown to exist in two modifications,  $\alpha$  and  $\beta$  for the reduced structure, and  $\gamma$  and  $\beta$ , for the oxidized structure. The reduced  $\alpha$  form has further been shown to have the formula  $3\text{Ni(OH)}_2 \cdot 2\text{H}_2\text{O}$ . These structures and their modifications are probably hydrated to a greater or lesser extent [49, 100]. In addition, phases  $\alpha$ ,  $\beta$ , and  $\gamma$  have layered structures [101]. The  $\beta$ -phase is an anhydrous phase but  $\alpha$ , and  $\gamma$  are hydrous phases. In the  $\alpha$ -phase the planar metal hydroxide layers are separated from each other by planes of water molecules whereas in the  $\gamma$ -phase the layers are separated by electrolyte [101, 102]. From the

preceding, the two peaks  $\beta$ -Ni(OH)<sub>2</sub> to  $\beta$ -NiOOH and  $\alpha$ -Ni(OH)<sub>2</sub> to  $\gamma$ -NiOOH would be expected on the anodic sweep with two more peaks on the subsequent cathodic sweep.

Hummel and collaborators [103] showed that in 0.15 N Na<sub>2</sub>SO<sub>4</sub> solutions, the anodic film observed on pure Ni was primarily Ni(OH)<sub>2</sub>. Also they showed that at different pH and potentials NiO may form simultaneously with Ni(OH)<sub>2</sub>. Thus at pH>8, the Ni(OH)<sub>2</sub> film is oxidized to NiOOH at potentials near those required for oxygen evolution and a deprotonation reaction converts the Ni(OH)<sub>2</sub> to NiOOH. However, according to Barnard and co-workers [140], formal E<sup>0</sup> potentials for activated and deactivated  $\beta$ -Ni(OH)<sub>2</sub>/ $\beta$ -NiOOH lie in the range of 0.443-0.470 V and for  $\alpha$ -Ni(OH)<sub>2</sub>/ $\gamma$ -NiOOH lie in the range of 0.393-0.440 V with respect to a Hg/HgO/KOH reference electrode. According to Tuomi [141],  $\gamma$ -NiOOH is less active than  $\beta$ -NiOOH and only discharges appreciably at a very low rate. Therefore it seems that the small shoulder (peak 5) could be related to the reduction of  $\gamma$ -NiOOH to  $\alpha$ -Ni(OH)<sub>2</sub>, and peak 4 could be attributed to the reduction of  $\beta$ -NiOOH to  $\beta$ -Ni(OH)<sub>2</sub>. Finally,  $\alpha$ -Ni(OH)<sub>2</sub> is unstable and converts to  $\beta$ -Ni(OH)<sub>2</sub> on standing in alkaline solution. This is believed to be the reason for the absence of peak 5 in Figures 4.25, 4.26, and 4.27.

It was found that although the corrosion resistance of EN coatings generally increased with an increase in phosphorus content the trend was observed only for samples where the difference in the P content was large.



For example, a very low P EN coating (2 w%) was more resistant in alkaline solution than two medium P (6.5, 8 w%) samples, and these in turn were more resistant than the high P (12.5 w%) coated sample. However, when comparing the 6.5 and 8 w% samples the higher P content showed more resistance (less corrosion current). Figure 4.24 (sample 1, 12.5 w% P) shows more peaks and hence more corrosion products, and a higher corrosion current compared to Figures 4.25, 4.26, and 4.27. Therefore, it seems that sample 4 (2 w% P) has higher corrosion resistance compared to samples 1, 2, and 3.

This behaviour can be explained in terms of the two counteracting effects, activating and inhibiting, of phosphorus on corrosion resistance. The activating effect is due to the lower protectiveness of the passivating film because of its lower thickness. As the P content increases, the inhibiting effect increases as a result of phosphate formation. Finally, the corrosion products, and cyclic voltammetric behaviour of the EN samples, varied with bath pH.

#### ***4.2.2 Cyclic voltammetric study of the electroless nickel-phosphorus coated AA6061 samples***

Following potentiodynamic experiments, multiple cyclic voltammograms (CV) of each sample were run in an attempt to grow an oxide layer on the surface. The multiple CV experiments were run at a scan rate of 100 mV/s, for 60 cycles. Single CVs at different scan rates were then obtained for each sample. Figures 4.28, 4.29, 4.30 and 4.31 show a single

CV for samples 1, 2, 3, and 4, respectively at different scan rates. It can be seen that, in CV of samples 1, 2, and 3, the anodic potential peak shifts towards a more positive potential and the cathodic potential peak shifts towards a more negative potential with increasing scan rate. As can be seen from Figure 4.31 the positions of the anodic and cathodic peaks do not change with increasing the scan rate. This indicates that the anodic and cathodic reactions are reversible. Also from Figures 4.28 to 4.31 it can be seen that the cathodic peak splits into two peaks at lower scan rates. The anodic and cathodic peaks in voltage range 0 - 0.800 V vs. Ag/AgCl, Figures 4.28 to 4.31, could be related to reaction (4.24). In the present system the splitting of the cathodic peak may be explained by considering the poor conductivity of  $\beta$ -phase compared to the  $\alpha$ -phase layer.  $\beta$ -phase is an anhydrous layer, whereas  $\alpha$ -phase is a hydrous layer. Therefore, the  $\beta$ -phase is expected to be covered by  $\alpha$ -phase, as shown in Figure 4.32.

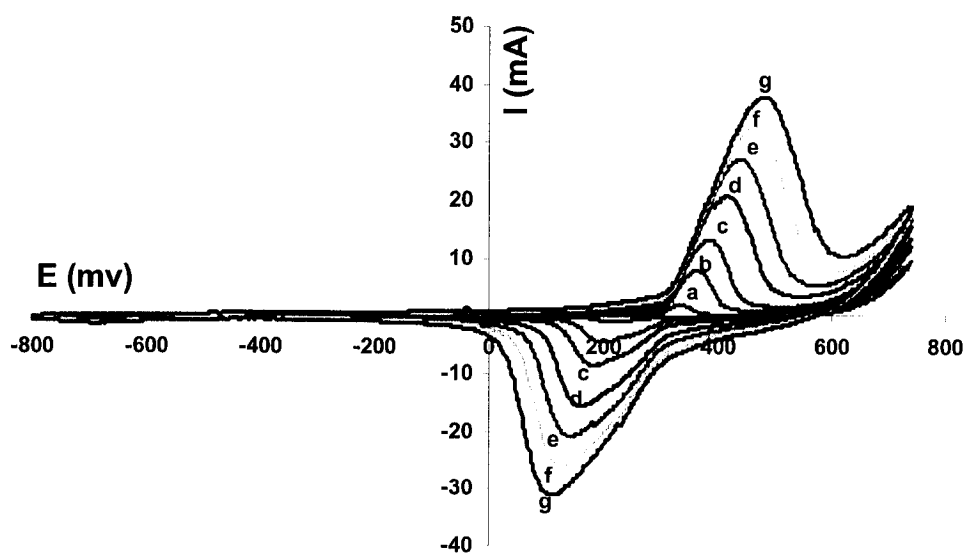


**Figure 4.28** Cyclic voltammogram of EN-P coated sample 1 in 0.5 M NaOH at different scan rates; (a) 0.010 V/s, (b) 0.05 V/s, (c) 0.100 V/s, (d) 0.200 V/s, (e) 0.300 V/s, (f) 0.400 V/s, (g) 0.500 V/s.

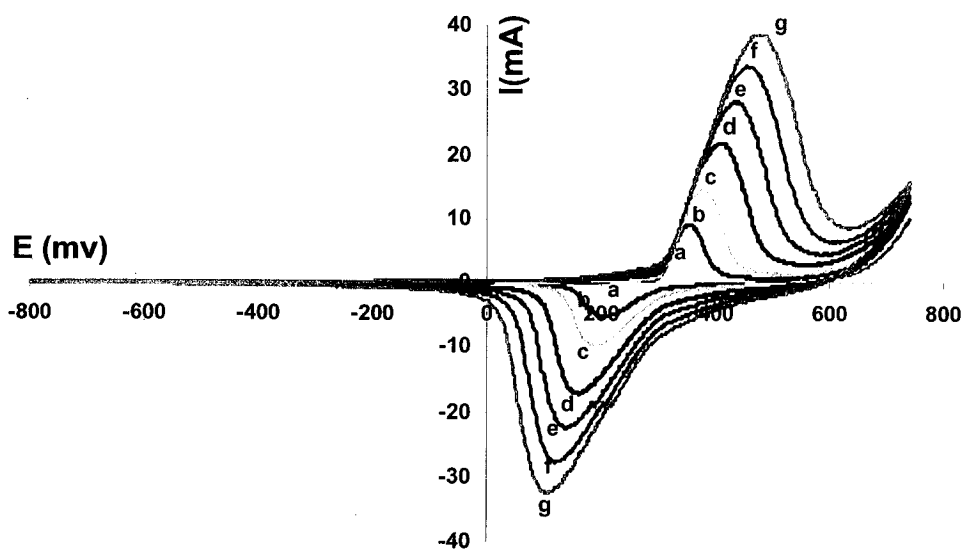


**Figure 4.29** Cyclic voltammogram of EN-P coated sample 2 in 0.5 M NaOH at different scan rates; (a) 0.010 V/s, (b) 0.050 V/s, (c) 0.100 V/s, (d) 0.200 V/s, (e) 0.300 V/s, (f) 0.400 V/s, (g) 0.500 V/s.

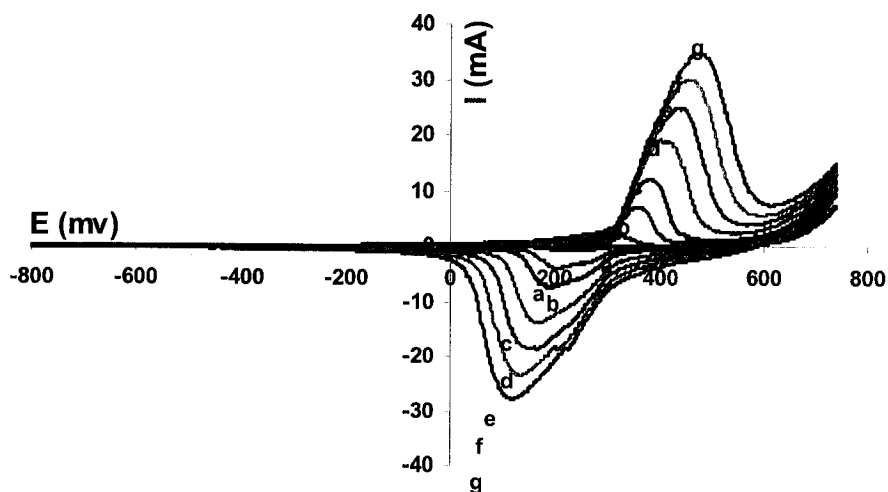


**Figure 4.30** Cyclic voltammogram of EN-P coated sample 3 in 0.5 M NaOH at different scan rates; (a) 0.010 V/s, (b) 0.050 V/s, (c) 0.100 V/s, (d) 0.200 V/s, (e) 0.300 V/s, (f) 0.400 V/s, (g) 0.500 V/s.

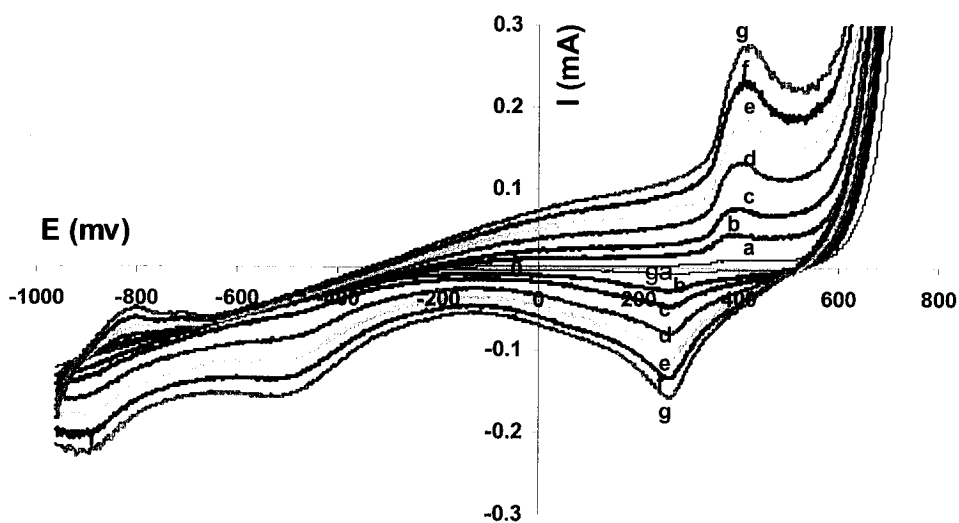


**Figure 4.31** Cyclic voltammogram of EN-P coated sample 4 in 0.5 M NaOH at different scan rates; (a) 0.010 V/s, (b) 0.050 V/s, (c) 0.100 V/s, (d) 0.200 V/s, (e) 0.300 V/s, (f) 0.400 V/s, (g) 0.500 V/s.

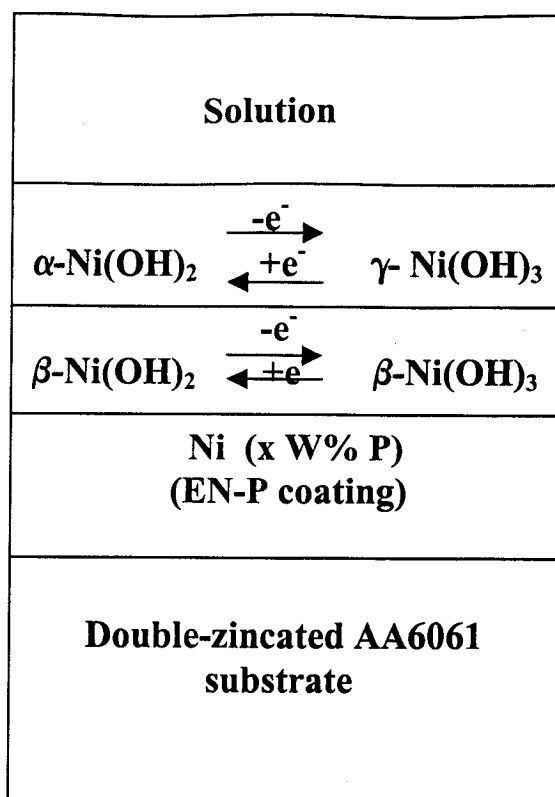


**Figure 4.32** A schematic diagram of EN-P coated AA6061 covered by  $\beta\text{-Ni(OH)}_2 / \beta\text{-Ni(OH)}_3$  and  $\alpha\text{-Ni(OH)}_2 / \gamma\text{-Ni(OH)}_3$  layers.

In anodic polarization, the  $\alpha\text{-Ni(OH)}_2$  is oxidized to  $\gamma\text{-Ni(OH)}_3$  and  $\beta\text{-Ni(OH)}_2$  is oxidized to  $\beta\text{-Ni(OH)}_3$ . The  $\alpha$ -phase is separated from the surface of EN-P coated AA6061 by a poorly conductive  $\beta$ -phase layer. This makes the oxidation of  $\alpha\text{-Ni(OH)}_2$  to  $\gamma\text{-Ni(OH)}_3$  more difficult. Therefore, only one peak is expected in anodic polarization. This peak is a result of  $\beta\text{-Ni(OH)}_2 / \beta\text{-Ni(OH)}_3$  transition. In cathodic polarization, the  $\gamma\text{-Ni(OH)}_3$  is reduced to  $\alpha\text{-Ni(OH)}_2$  and  $\beta\text{-Ni(OH)}_3$  is reduced to  $\beta\text{-Ni(OH)}_2$ . The oxidized form of nickel hydroxide,  $\text{Ni(OH)}_3$ , has higher conductivity relative to the reduced form,  $\text{Ni(OH)}_2$ , because of the existence of mixed oxidation states in the oxidized form. Therefore, in spite of the fact that the  $\beta$ -phase layer is poorly

conductive, the reduction of  $\gamma\text{-Ni(OH)}_3$  to  $\alpha\text{-Ni(OH)}_2$  can happen because of the higher conductivity of  $\text{Ni(OH)}_3$  compared to  $\text{Ni(OH)}_2$ . This may explain the splitting of the cathodic peak. These results compared favourably with those obtained by Burke and Twomey [99] at  $\text{pH} < 14$ .

As can be seen from Figures 4.28 to 4.31, the splitting of the cathodic peak is obvious only for low scan rates. This shows that the  $\gamma\text{-Ni(OH)}_3$  to  $\alpha\text{-Ni(OH)}_2$  transition proceeds very slowly relative to the  $\beta\text{-Ni(OH)}_3/\beta\text{-Ni(OH)}_2$  transition. Therefore, at high scan rates there will not be enough time for  $\gamma\text{-Ni(OH)}_3/\alpha\text{-Ni(OH)}_2$  conversion, and only one peak resulting from the  $\beta\text{-Ni(OH)}_3/\beta\text{-Ni(OH)}_2$  transition will be produced. This indeed is observed in Figure 4.31.

One advantage of cyclic voltammetry is that it is relatively easy to determine whether a system is reversible. The peak potential difference for an ideally reversible system is independent of the scan rate, and the peak currents, anodic and cathodic, are equal. If the electron transfer kinetics are slow, the peak potential separation is larger, and increases with increasing scan rate. It should be noted that this behaviour is also characteristic of uncompensated solution resistance; the two causes can be distinguished by running cyclic voltammograms at different base concentrations. If the redox reaction is coupled to chemical reactions, both the peak currents and peak potentials can be affected. For example, if there is a chemical reaction following the electron transfer reaction, the peak current on the reverse scan is decreased.

Figure 4.33 represents the data obtained from the CV experiments from all samples. The peak potential difference has been plotted as a function of scan rate. The data for Figure 4.33 are shown in Table D.1, Appendix D.

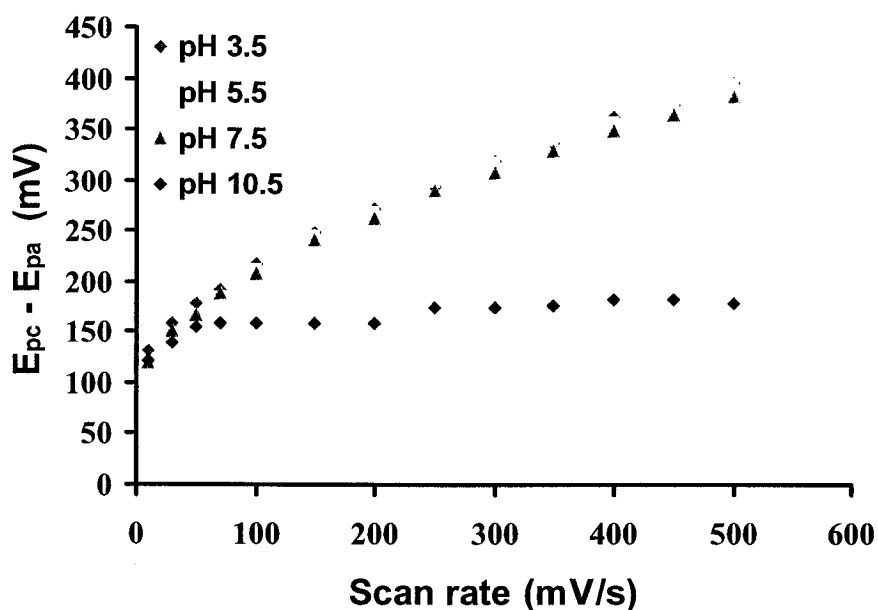


Figure 4.33 Peak potential difference vs. scan rate (mV/s).

As Figure 4.33 shows, for samples 1, 2, and 3 [baths 1, 2, and 3, Table 3.1] the peak separation increases with increasing scan rate. However, for sample 4 the peak separation remains constant thus indicating that it is independent of the scan rate. Therefore, for the sample with the lowest phosphorus content (2 w% P) which is obtained using bath 4 (pH 10.5), the

plot of peak potential difference versus scan rate showed a reversible behaviour. For the sample with the highest phosphorus content (12.5 w% P), the fact that the peak separation remains constant with a change in scan rate could be related to an irreversible behaviour or it may be related to very low peak current and therefore, the peak separation for different scan rates may not be obvious.

Figures 4.34, 4.35, 4.36, and 4.37 show the effect of upper limit voltages on voltammetric behaviour of samples 1, 2, 3, and 4, respectively. From Figures 4.34 to 4.36, it can be seen that at voltages above 0.300 V vs. Ag/AgCl, both the anodic and cathodic peaks appear and above about 0.350 V vs. Ag/AgCl, with an increase in the upper voltage limit, the cathodic peak remains constant, whereas for sample 4, Figure 4.37, at an upper limit voltage above 0.600 V vs. Ag/AgCl, the cathodic peak remains constant. After the third run at an upper voltages limit above 0.300 V vs. Ag/AgCl the cathodic peak appears, and by increasing this voltage in the 5<sup>th</sup> and 6<sup>th</sup> run, the cathodic peak grows. Therefore, it appears that the cathodic peak is related to the anodic peak and they belong to the same electrochemical reaction. In cathodic polarization, the electrochemical reaction proceeds in the reduction direction, whereas in anodic polarization it proceeds in the oxidation direction, equation (4.24). In the third run where the upper voltage limit is 0.300 V vs. Ag/AgCl, the cathodic peak is absent. By increasing the upper voltage limit, the cathodic peak appears and continues to grow with increasing voltage to about 0.600 V vs. Ag/AgCl. Therefore, it appears that at voltages above 0.300 V vs. Ag/AgCl in the anodic polarization region, the



oxidized form of nickel hydroxide,  $\text{Ni(OH)}_3$  is formed which can be subjected to the subsequent reduction reaction in cathodic polarization producing the cathodic peak. The increase in current at upper voltage limits higher than 0.600 V vs. Ag/AgCl is mainly related to the oxidation of water molecules which can produce oxygen. By increasing the voltage beyond 0.600 V vs. Ag/AgCl, the cathodic and anodic peaks remain constant. This shows that the oxygen produced from the oxidation of water molecules does not interfere with the oxidation and reduction of nickel hydroxide.

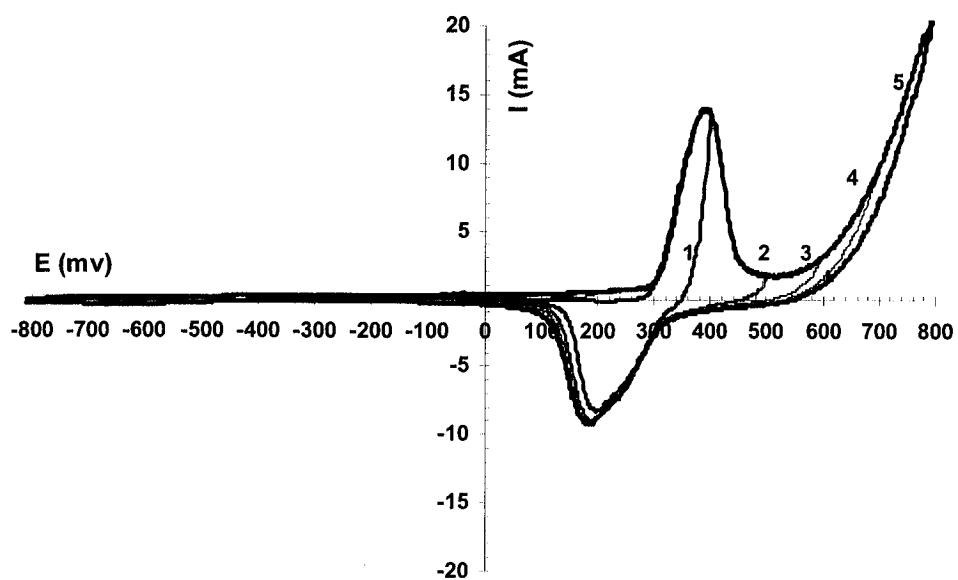


**Figure 4.34** Cyclic voltammograms of EN-P coated sample 1 at 0.100 V/s scan rate for different upper voltage limits.

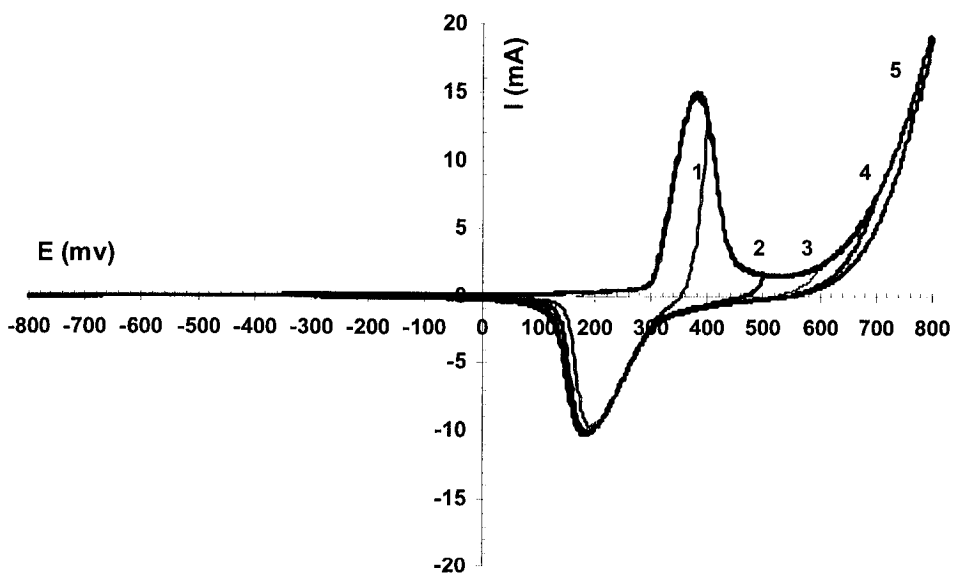


**Figure 4.35** Cyclic voltammograms of EN-P coated sample 2 at 0.100 V/s scan rate for different upper voltage limits.

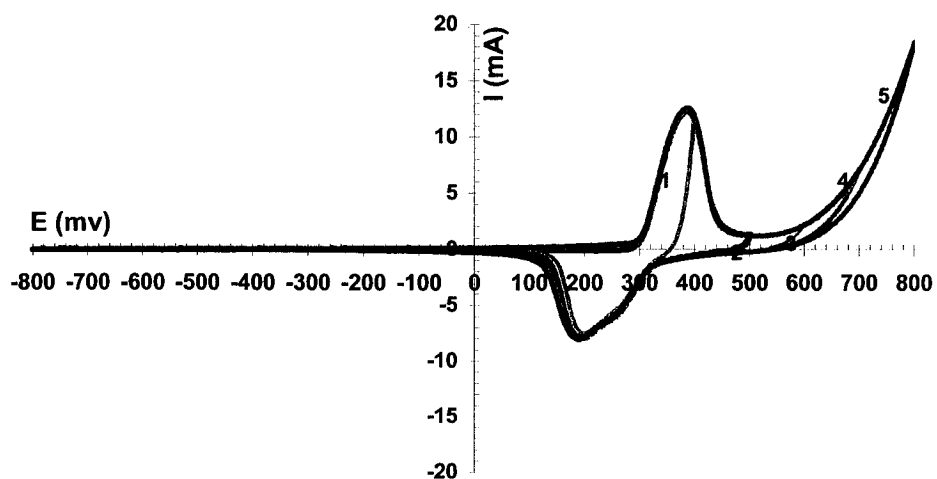


**Figure 4.36** Cyclic voltammograms of EN-P coated sample 3 at 0.100 V/s scan rate for different upper voltage limits.

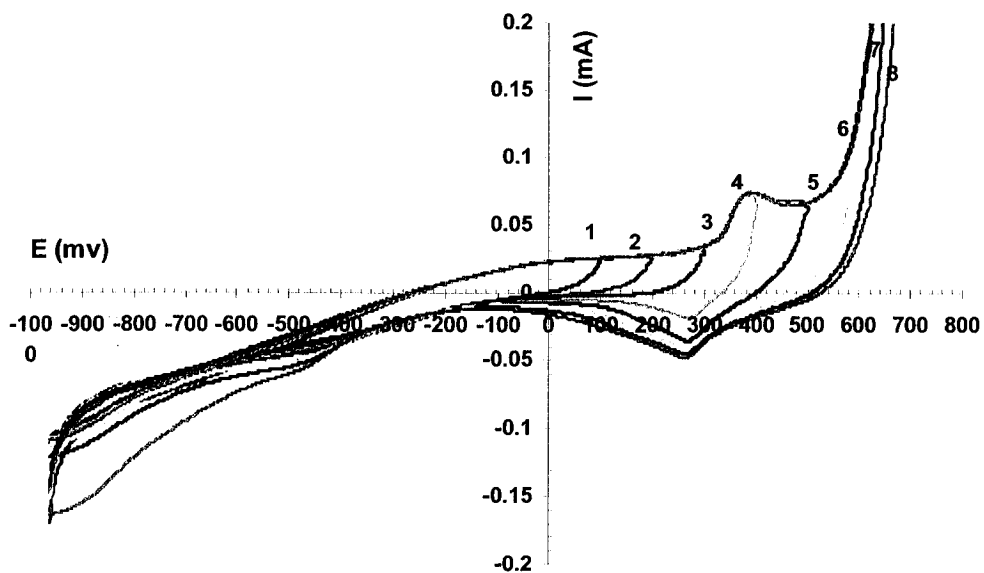


**Figure 4.37** Cyclic voltammograms of EN-P coated sample 4 at 0.100 V/s scan rate for different upper voltage limits.

Sample 4 was soaked in sulphuric acid (15% v/v) for 20 s, followed by rinsing with water, and then a single CV of the sample was obtained at 0.5 M NaOH. Figure 4.38 shows the CV for this sample immediately after soaking and rinsing in the first run (curve a), in a second run immediately following the first run (curve b), up to and including a 10<sup>th</sup> run (curve j). It can be seen that in the first run a very broad peak (peak a) appears in the cathodic region, which disappears in the second run. By soaking in sulfuric acid, it appears that the oxide film on the surface dissolves into the acid solution, and by repeating the cycling, the oxide film grows and becomes thicker, as after the first run the peak appearing in the region between 0.300 and 0.400 V vs. Ag/AgCl increases in height. It can also be seen that after the 5<sup>th</sup> run, the cathodic peak splits and a shoulder appears near 0.300 V vs. Ag/AgCl. By repeating the CV, the anodic and cathodic peaks grow in size. This single CV was repeated 5 times, each time for 20 cycles, at 0.100 V/s scan rate. Figure 4.39 shows the repetitive multiple CVs. As can be seen both the anodic and the cathodic peaks grow substantially with repeating multiple CVs. This can be attributed to oxide layer growth as a result of repeating the cyclic voltammograms.

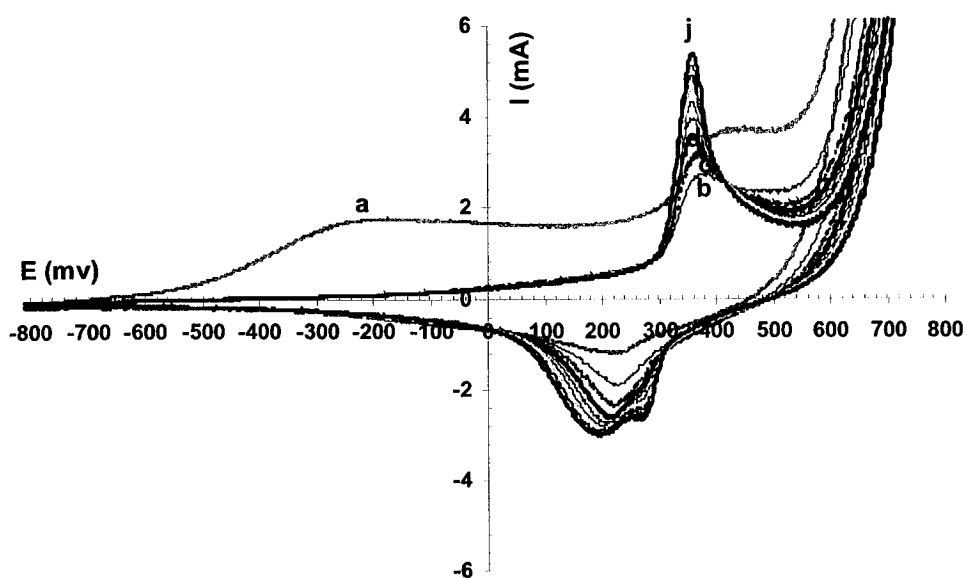


**Figure 4.38** Cyclic voltammogram of EN-P coated sample 4 after soaking in sulfuric acid (15% v/v) for 20 s in 0.5 M NaOH for different runs.

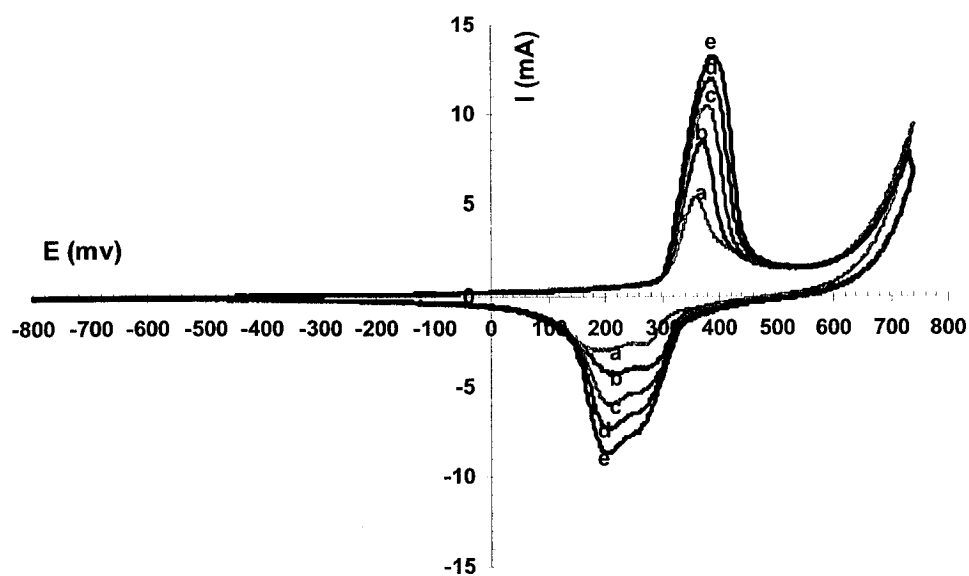


**Figure 4.39** Multiple cyclic voltammograms of EN-P coated sample 4 in 0.5 M NaOH at 0.100 V/s scan rate.

### 4.3 INVESTIGATION OF THE CORROSION BEHAVIOUR OF ELECTROLESS NICKEL-BORON COATINGS IN BASIC SOLUTIONS

The corrosion behaviour of electroless nickel-boron (EN-B) coatings with boron content of 6 w% was investigated using a potentiodynamic technique in 0.5 M sodium hydroxide, and the results were compared with those of a nickel-phosphorus coating with phosphorus content of 6 w%. As well, the effect of heat treatment on the corrosion resistance of the electroless nickel-boron coating was investigated.

In order to omit the deoxidizing/zincating pretreatments that were necessary for EN coating on the aluminum substrate, in this study brass was chosen as a substrate. In order to be able to compare the corrosion results with those of obtained from the Ni-P coated AA6061, following polishing the brass substrates were coated electrolessly with a 5  $\mu\text{m}$  intermediary Ni-P layer followed by heat- treatment at 220  $^{\circ}\text{C}$  in vacuum for 9h.

#### ***4.3.1 Potentiodynamic study of the electroless nickel-boron coated brass samples***

In order to avoid complications associated with the substrate and the corresponding necessity to perform the double zincating process required for EN-B coating of AA6061 samples, brass was chosen as a substrate.

Figures 4.40a.. k show first, ..., eleventh runs of EN-B coated sample 1 (no heat treatment) in 0.5 M NaOH solution. It can be seen that in the first run in the anodic polarization region, there is one sharp peak 1, and in the cathodic polarization region a very small broad peak 2 appears.

After the second run, the height of peak 1 increases but the position does not change, peak 2 becomes larger, and the passive anodic current does not change. The vertical line represents the logarithm of the cathodic current. Any decrease in cathodic current can be considered to be an increase in anodic current.

After the third run, the position of peak 1 changes toward a more negative potential, and the height of peak 1 does not change. In the cathodic polarization region, peak 2 grows, and the passive anodic current decreases.

In the fourth run (Figure 4.40d), in the anodic polarization region, peak 1 decreases in height and becomes broad, and changes slightly towards a more positive potential; the passive anodic current does not change. There is also no change in the height and position of peak 2.

In the fifth run (Figure 4.40e), in the anodic polarization region, peak 1 becomes slightly smaller, its position does not change, and two new peaks (peaks 3 and 4) appear. In the cathodic polarization region, the size and position of peak 2 remain constant. As well, the passive anodic current remains constant.

In the sixth, seventh,...ninth, it seems that the size and position of peaks 1, 2, and 3 remain constant, peak 4 grows slightly in size, but its position remains constant. As well, the anodic passive current remains constant.

Finally, in the tenth and eleventh runs, peak 1 becomes smaller, peak 2 remains constant, peak 3 grows in size, and peak 4 remains constant. As well the passive cathodic current remains constant.



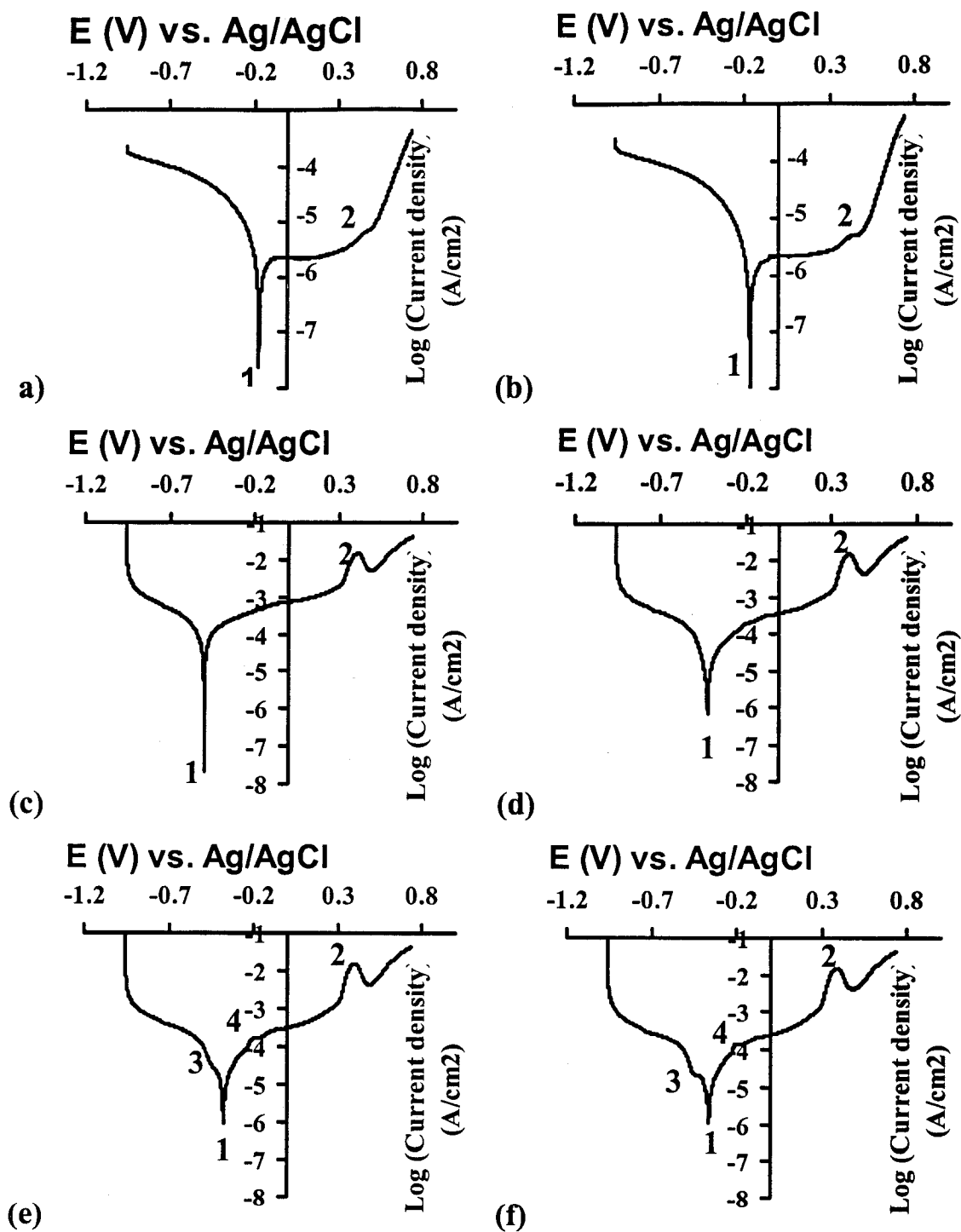


Figure 4.40 Polarization curves of EN-B coated sample 1 in 0.5 M NaOH solution for no heat treatment. (a) first run, (b) second run, (c) third run, (d) 4<sup>th</sup> run, (e) 5<sup>th</sup> run, (f) 6<sup>th</sup> run.

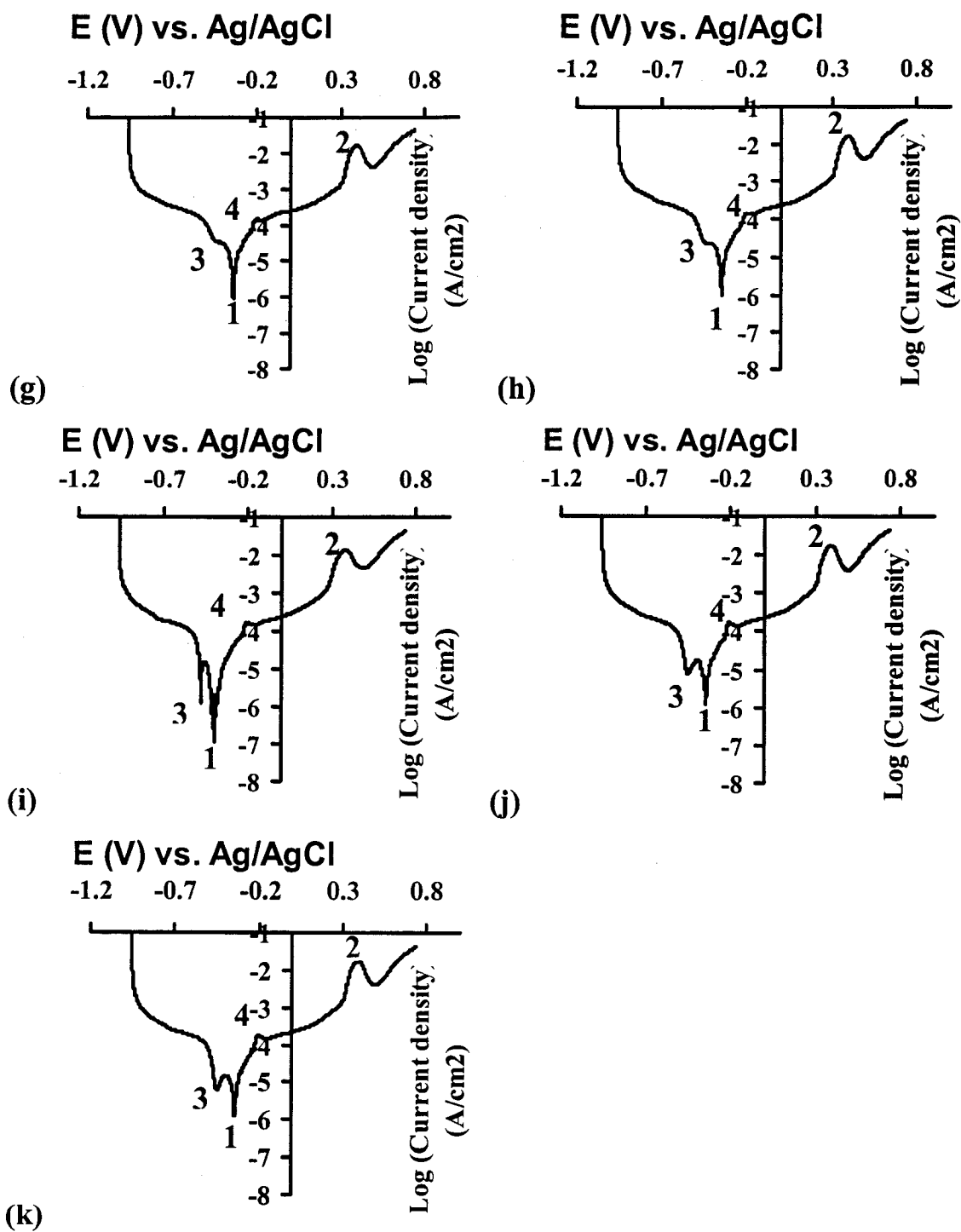


Figure 4.40 (Continued) Polarization curves of EN-B coated sample 1 in 0.5 M NaOH solution for no heat treatment. (g) 7<sup>th</sup> run, (h) 8<sup>th</sup> run, (i) 9<sup>th</sup> run, (j) 10<sup>th</sup> run, (k) 11<sup>th</sup> run.

Figures 4.41a.. k show first, ..., eleventh runs of EN-B coated sample 2 (48 h heat treatment) in 0.5 M NaOH solution. In the first run, in anodic polarization region, one sharp peak 1 appears and in the cathodic polarization region, one broad peak 2 appears. A comparison of Figures 4.41a, and 4.42a shows that in sample 2, the corrosion current is higher, and peak 1 appears at a more negative potential. Therefore, the heat treatment has decreased the corrosion resistance.

Continuing with polarization in the second run (Figure 4.41b), peak 1 shifts towards a more positive potential, and peaks 2 grows slightly in size and remains in the same position; in the third, fourth, fifth, and sixth runs (Figures 4.41c, 4.41d, 4.41e and 4.41f), peak 1 shifts towards more positive potentials, and peak 2 remains constant in size and position; in the seventh, eighth, and ninth runs (Figures 4.40g, 4.40h and 4.40i), peak 1 shifts towards more positive potentials, peak 2 remains constant in size and position, and two small peaks 3 and 4 appear and finally in the tenth and eleventh runs (Figures 4.41j and 4.41k), in the anodic polarization region, four peaks 1, 3, 5 and 4 appear. It seems that peaks 1 and 3 differ from the corresponding peaks 1 and 3 from previous runs. By comparing Figures 4.41j (sample 2, 10<sup>th</sup> run) and 4.41k (sample 2, 11<sup>th</sup> run) with Figures 4.40j (sample 1, 10<sup>th</sup> run) and Figure 4.40k (sample 1, 11<sup>th</sup> run), it can be seen that for sample 2 (24 h heat treatment at 220 °C) in 10<sup>th</sup> and 11<sup>th</sup> runs, four peaks appear in the anodic polarization region, whereas for sample 1 (no heat-treatment), three peaks appear in the 10<sup>th</sup> and 11<sup>th</sup> runs in the anodic polarization regions.

Therefore, it appears that again the heat treatment increases the number of peaks, which are representative of the various corrosion products.

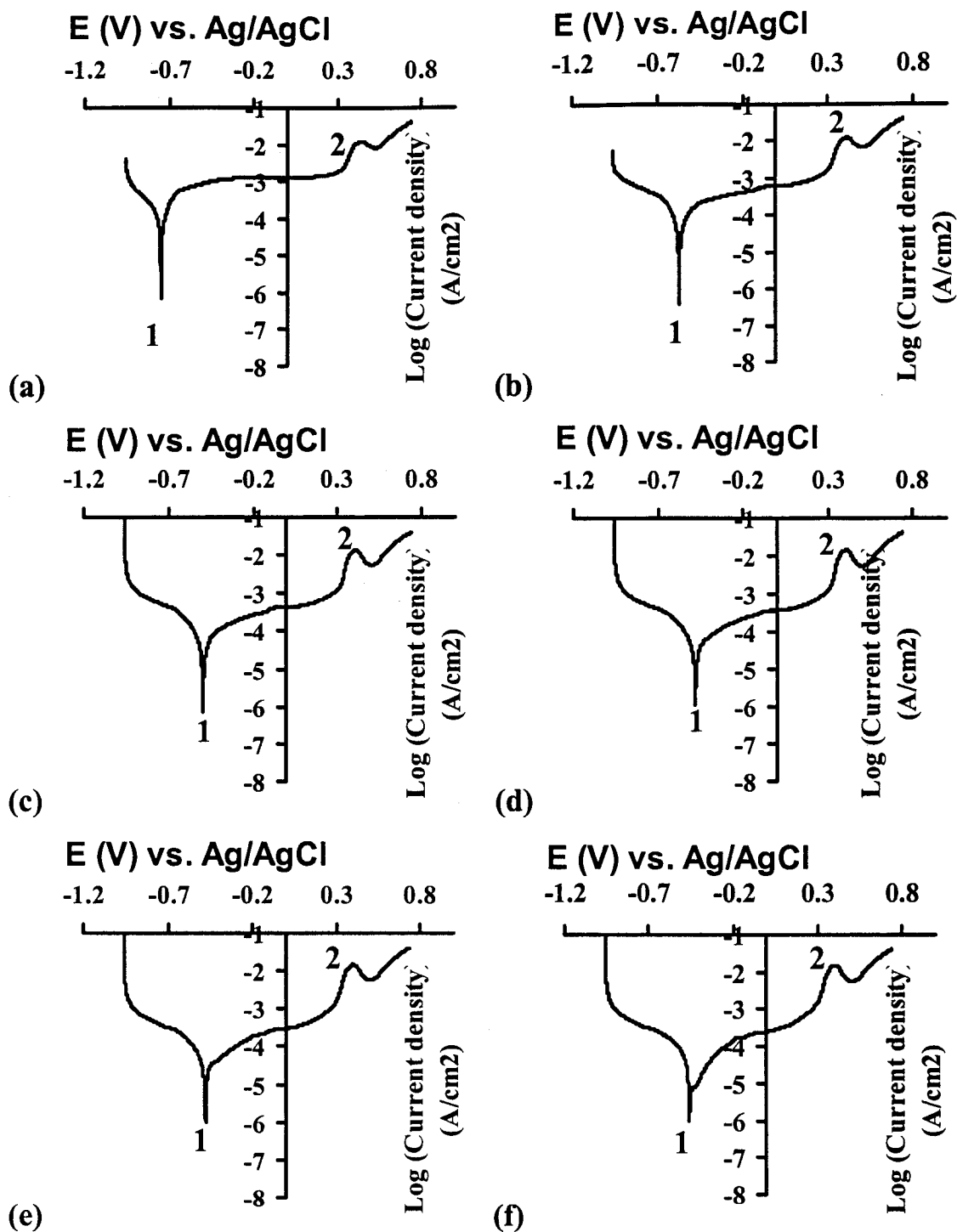


Figure 4.41 Polarization curves of EN-B coated sample 2 in 0.5 M NaOH solution for heat treatment duration of 24 h. (a) first run, (b) second run, (c) third run, (d) 4<sup>th</sup> run, (e) 5<sup>th</sup> run, (f) 6<sup>th</sup> run.

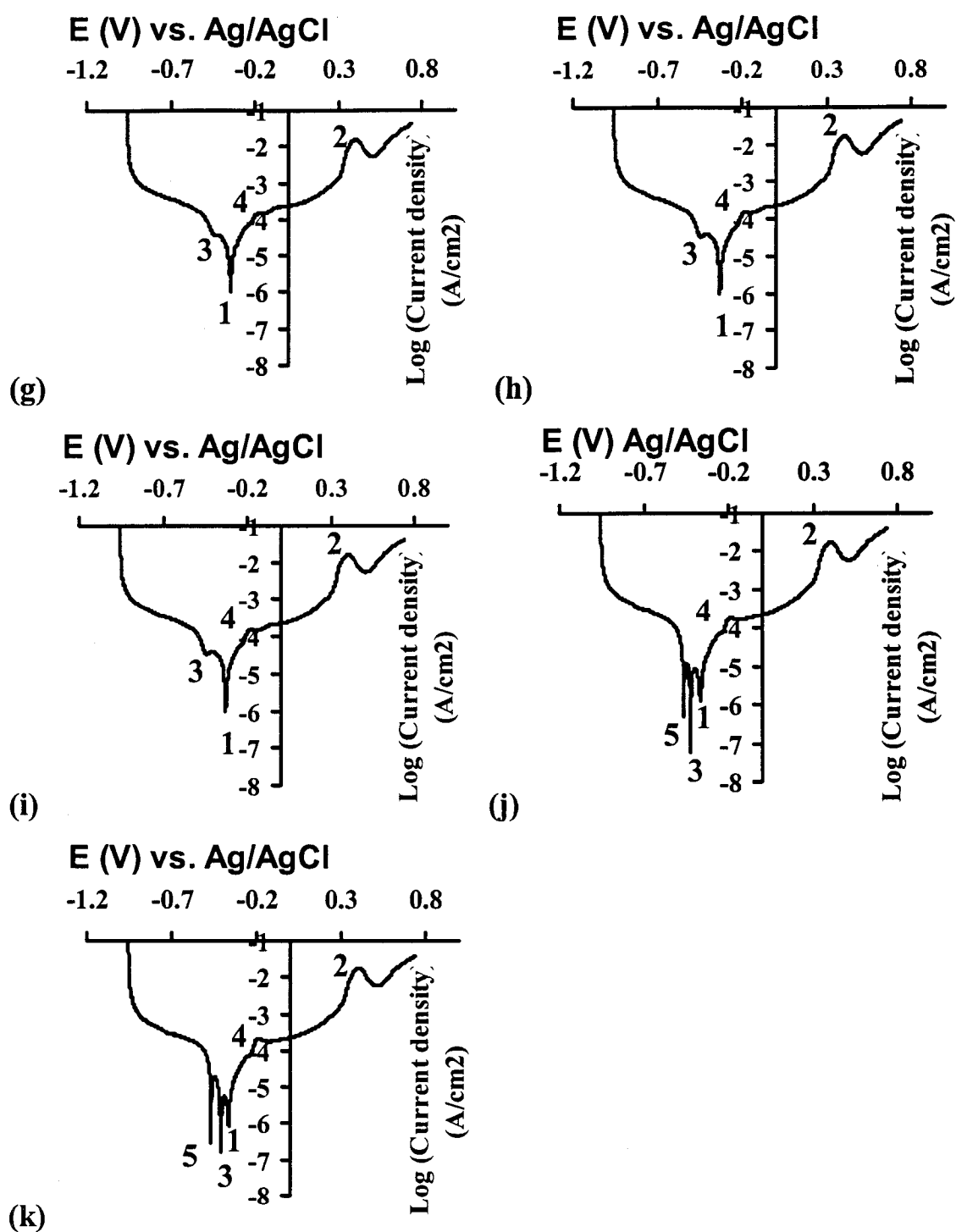


Figure 4.41 (Continued) Polarization curves of EN-B coated sample 2 in 0.5 M NaOH solution for heat treatment duration of 24 h. (g) 7<sup>th</sup> run, (h) 8<sup>th</sup> run, (i) 9<sup>th</sup> run, (j) 10<sup>th</sup> run, (k) 11<sup>th</sup> run.

Figures 4.42a...k show first, ..., eleventh runs of EN-B coated sample 3 (96h heat treatment) in 0.5 M NaOH solution. In the first run, in the anodic polarization region, one sharp peak 1 appears. In the cathodic polarization region, one broad peak 2 appears. Comparison of Figures 4.42a, and 4.41a shows that in sample 3, the passive cathodic current is higher compared to sample 1, and peak 1 appears at a more negative potential. Therefore, once again an increase in the heat treatment duration has decreased the corrosion resistance.

Figure 4.42b shows the second run for sample 3. Again it can be seen that peak 1 shifts towards more positive potentials and peak 2 slightly increases in size, but remains constant in position. This behaviour is similar to that for sample 2 for the second run.

Figures 4.42c, 4.42d, 4.42e, 4.42f, and 4.42g show the third, 4<sup>th</sup>, 5<sup>th</sup>, 6<sup>th</sup>, and 7<sup>th</sup> runs for sample 3, respectively. It can be seen that in these runs, three peaks 1, 3, and 4 appear in the anodic polarization region and one peak 2 appears in the cathodic polarization region.

Figures 4.42h, 4.42i, 4.42j, and 4.42k show the 8<sup>th</sup>, 9<sup>th</sup>, 10<sup>th</sup>, and 11<sup>th</sup> runs for sample 3, respectively. It can be seen that in the 7<sup>th</sup> run, peak 3 starts to split into two peaks 3' and 5. For sample 2 this splitting happened after the 9<sup>th</sup> run.

A comparison of Figures 4.41 and 4.42 shows that the anodic and cathodic polarization behaviour of samples 2 and 3 are similar. For both samples, four peaks are present in the final run for the anodic polarization region. This is in contrast to sample 1, where three peaks appear in the anodic polarization region for the final run. Therefore, heat treatment and its duration can decrease the corrosion behaviour of EN-B coated samples in 0.5M NaOH solution. This is apparent from Figures 4.40, 4.41, and 4.42. Figure 4.40 shows that fewer corrosion products are produced in the 10<sup>th</sup> and 11<sup>th</sup> runs. Also there is a lower corrosion current compared to Figures 4.41 and 4.42. Comparison of Figures 4.41 and 4.42 shows that higher heat-treatment duration decreases corrosion resistance, as in Figure 4.41 the corrosion current is lower relative to Figure 4.42. The results are related to crystallization of the Ni-B coating from an amorphous state. These coatings, however, are not completely amorphous. During heating to 220 °C, the amorphous Ni-B is crystallized. The crystallization is gradual and the amounts of Ni<sub>3</sub>B formed during crystallization increases gradually with an increase in heat treatment duration. Therefore, the corrosion resistance is expected to decrease with increase in heat-treatment duration.

In order to examine the effect of heat treatment and its duration on the amounts of crystallized phase, XRD spectra were taken from various Ni-B coatings on the brass substrate with as-plated and various heat treatment duration conditions. The results are shown in Figure 4.43. The as-plated condition is shown in Figure 4.43a. Here, the diffraction pattern for the brass substrate appears at Bragg angles of 42, 49, 73, and 80 degrees. The X-ray



diffraction spectrum for the coating is characteristic of an amorphous material, with the peak maximum at an angle of about 52.265 degrees. However, this peak angle coincides with that of the Ni(100) 51.9 diffraction peak and thus the coating is not completely amorphous.

Figure 4.43b, 4.43c, 4.43d, 4.43f, 4.43g, and 4.43f show XRD spectra for EN-B coated samples with heat-treatment durations of 5 h, 24 h, 48 h, 72 h, 96 h, and 120 h, respectively. It can be seen that by increasing the heat treatment time at 220 °C, the transition from amorphous to crystalline states occurs. This may explain the decrease in corrosion resistance with an increase in heat treatment time.

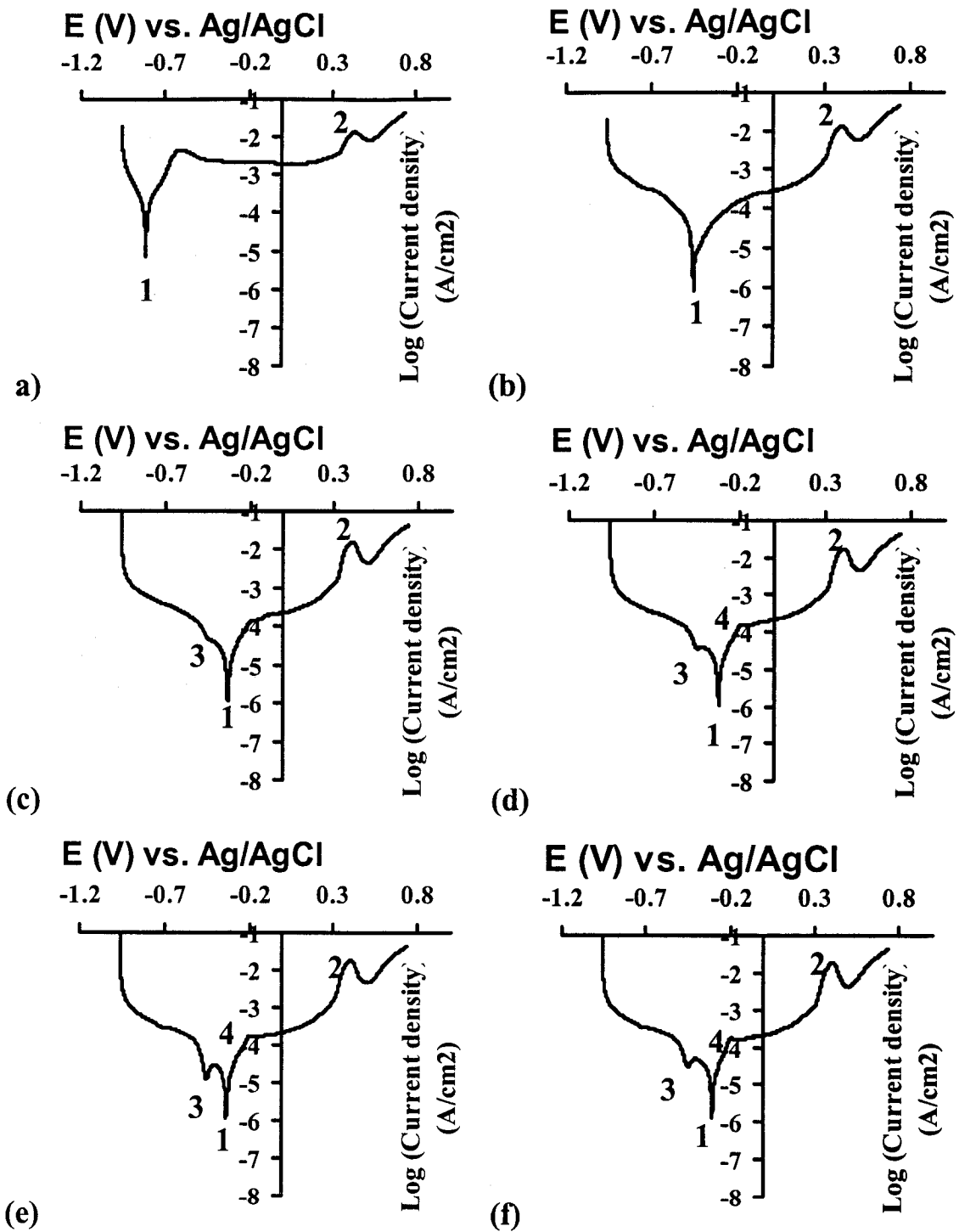


Figure 4.42 Polarization curves of EN-B coated sample 3 in 0.5 M NaOH solution for heat treatment durations of 96h. (a) first run, (b) second run, (c) third run, (d) 4<sup>th</sup> run, (e) 5<sup>th</sup> run, (f) 6<sup>th</sup> run.

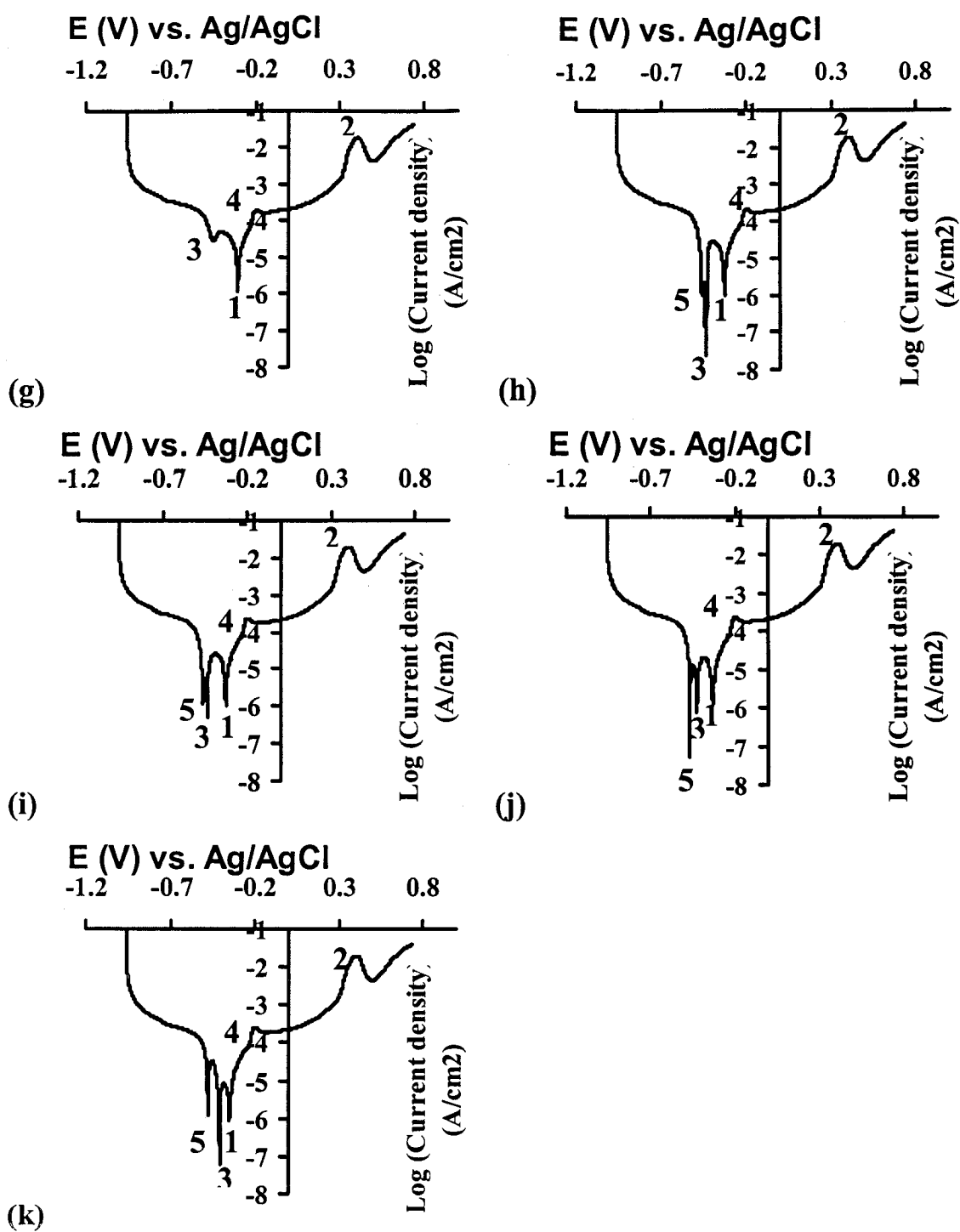


Figure 4.42 (Continued) Polarization curves of EN-B coated sample 3 in 0.5 M NaOH solution for heat treatment durations of 96 h. (g) 7<sup>th</sup> run, (h) 8<sup>th</sup> run, (i) 9<sup>th</sup> run, (j) 10<sup>th</sup> run, (k) 11<sup>th</sup> run.

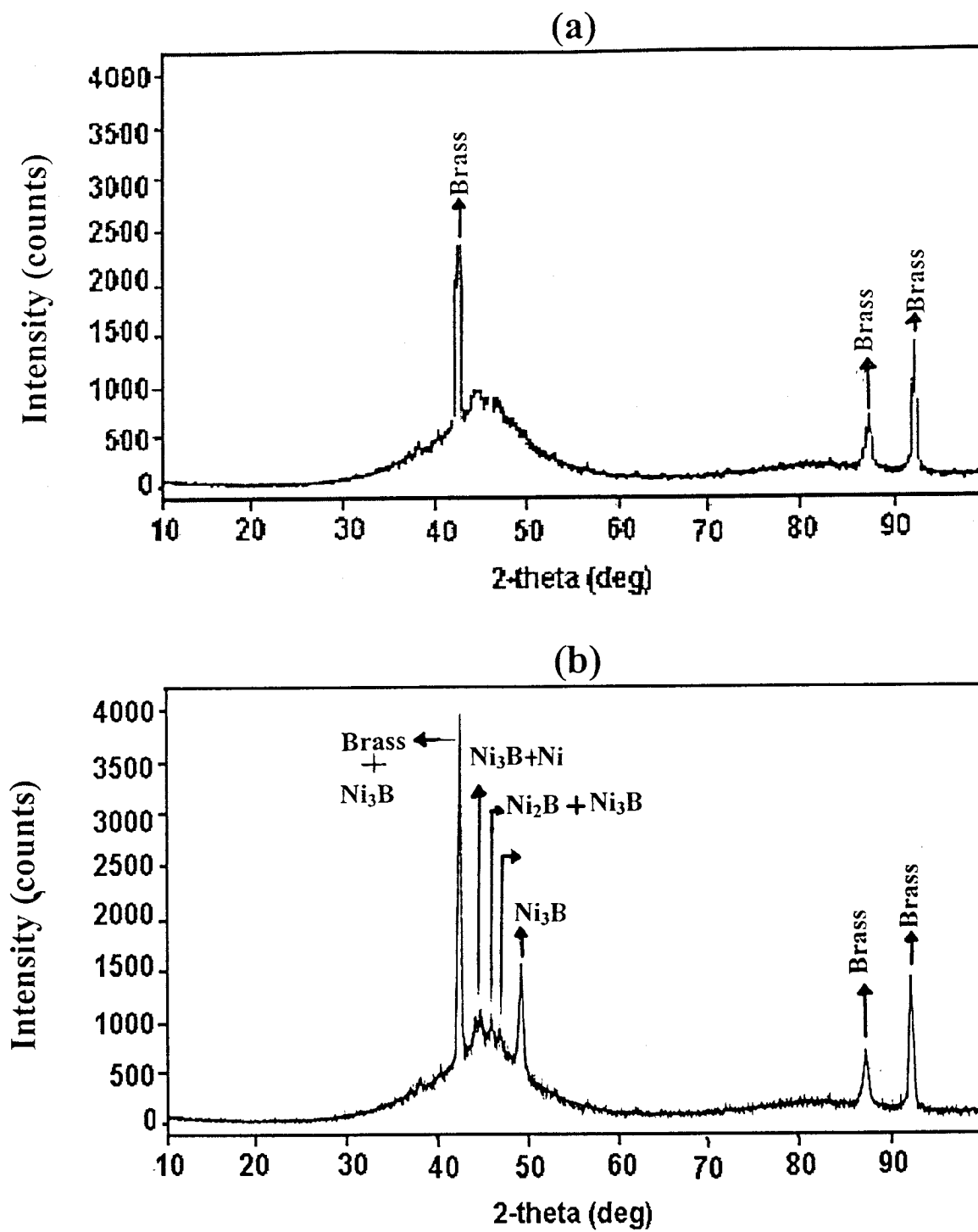


Figure 4.43 XRD spectra of various Ni-B coatings: (a) as-plated condition, (b) 5h heat treatment.

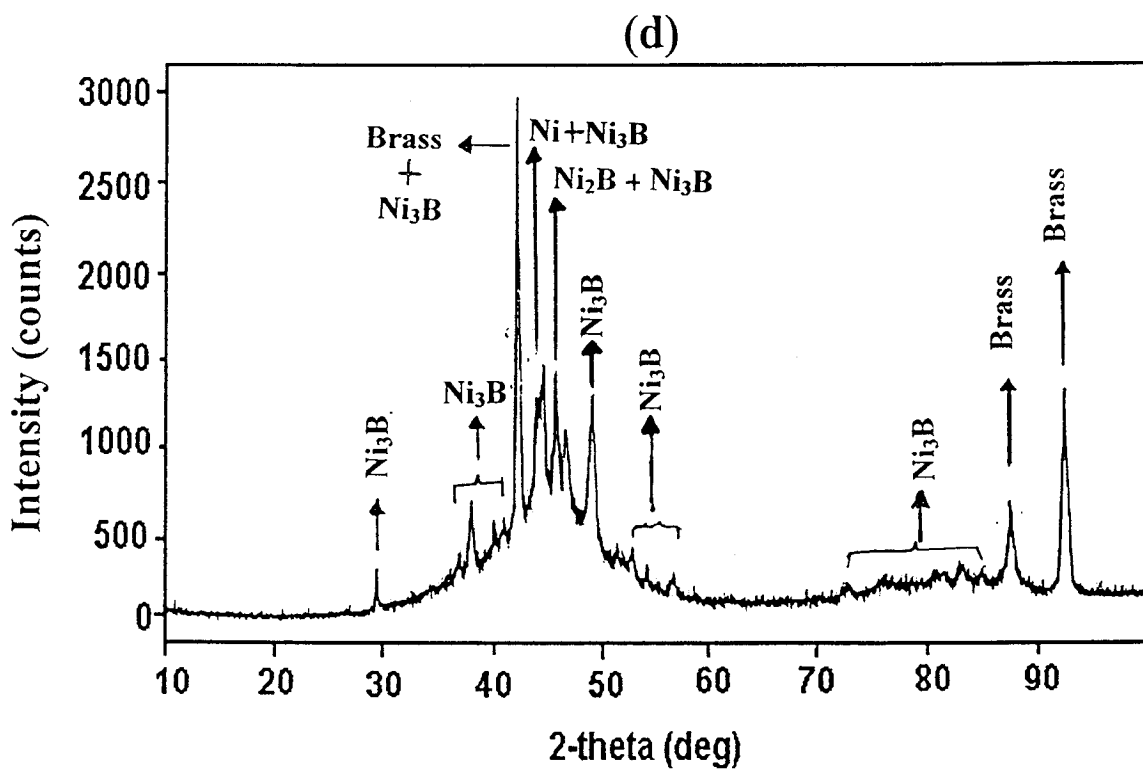
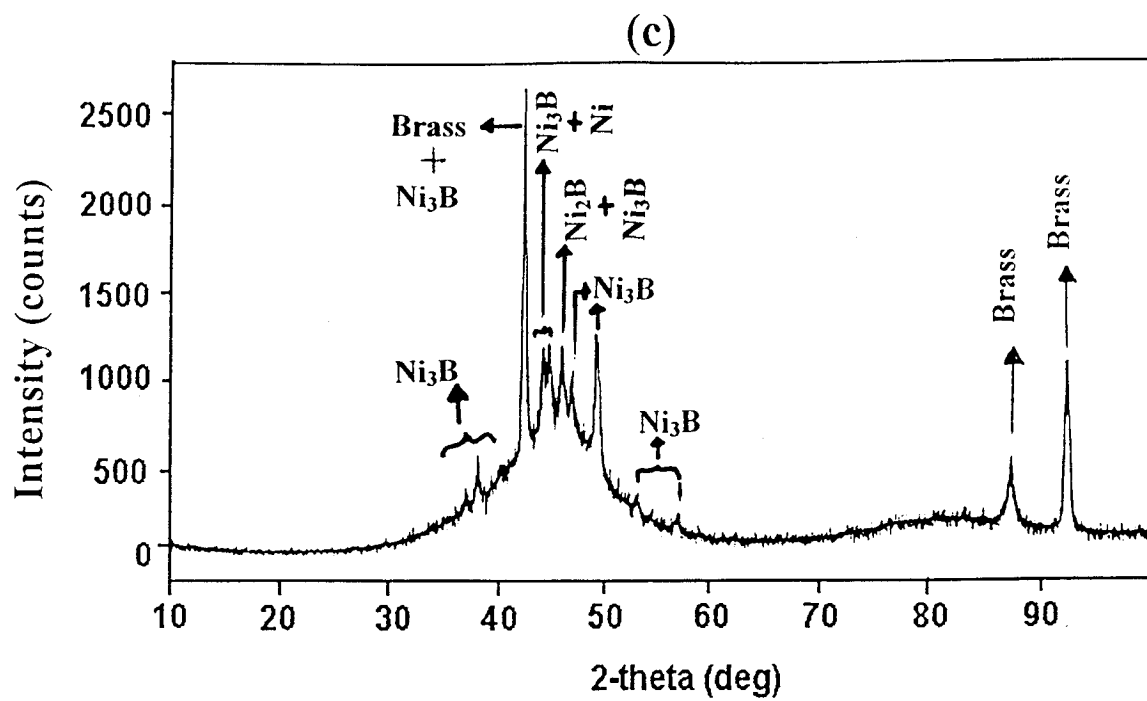
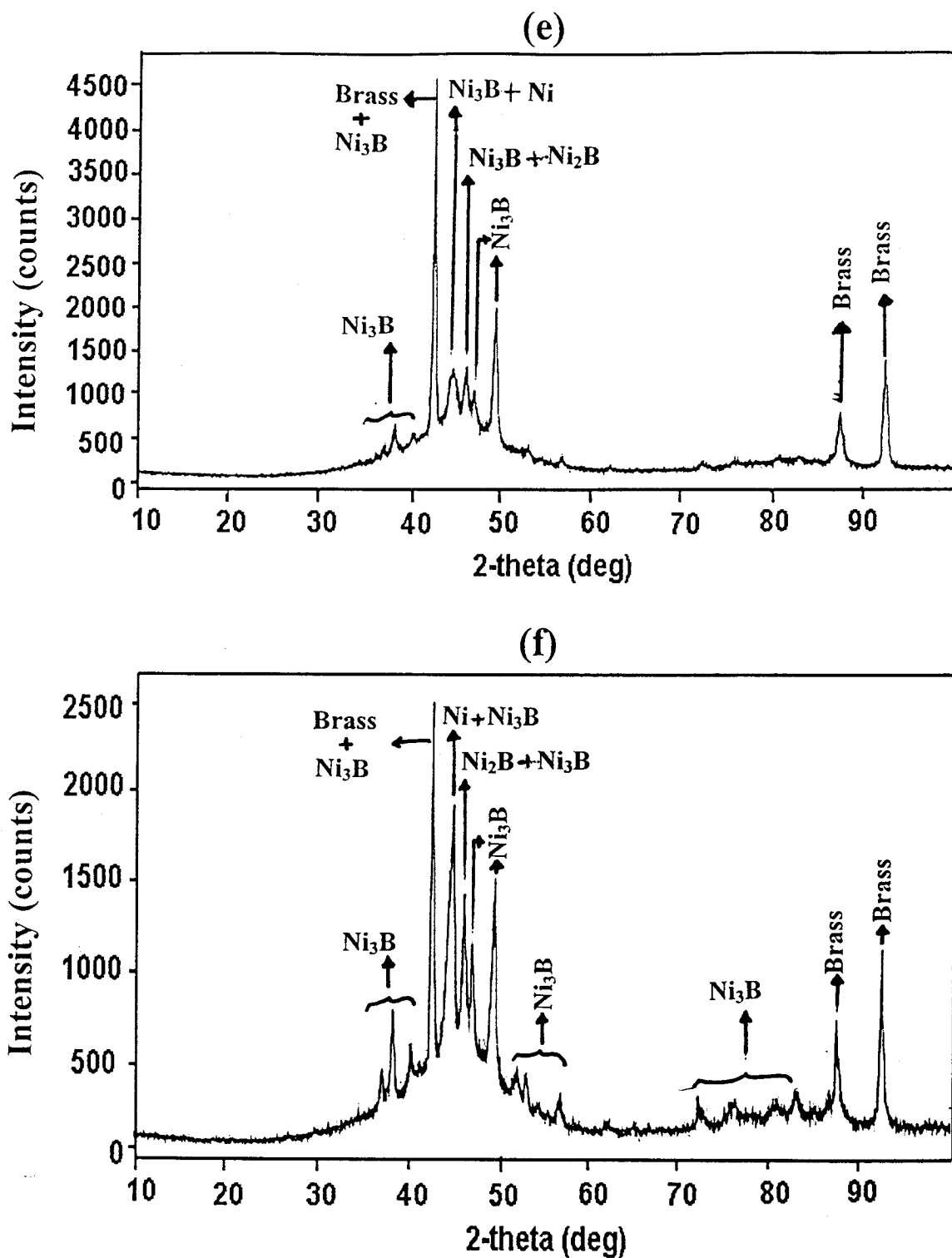


Figure 4.43 (continued) XRD spectra of various Ni-B coatings: (c) 24 h heat treatment, (d) 48 h heat treatment.



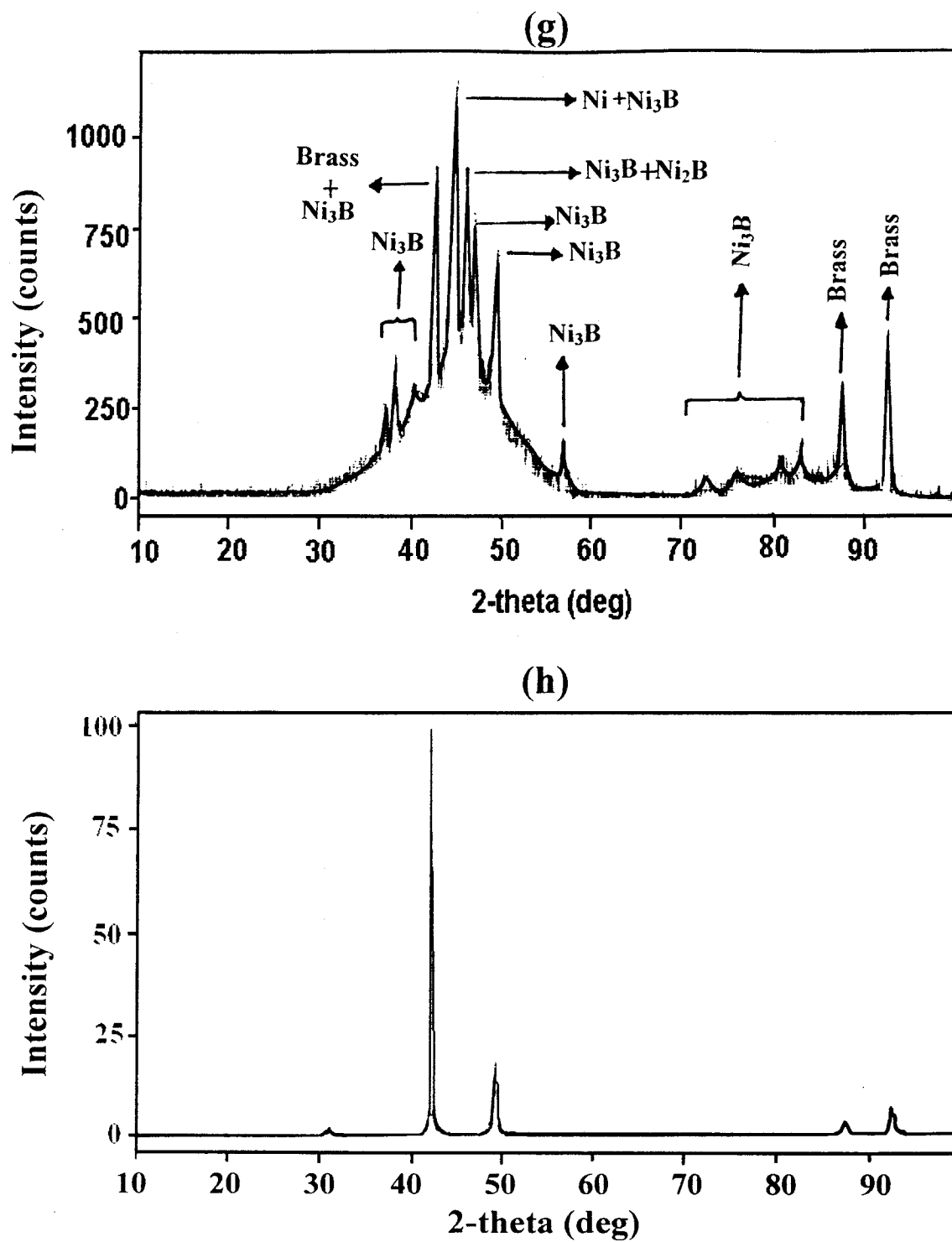
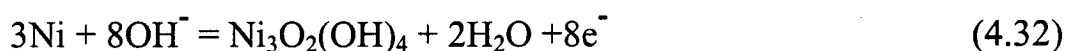


Figure 4.43 (continued) XRD spectra of various Ni-B coatings: (g) 120 h heat Treatment, (h) Brass (70:30) substrate.

There is a strong similarity between the reactions discussed in section for the EN-P coating (section 4.2) and the reactions occurring here during anodic and cathodic polarization. However, these reactions are related to phosphorus oxidation. There are no phosphorus species in the EN-B coating. Thus, thermodynamically, the possible oxidation reactions in the anodic region (-0.96 – 0 V), are reactions (4.30), (4.31), and (4.32):



As can be seen from Figures 4.39, 4.40, and 4.41, in the second run, the position of peak 1 changes towards a more positive potential. This peak may again be related to the oxidation of elemental nickel, which again becomes more difficult after the first run because of the formation of a surface oxide layer and may explain the shift of peak 1 towards more positive potentials. Therefore, peak 1 may be attributed to either of reactions (4.30), (4.31), (4.32) or a mixture of these reactions happening simultaneously.

In the cathodic region (0 – 0.74 V vs. Ag/AgCl), the reaction





is the most favorable from a thermodynamic viewpoint. Thus it appears that peak 2 in Figures 4.39, 4.40, and 4.41 is due to reaction (4.33). The reduced form is  $\text{Ni(OH)}_2$  and the oxidized form is generally believed to be  $\text{Ni(OH)}_3$ . Both these structures have been shown to exist in two modifications,  $\alpha$  and  $\beta$  for the reduced structure, and  $\gamma$  and  $\beta$ , for the oxidized structure. The two peaks  $\beta\text{-Ni(OH)}_2$  to  $\beta\text{-NiOOH}$  and  $\alpha\text{-Ni(OH)}_2$  to  $\gamma\text{-NiOOH}$  would be expected on the anodic sweep with two more peaks on the subsequent cathodic sweep.  $\gamma\text{-NiOOH}$  is less active than  $\beta\text{-NiOOH}$  and only discharges appreciably at a very low rate. Therefore the appearance of peak 3 and its splitting into two peaks may be related to  $\alpha\text{-Ni(OH)}_2/\gamma\text{-NiOOH}$  and  $\beta\text{-Ni(OH)}_2/\beta\text{-NiOOH}$  transitions.

In order to compare the corrosion behaviour of an EN-B coating with that of an EN-P coating, a potentiodynamic polarization curve was run repetitively. Results for the EN-P coated sample containing 8 w% P are shown in Figure 4.44.

Figures 4.44a, 4.44b, 4.44c, and 4.44d show first, second, third, and fourth run of EN-P coated sample (8 w% P) in 0.5M NaOH. It can be seen that in the first run, in the anodic polarization region, a sharp peak 1 appears at  $-0.642$  V and in the cathodic region a broad peak 2 appears at  $0.367$  V. In the second run (immediately following the first run), the position of peak 1 shifts towards more positive potential ( $-0.215$  V) and peak 2 grows slightly and shifts towards more negative potential ( $0.335$  V). In the third and fourth runs of sample 2, peaks 1 and 2 retain their positions, and peak 2 does not

grow further. Comparing Figure 4.44 with Figure 4.40 shows that the EN-P coated sample is more resistant to corrosion than the EN-B sample.

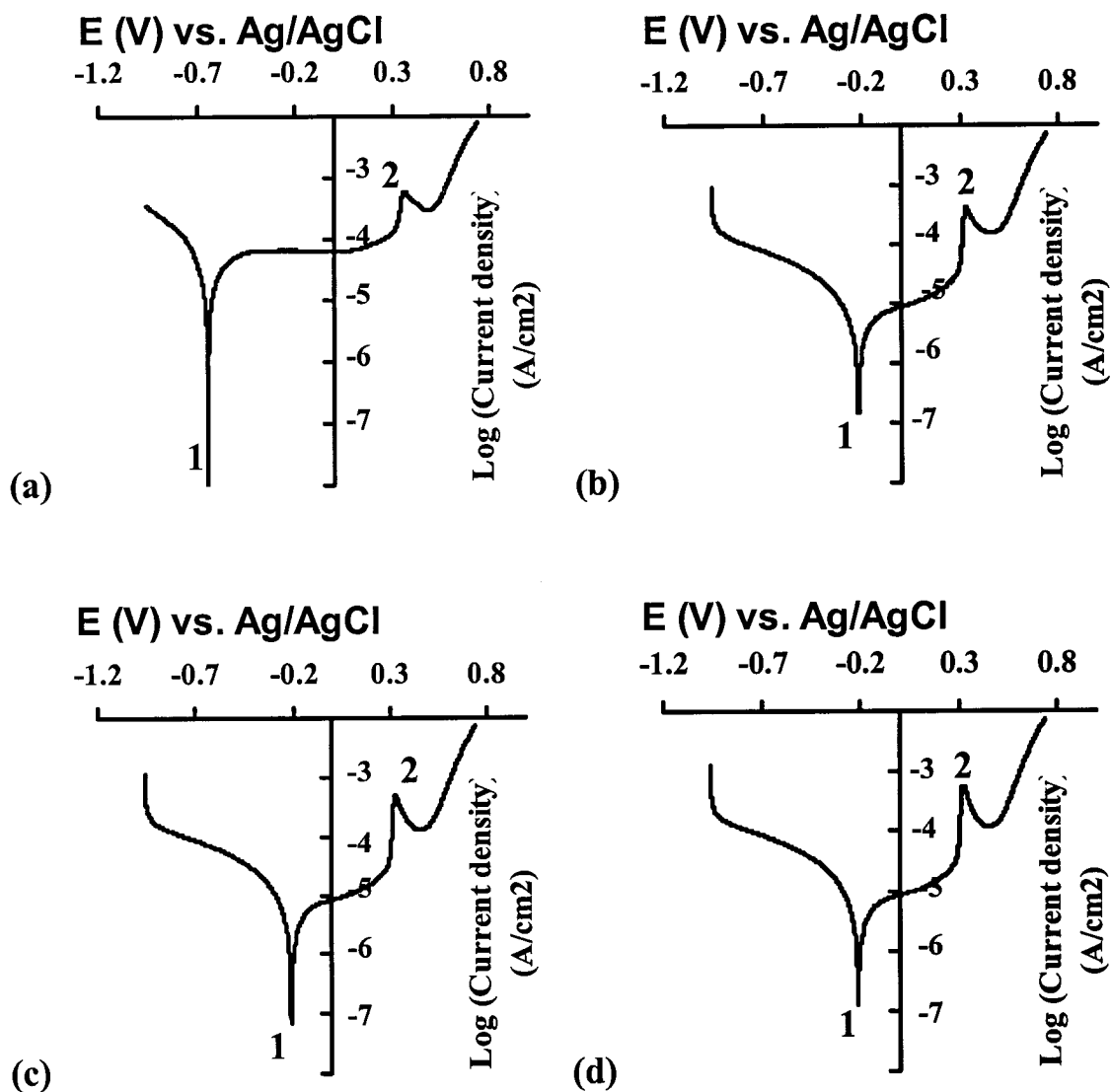


Figure 4.44 Polarization curves of EN-P coated sample (8 w% P) in 0.5 M NaOH at 5 mV/s scan rate; a) first run, b) second run, c) third run, d) fourth run.

### ***4.3.2 Potentiodynamic study of the electroless nickel-boron coated AA6061 samples***

In order to investigate the potential complication associated with the presence of an AA6061 substrate, experiments were conducted following the method described in section 4.3.1. A typical potentiodynamic polarization curve is shown in Figure 4.45.

From the comparison of Figure 4.45 to Figure 4.40, which was obtained using a brass substrate it is apparent that peak 2 is more pronounced and appears in all consecutive runs. A similar observation was noted with EN-B coated brass. Also peak 3, which in the case of the EN-B coated brass substrate appeared after the 9<sup>th</sup> run, appears in the 3<sup>rd</sup> run for AA6061. The final polarization curves for both the brass and the AA6061 substrates are almost identical. The difference between the two cases in the intermediate runs may be attributed to higher passivation of the AA6061 in the early stages.

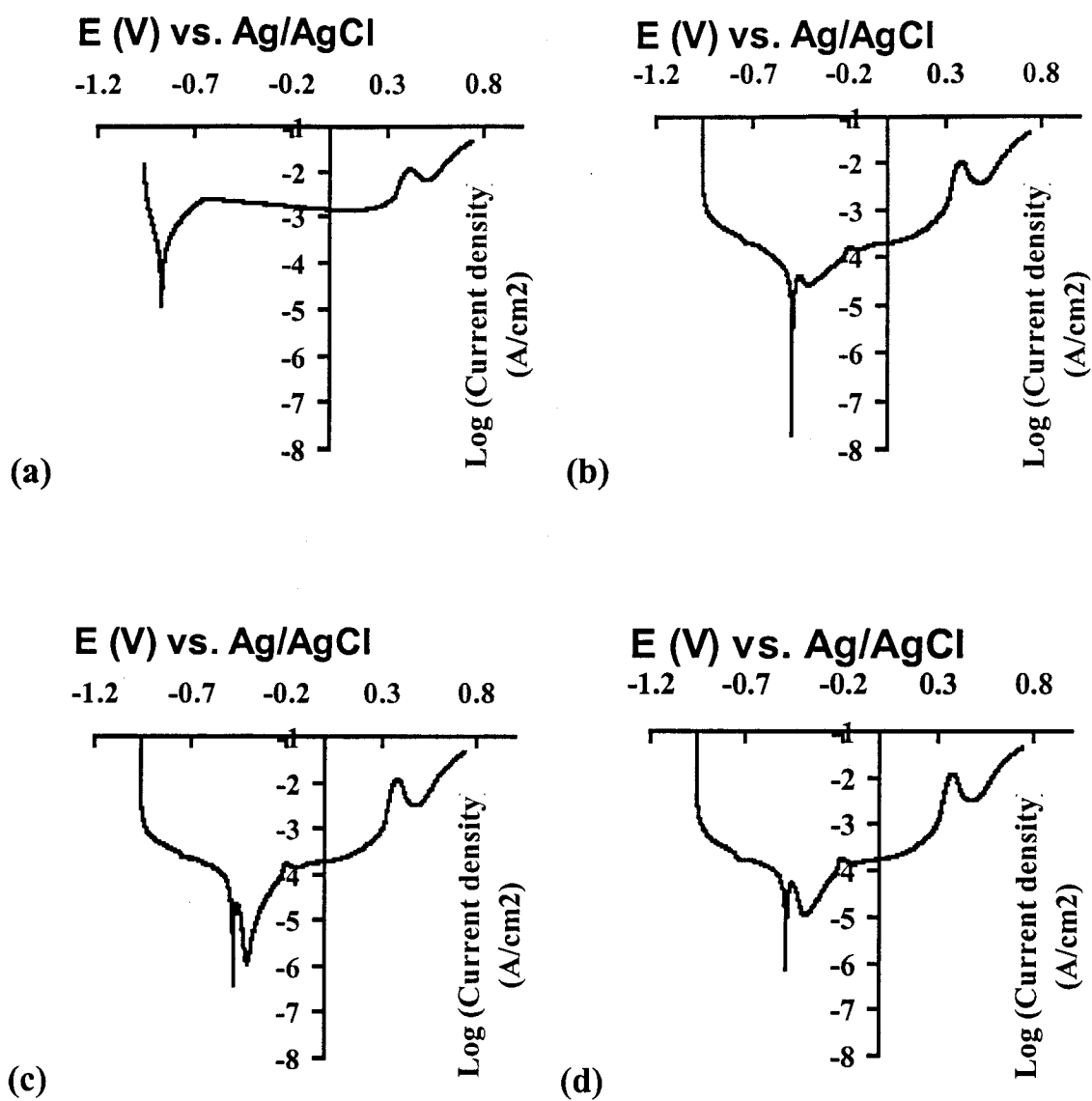


Figure 4.45 Polarization curves of EN-B coated AA6061 sample in 0.5 M NaOH solution for no heat treatment. (a) 1<sup>st</sup> run, (b) 2<sup>nd</sup> run, (c) 3<sup>rd</sup> run, (d) 4<sup>th</sup> run.

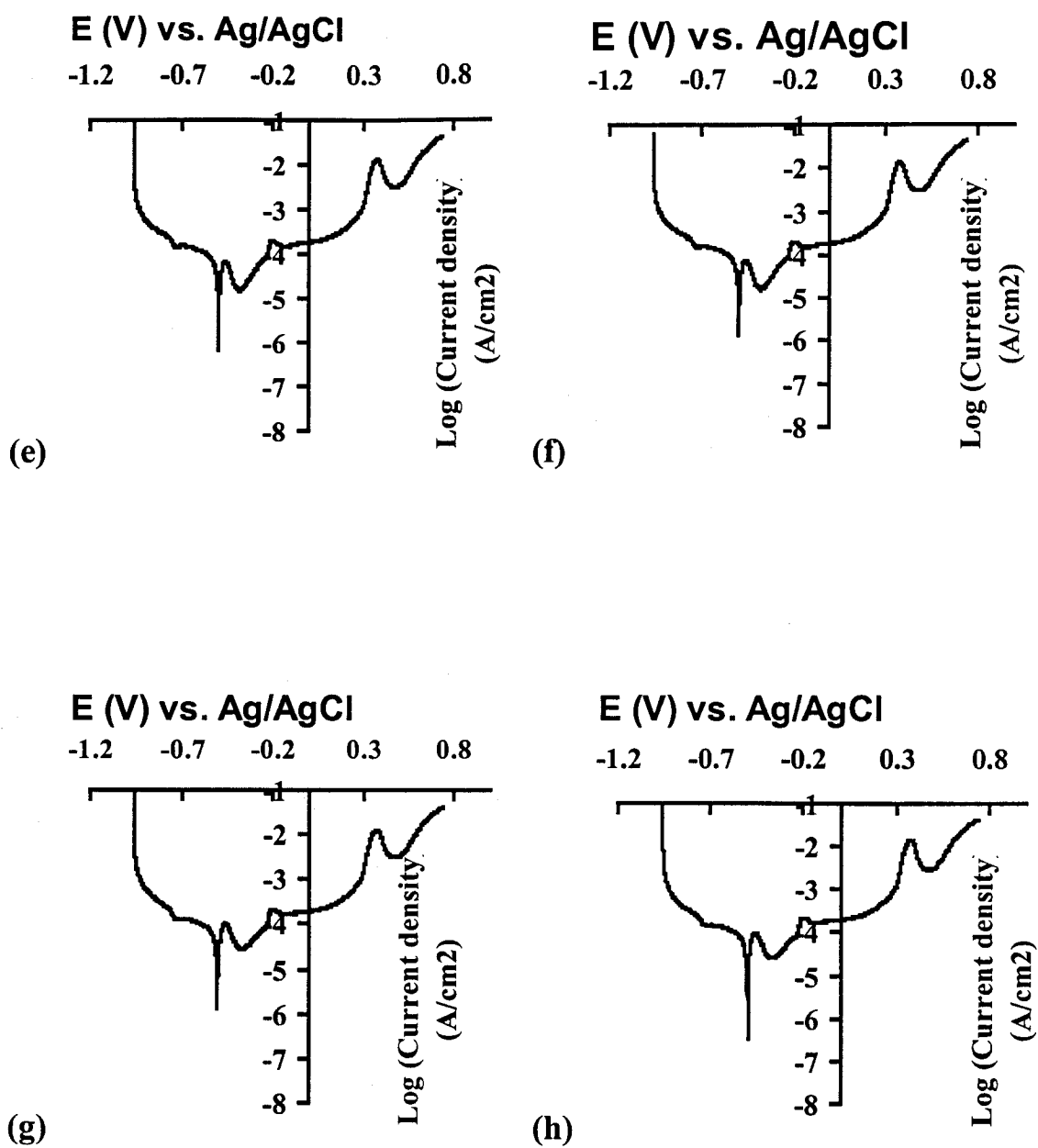


Figure 4.45 (Continued) Polarization curves of EN-B coated AA6061 sample in 0.5 M NaOH solution for no heat treatment. (e) 5<sup>th</sup> run, (f) 6<sup>th</sup> run, (g) 7<sup>th</sup> run, (h) 8<sup>th</sup> run.

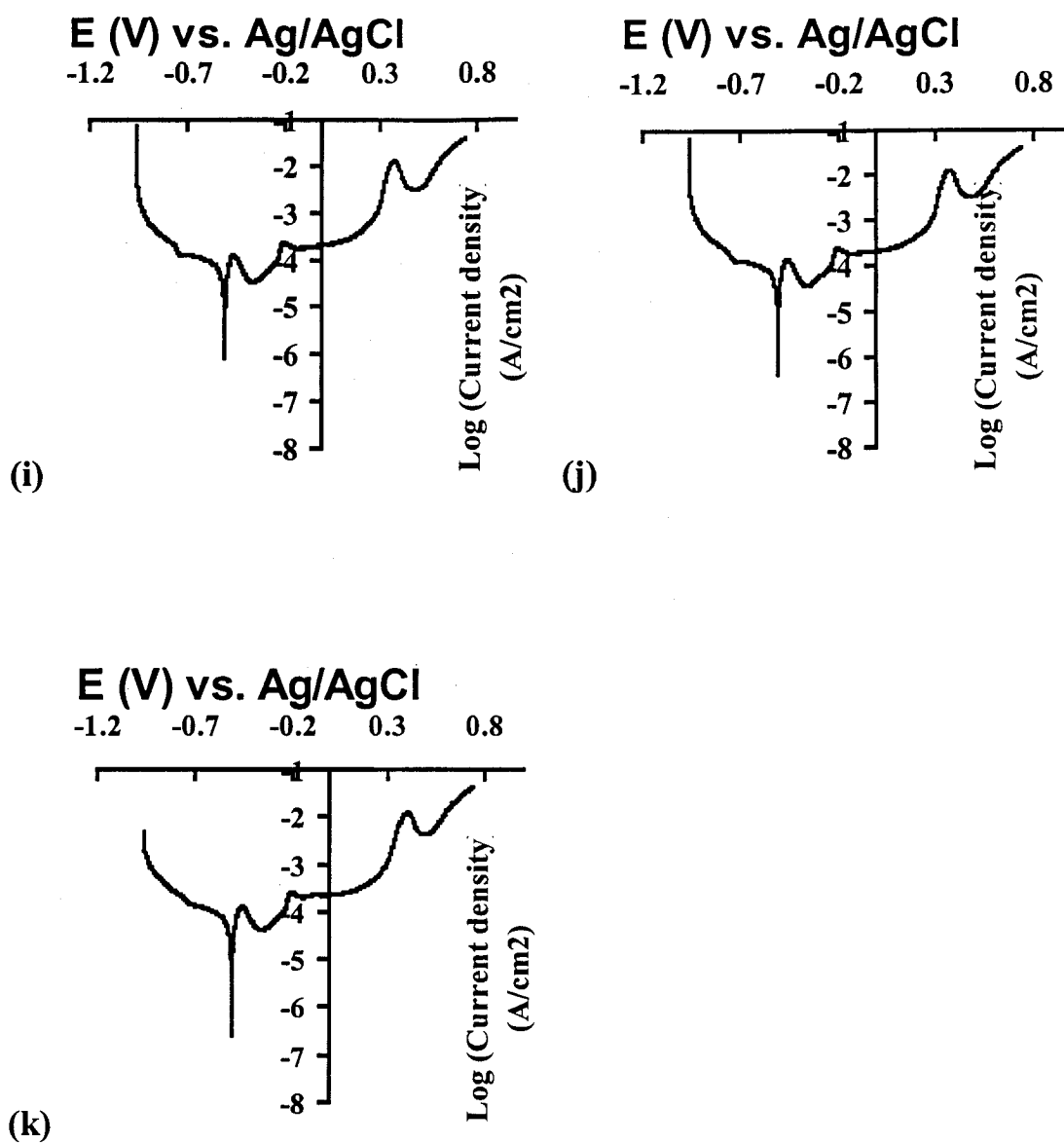


Figure 4.45 (Continued) Polarization curves of EN-B coated AA6061 sample in 0.5 M NaOH solution for no heat treatment. (i) 9<sup>th</sup> run, (j) 10<sup>th</sup> run, (k) 11<sup>th</sup> run.

## 5. CONCLUSIONS

A procedure to produce an electroless nickel coating on AA6061 was developed using a unique pretreatment process prior to deposition from a nickel boride bath. The pretreatment process consisted of preparation of the aluminum substrate, zincating conversion, intermediate electroless deposition of a thin layer of nickel-phosphorus, and heat treatment. The surface morphology of each coating was examined using scanning electron microscopy, and it was found that the surface morphology of the intermediate electroless nickel-phosphorus (EN-P) coating was dependent upon the thickness of the coating and the EN-P plating bath condition. Optimum conditions produced a continuous nodular coating which is expected to enhance the wear resistance of AA6061.

In the as-plated condition, a Vickers hardness value of  $111.76 \pm 2.43$  was obtained for uncoated AA6061, whereas for the EN-B coated AA6061 material (39  $\mu\text{m}$  thickness of coating containing 6.8 W% B), the Vickers hardness was measured to be  $384.96 \pm 8.75$ . It was found that the hardness was increased with an increase in heat-treatment duration.

A trend in dependency of corrosion resistance of EN coatings on P content in alkaline solutions was observed when the difference between the P content of the samples was very large. This behaviour can be explained by the two counteracting effects of activating and inhibiting of phosphorus on corrosion resistance. The activating effect is due to the lower protectiveness



of the passivating film because of lower thickness. As the P content increases, the activating effect decreases. The inhibiting effect can be explained by the formation of phosphates. Therefore, by increasing the P content the inhibiting effect increases.

The cyclic voltammetric behaviour of the EN samples prepared in baths of different pH, was also found to be different. The peak current for the sample with the lowest phosphorus content (2 w% P) was very low relative to other samples with higher amounts of phosphorus. As well, for the 2 w% P sample, the plot of peak potential difference versus scan rate showed a reversible behavior, whereas the plot for the samples with higher amounts of phosphorus showed an irreversible behaviour. This may be related to the very low peak current for the 2 w% P sample, and therefore, the peak separation for different scan rates may not be obvious. The implication of this finding is that for samples containing more than 2 w% P, once initiated, the degradation of the material would be difficult to arrest.

The potentiodynamic behaviour of electroless nickel-boron (EN-B) coated samples can be affected by heat treating the samples at 220 °C. As well the heat treatment duration affected this behaviour. XRD spectra of various EN-B coated samples (using different heat treatment times) showed that crystallinity increased with an increase in the time of heat treatment. Comparing the potentiodynamic polarization behaviour of EN-B coated samples with those from EN-P showed that the corrosion resistance of the EN-B coated samples was inferior to the EN-P products.

Finally, it is suggested that the process developed for the EN-P coatings will provide a valuable alternative to electroless nickel boron coating processes used at present in order to produce hard and wear resistant coating on aluminum alloys.

## 6. REFERENCES

- 1) Strafford K. N., Datta P. K. and Gray J. S., (1990) Surface engineering practice: processes, fundamentals and applications in corrosion and wear, Ellis Horwood, Chichester, U.K., pp. 5-120
- 2) Wernick S., Pinner R. and Sheasby P.B., (1987) The surface treatment and finishing of aluminum and its alloys, Finishing Publications Ltd. and ASM International, London, U.K., pp.1-102
- 3) King R. G., (1988) Surface treatment and finishing of aluminum, Elsevier Science, London, U.K, pp. 25-70
- 4) Boyer H. E., (1984) Practical heat treating, ASM publication, Ohio, USA.
- 5) Zinn S. and Semiatin S. L., (1988) Elements of induction heating: design, control, and applications, ASM publication, Ohio, USA.
- 6) Groenegrass H. W., (1964) Flame hardening, Springer-Verlag, New York, USA, pp.70-82.
- 7) Ready J. F. and Farson D. F., (2001) LIA handbook of laser materials processing, The Laser Institute of America, Orlando, Florida, USA, pp.1-100
- 8) Website by efunda (engineering fundamentals):  
[http://www.efunda.com/processes/heat\\_treat/hardening/selective.cfm](http://www.efunda.com/processes/heat_treat/hardening/selective.cfm),  
April 27, 2002.
- 9) Keller F., Hunter M. S., and Robinson D. L., (1953) Structural features of oxide coatings on alumina, Journal of Electrochemical Society, vol. 100, pp. 411-419.

- 10) Masuda H. and Hasegwa F., (1997) Self-ordering of cell arrangement of anodic porous alumina formed in sulfuric acid solution, Journal of Electrochemical Society, vol. 144, pp. L127-L130.
- 11) Dorsey, G. A. (1966) The characteristics of anodic aluminas I. Composition films from acidic anodizing electrolytes, Journal of Electrochemical Society, vol. 113, pp. 169-176.
- 12) Holmes A. J. T., (1979) Beam Transport, Gordon and Breach Science Publishing, New York, USA, pp.25-90
- 13) Rimini E., (1994) Ion implantation, Kluwer Academic Publishers, Boston, USA, pp. 37-42.
- 14) Website by AEA Technologies plc:  
<http://www.aeat.co.uk/net/courses/coating.htm>, March 31, 2001.
- 15) Selvan J. S., Soundararajan G. and Subramanian K., (2000) Laser alloying of aluminum with electrodeposited nickel: optimisation of plating thickness and processing parameters, Surface and Coatings Technology, vol. 124, pp. 117-127.
- 16) Vilar R., (1999) Laser alloying and laser cladding, Lasers in Material Science Materials Science Forum, vol. 301, pp. 229-251.
- 17) Fishman M. R. and Zahavi J., (1996) Laser alloying and cladding for improving the surface properties, Applied Surface Science, vol. 106, pp. 263-267.
- 18) Schuöcker D., Website, Handbook on Industrial Laser Safety  
[http://www.tuwien.ac.at/islt/safety/misc/ba\\_35.htm](http://www.tuwien.ac.at/islt/safety/misc/ba_35.htm), April 27, 2002.
- 19) Vilar R., (2001) Laser cladding, International Journal of Powder Metallurgy, vol. 37, pp. 31-32.

- 20) Sexton C. L., Byrne G., and Watkins K. G., (2001) Alloy development by laser cladding: An overview, *Journal of Laser Applications*, vol. 13, pp. 2-11.
- 21) Migliore L., (1996) *Laser materials processing*, Marcel Dekker Inc., New York, USA, pp.1-45
- 22) Grainger S. and Blunt J., (1999) *Engineering coating*, Woodhead Publishing Limited, Cambridge, U.K., pp.10-27.
- 23) Sampath S. and Berndt C. C., (1995) *Advances in thermal spray science and technology*, A. S. M. International, Ohio, USA, pp.28-42.
- 24) National Association of Colleges and Employers (NACE) Staff, (1994) *Thermal spray coating applications in the chemical Process industries*, NACE International, New York, USA, pp. 1-29.
- 25) Steffens H. D., Babiak Z. and Wewel M.,(1990) Recent developments in arc spraying, *IEEEET Plasma Science.*, vol. 18, pp. 974-979.
- 26) Cheng D., Trapaga G. and McKelliget J. W., (2001) Mathematical modeling of high velocity oxygen fuel thermal spraying: An overview, *Key Engineering Materials*, vol. 197, pp. 1-25.
- 27) Matejka D. and Benko B., (1990) *Plasma spraying of metallic and ceramic materials*, John Wiley & Sons, New York, USA.
- 28) Website, Judy J. and Motta P., MEMS Nickel Electroplating  
<http://www.ee.ucla.edu/research/judylab/procedures/nickelectroplate/>  
April 27, 2002
- 29) Dini J.W., (1992) Perspective on plating for precision finishing, *Plating and Surface Finishing*, vol. 79, pp. 121-128.

- 30) Dini J. W., (1993) Electrodeposition, the materials science of coatings and substrates, Noyes Publications, New Jersey, USA, 61-75.
- 31) Durney L. J., (1984) Electroplating engineering handbook, Van Nostrand Reinhold, New York, USA, pp.1-80.
- 32) Hitchman M. L. and Jensen K. F., (1993) Chemical vapour deposition, Academic Press, Incorporated, New York, USA, pp.1-45.
- 33) Mattox D. M., (1998) Handbook of physical vapour deposition processing, William Andrews/Noyes Publications, New Jersey, USA.
- 34) Ohring M., (1992) The materials science of thin films, Academic Press, Incorporated. New York, USA, pp. 24-40.
- 35) Maissel L. I. and Glang R., (1970) Handbook of thin film technology, McGraw Hill book company, New York, USA.
- 36) Holland L., (1956) Vacuum deposition of thin films, John Wiley & Sons, New York, USA, pp.56-69.
- 37) Ahmed N. A., (1987) Ion plating technology, Books on Demand, Norderstedt, Germany, pp. 1-70.
- 38) Riedel W., (1991) Electroless nickel plating, The American Electroplaters and Surface Society, Incorporated, Orlando, Florida, USA, pp. 1-90
- 39) Parker K., (1972) Recent advances in electroless nickel deposits, 8<sup>th</sup> interfinish conference, Basel, Swiss, pp. 28-100.

- 40) Mallory G. O. and Hajdu J. B., (1990) *Electroless plating*, William Andrew Publishing, New York, USA, pp.1-85..
- 41) Mallory G. O., (1979) *The electroless nickel plating bath, electroless nickel conference*, Products Finishing, Cincinnati, Ohio, USA, pp.1-90.
- 42) Gawrilov G. G., (1979) *Chemical (electroless) nickel plating*, Portcullis Press, Redhill, England, pp.1-65.
- 43) Gutzeit G., (1959) *An outline of the chemistry involved in the process of catalytic nickel deposition from aqueous solution*, *Plating and surface finishing*, vol. 46, pp. 1158-1164.
- 44) Stallman K. and Speckhardt H., (1981) *Deposition and properties of nickel-boron coatings*, *Metalloberflaeche Angewandte Elektrochemie*, vol. 35, pp. 979-988.
- 45) Lelental M., (1973) *Dimethylamine borane as the reducing agent in electroless plating systems*, *Journal of Electrochemical Society*, vol. 120, pp. 1650-1654.
- 46) Gorbunova K. M. and Nikiforova A. A., (1960) *Physiochemical principles of nickel plating*, Moscow: Izdatel'stvo Akademii Nauk SSSR, pp. 1-40.
- 47) kumar P. S. and Nair P. K., (1996) *Studies on crystallization of electroless Ni-P deposits*, *Journal of Material Processing Technology*, vol. 56, pp. 511- 520.
- 48) Chow S. L., Hedgecock N.E., Schiesinger M. and Rezek J., (1972) *Electron microscope study of the nucleation and growth of electroless cobalt and nickel*, *Journal of Electrochemical Society*, vol. 119, pp. 1614-1619.

- 49) Sugita K. and Ueno N., (1984) Composition and crystallinity of electroless nickel, *Journal of Electrochemical Society*, vol. 131, pp. 111-114.
- 50) Goldenstein A. W., Rostoker W., Schossberger F. and Gutzeit G., (1957) Structure of chemically deposited nickel, *Journal of Electrochemical Society*, vol. 104, pp. 104-110.
- 51) Park S. H. and Lee D. N., (1988) Microstructure of electroless nickel-phosphorus deposits, *Journal of Materials Science*, vol. 23, pp. 1634-1639.
- 52) Makhsoos E. V., Thomas E. L. and Toth L. E., (1978) heat treatment effects on crystallization behavior of electroless nickel-phosphorus deposits, *Metallurgical Transactions*, vol. 9A, pp. 1449-1453.
- 53) Hur K. H., Jeong J. H. and Lee D. N., (1990) Microstructures and crystallization of electroless Ni-P deposits, *Journal of Materials Science*, vol. 25, pp. 2573-2584.
- 54) Tyagi S. V. S., Barthwal S. K., Tandon V. K., and Ray S., (1989) Annealing behavior of electroless noncrystalline nickel phosphorus films, *Thin Solid Films*, vol. 169, pp. 229-233.
- 55) Duncan R. N., (1981) Properties and applications of electroless nickel deposits, *Finishers' Management*, vol. 26, pp. 5-9.
- 56) Parker K. and Shah H., (1971) Residual stresses in electroless nickel plating, *plating*, vol. 58, pp. 230-237.
- 57) Duncan R. N., (1982) Performance of electroless nickel coatings in oil field environments, *Corrosion/82 Conference*, National Association of Corrosion Engineers, Houston, Texas, USA, pp. 12-27.



- 58) Metzger W. H., (1959) Characteristics of deposits, Symposium on Electroless Nickel Plating, STP 265, American Society for Testing and Materials, Philadelphia, USA.
- 59) Parker K., (1981) Effects of heat treatment on the properties of electroless nickel deposits, *Plating and Surface Finishing*, vol. 68, pp. 71-76.
- 60) Jarrett G. D. R., (1966) Electroless nickel plating, *Industrial Finishing*, vol. 18, pp. 41-46.
- 61) Fitzgerald L. G., (1960) Chemical nickel plating, *Products Finishing* vol. 13, pp. 68-73.
- 62) Roberts W. H., (1964) Coating Beryllium with electroless nickel, U.S. Atomic Energy Commission, Report RFP478.
- 63) Staia M. H., Puchi E. S., Castro G., Ramirez F. O. and Lewis D. B., (1999) Effect of thermal history on the microhardness of electroless Ni-P, *Thin Solid Films*, vol. 356, pp. 472-479.
- 64) Baldwin C. and Such T. E., (1968) The plating rates and physical properties of electroless nickel/phosphorus alloy deposits. *Transactions of the Institute of Metal Finishing*, vol. 46, pp.73-79.
- 65) Spencer L. F., (1974) Electroless nickel plating-A Review, *Metal Finishing*, vol. 72, pp. 58-62.
- 66) Graham A. H., Lindsay R. W. and Read H. J., (1965) The structure and mechanical properties of electroless nickel, *Journal of Electrochemical Society*, vol. 112, pp. 401-413.
- 67) Nemoto K., (1990) The study on hardness of non-electrolytically plated

Ni-P deposits at high temperatures and effects given by heat treatments, *Journal of the Metal Finishing Society of Japan*, vol. 16, pp. 106-110.

- 68) Domnikov L., (1962) Chromium and electroless nickel deposits, hardness at high temperatures, *Metal Finishing*, vol. 60, pp. 67-74.
- 69) Parker K., (1974) Hardness and wear resistance tests of electroless nickel deposits, *Plating*, vol. 61, pp. 834-841.
- 70) Randin J. P. and Hintermann H. E., (1967) Electroless nickel deposited at controlled pH; Mechanical properties as a function of phosphorus content, *Plating*, vol. 54, pp. 523-528.
- 71) Bandrand D. W., (1981) Use of electroless nickel to reduce gold requirements, *Plating and Surface Finishing*, vol. 68, pp. 57-60.
- 72) Duncan R. N., (1982) Corrosion control with electroless nickel coatings, *Electroless Plating Symposium*, American Electroplaters' Society, St. Louis, USA.
- 73) Klein H. G., (1971) Study of chemically deposited nickel-boron coatings on metals (Untersuchungen an chemisch abgeschiedenen nickel-bor-schichten auf metallen), *Metalloberflaeche Angewandte Elektrochemie*, vol. 25, pp. 305-317.
- 74) Totlani M. K. and Athavale S. N., (2000) Electroless nickel for corrosion control in chemical, oil and gas industries, *Corrosion reviews*, vol. 18, pp. 155-179.
- 75) Bielinski J., Krolikowski A., Kedzierska I. and Stokarski W., (1995) Compositional and structural factors in corrosion characteristics of Ni-P deposits, *Models in Chemistry*, vol. 32, pp. 685-695.
- 76) Mallory G. O., (1974) Influence of the electroless plating bath on the

corrosion resistance of the deposits, *Plating and Surface Finishing*, vol. 61, pp. 1005-1014.

- 77) Rajam K. S., Rajagopal I., and Rajagopalan S. R., (1990) Phosphorus-content and heat-treatment effects on the corrosion resistance electroless nickel, *Plating and Surface Finishing*, vol. 77, pp. 63-66.
- 78) Kerr C., Barker D. and Walsh F., (1997) Porosity and corrosion rate measurements for electroless nickel deposits on steel using electrochemical techniques, *Transactions of the Institute of Metal Finishing*, vol. 75, pp. 81-87.
- 79) Delaunois F., Petitjean J. P., Lienard P., and Jacob-Duliere M., (2000) Autocatalytic electroless nickel-boron plating on light alloys, *Surface and Coatings Technology*, vol. 124, pp. 201-209.
- 80) Zhang H., Zhang X. J., and Zhang Y. K., (1993) Structure and properties of electroless nickel-boron alloys, *Plating and Surface Finishing*, vol. 80, pp. 80-84.
- 81) Talaat EI-Mallah A., Abbas M. H., Shafei M. F., El-Sayed Aboul-Hassan M. and Nagi I., (1989) Structure of electroless nickel deposits from bath containing sodium hypophosphite and potassium borohydride, *Plating and Surface Finishing*, vol. 76, pp. 124-128.
- 82) Lelental M., (1973) Dimethylamine borane as the reducing agent in electroless plating systems, *Journal of Electrochemical Society*, vol. 120, pp. 1650-1654.
- 83) Duncan R. N. and Arney T., (1984) Operation and use of sodium-borohydride-reduced electroless nickel, *Plating and Surface Finishing*, vol. 71, pp. 49-54.
- 84) ASTM Standard D2714, (1978) Calibration and Operation of the Alpha

Model LFW-1 Friction and Wear Testing Machine, Part 24, American Society for Testing and Materials, West Conshohocken, PA.

- 85) Test Method G59-97 Standard Test Method for Conducting Potentiodynamic Polarization Resistance Measurements, American Society for Testing and Materials, West Conshohocken, PA.
- 86) Test Method G5-94 (1994) Standard Reference Test Method for Making Potentiostatic and Potentiodynamic Anodic Polarization Measurements, American Society for testing and Materials, West Conshohocken, PA, USA.
- 87) Practice G3-89(2001) Standard Practice for Conventions Applicable to Electrochemical Measurements in Corrosion Testing, American Society for testing and Materials, West Conshohocken, PA, USA.
- 88) Hack H. P., (1995) Atlas of polarization diagrams for naval materials in sea water, Carderock Division, Naval Surface Warfare Centre, Bethesda, CARDIVNSWC-TR-61-94/44 April 1995; Survivability, Technical Report.
- 89) Gosser D., (1993) Cyclic voltammetry, John Wiley & Sons, New York, USA.
- 90) Test Method G5-94(2001) Standard Reference Test Method for Making Potentiostatic and Potentiodynamic Anodic Polarization Measurements, American Society for testing and Materials, West Conshohocken, PA, USA.
- 91) Test Method G59-97 (2001) Standard Test Method for Conducting Potentiodynamic Polarization Resistance Measurements,

American Society for testing and Materials, West Conshohocken, PA, USA.

- 92) Kinsella T. Y. J. and Bailey B., (1996) Use of electrochemical techniques for monitoring the formation and corrosion protective ability of corrosion product scales and inhibitor films, 13th International Corrosion Congress, 25-29 November 1996, Melbourne, Australia.
- 93) Wang J., (2000) Analytical electrochemistry, 2th edition reviewed by Langhus D. L., John Wiley & Sons, New York, USA.
- 94) A review of techniques for electrochemical analysis, (1996) EG&G Princeton Applied Research, Electrochemical instruments group, Application Note: E-4.
- 95) Burke L. D., and Twomey T. A. M., (1984) Voltammetric behavior of nickel in base with particular reference to thick oxide growth, Journal of Electrochemical Society, vol. 162, pp. 101-119.
- 96) Milner P. C. and Thomas U. S., (1967) Advances in electrochemistry and electrochemical engineering, Vol. 5, pp. 1-207, Wiley, New York, USA.
- 97) Briggs G. W. D., (1974) Specialist Periodical Reports, Electrochemistry, vol. 4, pp. 1-330, The Chemical Society, London, U.K.
- 98) Arvia A. J. and Posadas D., (1975) Encyclopaedia of electrochemistry of the elements, Vol. 3, Marcel Dekker, New York, pp. 349-350.
- 99) Burke L. D. and Twomey T. A. M., (1982) Influence of pH on the redox behavior of hydrous nickel oxide, Journal of Electroanalytical Chemistry, vol. 134, pp. 353-362.
- 100) Bode H., Dehmelt K. and Witte J., (1966) Zur kenntnis der

nickelhydroxidelektrode – I. Über das nickel (II) – hydroxidhydrat, *Electrochimica Acta*, vol. 11, pp. 1079-1087.

- 101) Burke L. D. and Twomey T. A. M., (1984) Influence of the acid/base character of the surface on the electrocatalytic behavior of both nickel and nickel oxide anodes, with particular reference to oxygen gas evolution, *Journal of Electroanalytical Chemistry*, vol. 67, pp. 285-290.
- 102) Burke L. D. and Whelan D. P., (1980) Growth of an electrochromic film on nickel in base under potential cycling conditions, *Journal of Electroanalytical Chemistry*, vol. 109, pp. 385-388.
- 103) Smith R. J., Hummel R. E. and Ambrose J. R., (1987) The passivation of nickel in aqueous solutions-II. An in situ investigation of the passivation of nickel using optical and electrochemical techniques, *Corrosion Science*, vol. 27, pp. 815-826.
- 104) Visscher W. and Barendrecht E., (1983) Anodic oxide films of nickel in alkaline electrolyte, *Surface Science*, vol. 135, pp. 436-452.
- 105) Shumilova N. A. and Bagotzky V. S., (1968) Oxygen ionization on nickel in alkaline solutions, *Electrochimica Acta*, vol. 13, pp. 285-293.
- 106) Barnard R., Crickmore C. T., Lee J. A. and Tye F. L., (1980) The cause of residual capacity in nickel oxyhydroxide electrodes, *Journal of Applied Electrochemistry*, vol. 10, pp. 61-70.
- 107) Pourbaix M., (1966) *Atlas of electrochemical equilibria in aqueous solutions*, Pergamon Press, London, pp. 330-342.
- 108) Sokol'skii D. V., Zabotin P. I. and Druz S. V., (1979) Abscheidung und eigenschaften von niodur-uberzugen, *Elektrokhimiya*, vol. 15, pp. 881-883.
- 109) Guzman R. S., Vilche J. R. and Arvia A. J., (1978) The potentiodynamic behaviour of nickel in potassium hydroxide

- solutions, *Journal of Applied Electrochemistry*, Vol. 8, pp. 67-70.
- 110) Burke L. D. and Roche C. M. B., (1983) The possible importance of hydrolysis effects in the early stages of metal surface electrooxidation reactions – with particular reference to platinum, *Journal of Electroanalytical Chemistry*, vol. 159, pp. 89-99.
  - 111) Gassa L. M. H, Vilche J. R. and Arvia A. J., (1983) A potentiodynamic study of anodic film formation on nickel in borate solutions, *Journal of Applied Electrochemistry*, vol. 13, pp. 135-145.
  - 112) Conway B. E. and Angerstein-Kozłowska H., (1981) Electrochemical study of multiple state adsorption in monolayers, *Accounts of Chemical Research*, vol. 14, pp. 49-56.
  - 113) Meier J. G., Vilche J. R. and Arvia A. J., (1980) The influence of temperature on the current peak multiplicity related to the nickel hydroxide electrode, *Journal of Applied Electrochemistry*, vol. 10, pp. 611-621.
  - 114) Guzman R. S. S., Vilche J. R. and Arvia A. J., (1979) Non-equilibrium effects in the nickel hydroxide electrode, *Journal of Applied Electrochemistry*, vol. 9, pp. 183-189.
  - 115) Briggs G. W. D. and Snodin P. R., (1982) Ageing and the diffusion process at the nickel hydroxide electrode, *Electrochimica Acta*, vol. 27, pp. 565-572.
  - 116) Burke L. D. and Twomy T. A. M., (1982) Proceedings of the symposium on the nickel electrode. The Electrochemical Society, Pennington, pp. 75-96.
  - 117) Tjong S. C. and Yeager E., (1981) ESCA and SIMS studies of the passive film on iron, *Journal of Electrochemical Society*, vol. 128, pp. 2251-2254.

- 118) Murphy O. J., Bockris J. O. M., Pou T. E., Cocke D. L. and Sparrow G., (1982) SIMS evidence concerning water in passive layers, *Journal of Electrochemical Society*, vol. 129, pp. 2149-2151.
- 119) Brenner A. and Riddel G., (1946) Nickel plating on steel by chemical reduction, *Journal of Research*, vol. 37, pp. 31-34.
- 120) Hersch P., (1955) Study of the mechanism of the electroless deposition of nickel, *Transactions of Institute of Metal Finishing*, 33, pp. 417420.
- 121) Lukes R. M., (1964) Mechanism for autocatalytic reduction of nickel by hypophosphite ion, *Plating*, vol. 51, pp. 969-971.
- 122) Abrantes L. M. and Correia J. P., (1994) On the mechanism of electroless Ni-P plating, *Journal of Electrochemical Society*, Vol. 141, pp. 2356-2360.
- 123) Smith S. F., (1979) Mechanics of electroless nickel deposition, *Metal Finishing*, vol. 77, pp. 60-62.
- 124) Lowenheim F. A., (1978) *Electroplating*, McGraw-Hill, Inc., New York, USA.
- 125) Harris S. J., Gould A. J. and Boden P. J., (1986) Influence of cathodic polarization on the plating rate and properties of electroless Ni-P coatings, *Transactions of Institute of Metal Finishing*, vol. 64, pp. 24-29.
- 126) Malecki A. and Micek-Ilnicka A., (2000) Electroless nickel plating, *Surface and Coatings Technology*, vol. 123, pp. 72-77.
- 127) Duncan R. N. and Arney T. L., (1984) Operation and use of sodium-borohydride-reduced electroless nickel, *Plating and Surface Finishing*, vol. 71, pp. 49-54.



- 128) Gawrilov G. G., (1979) Chemical (electroless) nickel plating, Portcullis Press, Redhill, England.
- 129) Van Den Meerakker J. E. A. M., (1981) On the mechanism of electroless plating-II. One mechanism of different reductants, Journal of Applied Electrochemistry, vol. 11, pp. 395-400.
- 130) Mallory G. O., (1971) The electroless nickel-boron plating bath; effects of variables on deposit properties, Plating, vol. 58, pp. 319-327.
- 131) Yarkosky E. F., Affeldt D. C., Cacciatore P. A. and Nargi C. P., Strategies for electroless nickel plating aluminum, Enthone Incorporated, West Haven, CT 06516, pp. 1-16.
- 132) Website: <http://www.chem.vt.edu/chem-ed/spec/atomic/aa.html>  
Brian M. Tissue, January 2002.
- 133) Ebdon L., (1998) Analytical atomic absorption spectroscopy, John Wiley & Sons, Inc., New York, USA.
- 134) Zelle W. G., (1953) Formation of immersion zinc coatings on aluminum, Journal of Electrochemistry Society, vol. 100, pp. 328-332.
- 135) Mallory G. O. and Lloyd V. A., (1985) Kinetics of electroless nickel deposition with sodium hypophosphite – An empirical rate law, Plating and Surface Finishing, vol. 72, pp. 52-57.
- 136) Latimer W. M., (1952) Oxidation potentials (2 Edn.) pp.198-200, Prentice Hall, Englewood Cliffs, New York, USA.
- 137) Hummel R. E., Smith R. J. and Vernik E. D., (1987) The passivation of nickel in aqueous solutions – I. The identification of insoluble corrosion products on nickel electrodes using optical and ESCA techniques, Corrosion Science, vol. 27, pp. 803-813.

- 138) El Wakkard, S. E. and Emara, E. S., (1953) Anodic oxidation of nickel in basic solution, *Journal of the Chemical Society*, vol.4, pp. 3504-3509.
- 139) Briggs G. W. D., Jones E. and Wynne W. F. K., (1955) The nickel oxide electrode, *Transactions of Faraday Society*, vol. 51, pp. 1433-1442.
- 140) Barnard R., Randell C. F. and Tye F. L., (1980) Studies concerning charged nickel hydroxide electrodes, I. Measurement of reversible potentials, *Journal of Applied Electrochemistry*, vol. 10, pp. 109-125.
- 141) Tuomi D., (1965) The forming process in nickel positive electrodes, *Journal of Electrochemical Society*, vol. 112, pp. 1-10.

## APPENDIX A: Electroless plating EN-P and EN-B

The sample is of cylindrical disk shape.

C: Concentration (M) of electroless plating bath

$W_1$ : Weight of the sample before electroless nickel coating (g)

$W_2$ : Weight of the sample after electroless nickel coating (g)

D: Diameter of the sample (cm)

H: The thickness of the sample (cm)

A: total area of the sample ( $\text{cm}^2$ )

$\Delta X$  : thickness of the coating ( $\mu\text{m}$ )= $\Delta W/A$

v: deposition rate ( $\mu\text{m/h}$ ) =  $\Delta X/t$

$\Delta W$ : Weight gain =  $W_2 - W_1$

t: plating duration = 2h

T: Temperature (k)

D: Diameter of the sample (cm) =  $2r$

r: radius of the sample

A: Total area of the sample =  $2 \times 3.14 \times R \times (D + r)$

$\Delta X = \Delta m/A.d$

d: density of the deposit ( $\text{g/cm}^3$ )

$\Delta m = m_2 - m_1$  (g)

$m_2$  = The weight of sample before electroless coating (g)

$m_1$  = The weight of sample after electroless coating (g)

Table A.1 Data for the plot of time versus thickness of coating.

Time (min)	$W_1$ (g)	$W_2$ (g)	$\Delta W$ (g)	D (cm)	H (cm)	A (cm <sup>3</sup> )	$\Delta X$ ( $\mu\text{m}$ )
0	1.8025	1.8025	0.0000	1.30	0.46	4.53	0.00
20	1.9231	1.9347	0.0116	1.30	0.46	4.53	3.31
40	1.8765	1.8966	0.0201	1.30	0.36	4.12	6.29
60	1.8965	1.9287	0.0322	1.30	0.29	3.84	10.81
80	1.9322	1.9890	0.0568	1.28	0.72	5.47	13.41
100	1.7654	1.8273	0.0619	1.29	0.59	5.00	15.96
120	1.8001	1.8597	0.0596	1.30	0.38	4.20	18.30
140	1.9876	2.0537	0.0661	1.29	0.37	4.11	20.75
180	1.6999	1.8057	0.1058	1.28	0.47	4.46	30.61

Table A.2 Data for the plot of nickel sulfate concentration versus deposition rate of EN-P coating.

Concentration (M)	$W_1$ (g)	$W_2$ (g)	$\Delta W$ (g)	D (cm)	H (cm)	A ( $\text{cm}^3$ )	$\Delta X$ ( $\mu\text{m}$ )	v ( $\mu\text{m}/\text{h}$ )
0.0107	1.8234	1.8296	0.0062	1.29	0.34	3.99	2.00	1.00
0.0428	1.5793	1.6331	0.0538	1.29	0.76	5.69	12.20	6.10
0.1070	1.9035	1.9849	0.0814	1.29	0.56	4.88	21.49	10.75
0.1498	2.0912	2.1725	0.0813	1.29	0.46	4.48	23.45	11.72
0.2140	1.8675	1.9649	0.0974	1.29	0.62	5.12	24.52	12.26
0.2568	1.7903	1.8857	0.0954	1.29	0.58	4.96	24.80	12.40

**Table A.3 Data for the plot of sodium hypophosphite concentration versus deposition rate of EN-P coating.**

Concentration (M)	$W_1$ (g)	$W_2$ (g)	$\Delta W$ (g)	D (cm)	H (cm)	A ( $\text{cm}^3$ )	$\Delta X$ ( $\mu\text{m}$ )	v ( $\mu\text{m/h}$ )
0.0000	1.7356	1.7356	0.0000	1.29	0.67	5.33	0.00	0.00
0.0107	1.8976	1.9016	0.0040	1.29	0.51	4.68	1.11	0.55
0.0267	1.5675	1.5862	0.0187	1.30	0.38	4.20	5.73	2.86
0.0533	1.9432	1.9893	0.0461	1.27	0.72	5.40	11.00	5.50
0.1067	1.7777	1.8322	0.0545	1.28	0.24	3.54	19.88	9.94
0.2670	2.0012	2.1235	0.1223	1.30	0.68	5.43	29.07	14.54
0.3730	1.8712	2.0141	0.1429	1.29	0.88	6.18	29.84	14.92
0.4800	1.7986	1.9388	0.1402	1.30	0.78	5.84	31.00	15.50

**Table A.4 Data for the Plot of logarithm of nickel sulfate concentration versus logarithm of deposition rate.**

Concentration (M)	Log (C) (M)	W <sub>1</sub> (g)	W <sub>2</sub> (g)	ΔW (g)	D (cm)	H (cm)	A (cm <sup>3</sup> )	ΔX (μm)	v (μm/h)	Log (v) (μm/h)
0.0107	-1.9706	1.8234	1.8296	0.0062	1.29	0.34	3.99	2.00	1.00	0.00
0.0428	-1.3686	1.5793	1.6331	0.0538	1.29	0.76	5.69	12.21	6.10	0.79
0.1070	-0.9706	1.9035	1.9849	0.0814	1.29	0.56	4.88	21.49	10.75	1.03
0.1498	-0.8245	2.0912	2.1725	0.0813	1.29	0.46	4.48	23.45	11.72	1.07

**Table A.5 Data for plot of logarithm of sodium hypophosphite concentration versus logarithm of deposition rate.**

Concentration (M)	Log (C) (M)	$W_1$ (g)	$W_2$ (g)	$\Delta W$ (g)	D (cm)	H (cm)	A (cm <sup>3</sup> )	$\Delta X$ ( $\mu\text{m}$ )	$v$ ( $\mu\text{m}/\text{h}$ )	Log (v) ( $\mu\text{m}/\text{h}$ )
0.0107	-1.9718	1.8976	1.9016	0.0040	1.29	0.51	4.68	1.11	0.55	-0.26
0.0267	-1.5735	1.5675	1.5862	0.0187	1.30	0.38	4.20	5.73	2.86	0.46
0.0533	-1.2733	1.9432	1.9893	0.0461	1.27	0.72	5.40	11.00	5.50	0.74
0.1067	-0.9718	1.7777	1.8322	0.0545	1.28	0.24	3.54	19.88	9.94	0.99



Table A.6 Data for the plot of glycine concentration versus deposition rate of EN-P coating.

Concentration (M)	$W_1$ (g)	$W_2$ (g)	$\Delta W$ (g)	D (cm)	H (cm)	A (cm <sup>3</sup> )	$\Delta X$ ( $\mu\text{m}$ )	$v$ ( $\mu\text{m}/\text{h}$ )
0.0000	2.1301	2.3020	0.1719	1.28	0.55	4.78	46.37	23.19
0.0133	1.8834	2.0741	0.1907	1.29	0.67	5.33	46.20	23.10
0.0533	1.7689	1.9179	0.1490	1.29	0.44	4.39	43.74	21.88
0.1333	1.8734	1.9889	0.1155	1.28	0.39	4.14	36.00	18.00
0.2667	1.9825	2.1379	0.1554	1.29	0.74	5.61	35.75	17.87
0.4000	2.0070	2.1416	0.1346	1.30	0.61	5.14	33.77	16.89
0.5334	1.8356	1.9672	0.1316	1.30	0.65	5.31	32.00	16.00

Table A.7 Data for the Plot of logarithm of glycine concentration versus logarithm of deposition rate.

Concentration (M)	Log (C) (M)	W <sub>1</sub> (g)	W <sub>2</sub> (g)	ΔW (g)	D (cm)	H (cm)	A (cm <sup>3</sup> )	ΔX (μm)	v (μm/h)	Log (v) (μm/h)
0.0133	-1.8761	1.8834	2.0741	0.1907	1.29	0.67	5.33	46.20	23.10	1.36
0.0533	-1.2730	1.7689	1.9179	0.1490	1.29	0.44	4.39	43.74	21.88	1.34
0.1333	-0.8752	1.8734	1.9889	0.1155	1.28	0.39	4.14	36.00	18.00	1.26
0.2667	-0.5740	1.9825	2.1379	0.1554	1.29	0.74	5.61	35.75	17.87	1.25
0.4000	-0.3979	2.0070	2.1416	0.1346	1.30	0.61	5.14	33.77	16.89	1.23
0.5334	-0.2729	1.8356	1.9672	0.1316	1.30	0.65	5.31	32.00	16.00	1.23

Table A.8 Data for the plot of pH versus deposition rate of EN-P

PH	$W_1$ (g)	$W_2$ (g)	$\Delta W$ (g)	D (cm)	H (cm)	A ( $\text{cm}^3$ )	$\Delta X$ ( $\mu\text{m}$ )	$v$ ( $\mu\text{m/h}$ )
3.80	1.8092	1.8322	0.0230	1.30	0.55	4.90	6.06	3.03
4.87	1.4567	1.5813	0.1246	1.30	0.67	5.39	29.84	14.92
5.00	1.9735	2.0831	0.1096	1.30	0.44	4.45	31.77	15.89
6.00	1.9823	2.1928	0.2105	1.28	0.39	4.14	65.62	32.81
7.00	2.1124	2.4391	0.3267	1.29	0.74	5.61	75.14	37.57
8.08	2.1309	2.2050	0.0741	1.30	0.61	5.14	18.59	9.29
9.30	1.7589	1.7910	0.0321	1.29	0.65	5.25	7.90	3.95

Table A.9 Data for the Plot of logarithm of deposition rate versus logarithm of hydrogen ion concentration ( $\text{pH} < 7$ )

pH	-pH	$W_1$ (g)	$W_2$ (g)	$\Delta W$ (g)	D (cm)	H (cm)	A ( $\text{cm}^3$ )	$\Delta X$ ( $\mu\text{m}$ )	v ( $\mu\text{m}/\text{h}$ )	Log(v) ( $\mu\text{m}/\text{h}$ )
3.80	-3.8	1.8092	1.8322	0.0230	1.30	0.55	4.90	6.06	3.03	0.48
4.87	-4.87	1.4567	1.5813	0.1246	1.30	0.67	5.39	29.84	14.92	1.17
5.00	-5.00	1.9735	2.0831	0.1096	1.30	0.44	4.45	31.77	15.89	1.20
6.00	-6.00	1.9823	2.1928	0.2105	1.28	0.39	4.14	65.62	32.81	1.52

Table A.10 Data for the Plot of logarithm of deposition rate versus logarithm of hydrogen ion concentration (pH&gt;7)

pH	-pH	$W_1$ (g)	$W_2$ (g)	$\Delta W$ (g)	D (cm)	H (cm)	A ( $\text{cm}^3$ )	$\Delta X$ ( $\mu\text{m}$ )	v ( $\mu\text{m}/\text{h}$ )	Log (v) ( $\mu\text{m}/\text{h}$ )
7.00	-7.00	2.1124	2.4391	0.3267	1.29	0.74	5.61	75.14	37.57	0.85
8.08	-8.08	2.1309	2.2050	0.0741	1.30	0.61	5.14	18.59	9.29	0.91
9.30	-9.30	1.7589	1.7910	0.0321	1.29	0.65	5.25	7.90	3.95	0.97

**Table A.11 Data for the plot of temperature versus rate of deposition of nickel-phosphorus**

T (K)	$W_1$ (g)	$W_2$ (g)	$\Delta W$ (g)	D (cm)	H (cm)	A ( $\text{cm}^3$ )	$\Delta X$ ( $\mu\text{m}$ )	$v$ ( $\mu\text{m}/\text{h}$ )
312	1.8997	1.9021	0.0024	1.28	0.51	4.62	0.68	0.34
322	1.6734	1.6801	0.0067	1.29	0.47	4.52	1.90	0.96
331	1.9008	1.9168	0.0160	1.29	0.48	4.56	4.54	2.27
340	1.8729	1.9106	0.0377	1.28	0.42	4.26	11.43	5.72
349	2.0124	2.0949	0.0825	1.30	0.59	5.06	21.03	10.53
360	1.8914	2.0294	0.1380	1.30	0.62	5.18	34.35	17.18

**Table A.12 Data for temperature dependence plot of logarithm of deposition rate of nickel-phosphorus versus reciprocal of temperature (K).**

T (K)	1/T (K)	W <sub>1</sub> (g)	W <sub>2</sub> (g)	ΔW (g)	D (cm)	H (cm)	A (cm <sup>3</sup> )	ΔX (μm)	v (μm/h)	Log (v) (μm/h)
310	0.0033	1.9245	1.9270	0.0025	1.29	0.55	4.85	0.68	0.34	-0.47
320	0.0032	1.6739	1.6817	0.0078	1.29	0.67	5.33	1.90	0.96	-0.02
330	0.0030	1.8934	1.9089	0.0155	1.29	0.44	4.39	4.54	2.27	0.36
340	0.0029	2.1801	2.2177	0.0376	1.30	0.39	4.25	11.43	5.72	0.76
350	0.0029	1.8829	1.9743	0.0914	1.29	0.74	5.61	21.03	10.51	1.02
360	0.0028	1.8934	2.0287	0.1353	1.29	0.61	5.08	34.35	17.17	1.23

**Table A.13 Data for the plot of temperature versus phosphorus content of an EN-P deposit (w%).**

T (K)	Phosphorus (w%)
310	10.78
320	10.58
330	10.43
340	10.05
350	9.74
360	9.85



**Table A.14 Data for the plot pH versus phosphorus content EN-P deposit (w%).**

pH	Phosphorus (w%)
3.8	12.5
5	10
6	7.2
7	6.8
8	6
9.25	4.2

**Table A.15 Data for the plot of sodium borohydride concentration versus deposition rate of EN-B.**

Concentration (M)	$W_1$ (g)	$W_2$ (g)	$\Delta W$ (g)	D (cm)	H (cm)	A ( $\text{cm}^3$ )	$\Delta X$ ( $\mu\text{m}$ )	$v$ ( $\mu\text{m/h}$ )
0.0200	1.7324	1.7324	0.0000	1.29	0.51	4.68	0.00	0.00
0.0425	2.1113	2.2781	0.1668	1.29	0.51	4.68	46.00	23.00
0.0550	1.9008	2.0353	0.1345	1.29	0.32	3.91	44.40	22.20
0.0725	1.7682	1.8952	0.1270	1.28	0.45	4.39	37.40	18.70
0.0950	1.9468	2.0439	0.0971	1.30	0.31	3.92	32.00	16.00
0.1515	1.8926	2.0129	0.1203	1.30	0.68	5.43	28.60	14.30
0.1800	1.9082	2.0031	0.0949	1.29	0.54	4.80	25.50	12.75

**Table A.16 Data for the plot of sodium borohydride concentration versus boron content of EN-B coating (w%).**

Concentration (M)	Boron (w%)
0.0000	0.00
0.0430	6.46
0.0543	6.76
0.0733	7.31
0.0951	7.40
0.1524	9.00
0.1795	8.44

## APPENDIX B: Vickers hardness measurement of EN-B coated AA6061 aluminum alloy

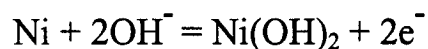
**Table B.1 Vickers hardness measurements of Ni-B coated AA6061 aluminum alloy samples subjected to various heat treatment durations at 220 °C in vacuum.**

Heat-treatment duration (h)	Diameter of indentation ( $\mu\text{m}$ )	Average diameter of indentation ( $\mu\text{m}$ )	Hardness (Vickers)
9	4.70, 4.70, 4.55, 4.65, 4.65, 4.70, 4.60	4.65 $\pm$ 0.06	875.48 $\pm$ 19.97
12	4.60, 4.55, 4.65, 4.65, 4.65, 4.50, 4.60	4.60 $\pm$ 0.06	876.22 $\pm$ 20.63
24	4.80, 4.65, 4.70, 4.60, 4.50, 4.60, 4.70	4.65 $\pm$ 0.10	857.48 $\pm$ 32.77
36	4.85, 4.75, 4.65, 4.70, 4.60, 4.60, 4.75	4.70 $\pm$ 0.09	839.33 $\pm$ 29.95
48	4.80, 4.70, 4.60, 4.50, 4.65, 4.60, 4.70	4.65 $\pm$ 0.10	857.48 $\pm$ 32.77
60	4.50, 4.70, 4.50, 4.55, 4.55, 4.55, 4.50	4.60 $\pm$ 0.07	876.22 $\pm$ 24.97
72	4.70, 4.50, 4.50, 4.60, 4.60, 4.60, 4.70	4.60 $\pm$ 0.08	876.22 $\pm$ 28.83
84	4.50, 4.40, 4.40, 4.60, 4.60, 4.50, 4.50	4.55 $\pm$ 0.08	895.59 $\pm$ 35.71
96	4.70, 4.55, 4.65, 4.80, 4.60, 4.65, 4.60	4.60 $\pm$ 0.08	876.22 $\pm$ 27.42
108	4.60, 4.40, 4.45, 4.40, 4.60, 4.55, 4.50	4.55 $\pm$ 0.09	895.59 $\pm$ 32.66
120	4.00, 4.50, 4.35, 4.50, 4.60, 4.45, 4.40	4.45 $\pm$ 0.19	936.29 $\pm$ 85.68
132	4.40, 4.40, 4.60, 4.50, 4.50, 4.50, 4.60	4.50 $\pm$ 0.08	915.60 $\pm$ 34.00
144	4.20, 4.50, 4.40, 4.30, 4.50, 4.40, 4.50	4.40 $\pm$ 0.12	957.69 $\pm$ 47.88

## APPENDIX C

The  $E^0$  value for each reaction was calculated from the free energy of formation of the compounds.  $E_{eq}$  values were calculated from the  $E^0$  value and using the Nernst equation for a pH 11.6. The calculations are shown below. Standard  $G^0$  values were taken from Latimer [145].

1) For equation (4.17):



$$\Delta G^0 = G^0_{\text{Ni}(\text{OH})_2} - G^0_{\text{Ni}} - 2G^0_{\text{OH}^-}$$

$$\Delta G^0 = -108.3 - 2(-37.595)$$

$$\Delta G^0 = -33.11$$

$$E^0 = \frac{\Delta G^0}{nF}$$

$$E^0 = \frac{-33.11 \times 10^3}{2 \times 23060} = -0.72$$

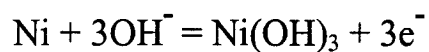
$$E^0 = -0.72 \quad E_{eq} = E^0 + (0.059/2)\log(1/a_{\text{OH}^-})$$

$$E_{eq} = E^0 + (0.059)\text{pOH}$$

$$\text{pOH} = 14 - \text{pH} \quad \text{pH} = 11.6 \rightarrow \text{pOH} = 2.4$$

$$E_{eq} = -0.72 + (0.059)(2.4) \rightarrow E_{eq} = -0.58 \text{ V}$$

2) For equation (4.18):



$$\Delta G^0 = G_{\text{Ni}(\text{OH})_3}^0 - G_{\text{Ni}}^0 - 3G_{\text{OH}^-}^0$$

$$\Delta G^0 = -129.5 - 3(-37.595)$$

$$\Delta G^0 = -16.715$$

$$E^0 = \frac{-\Delta G^0}{nF}$$

$$E^0 = \frac{-16.715 \times 10^3}{3 \times 23060} = -0.24$$

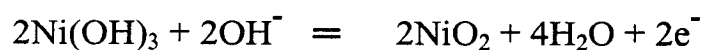
$$E^0 = -0.24 \text{ V} \quad E_{\text{eq}} = E^0 + (0.059/2)\log(1/a_{\text{OH}^-})$$

$$E_{\text{eq}} = E^0 + (0.059)\text{pOH}$$

$$\text{pOH} = 14 - \text{pH} \quad \text{pH} = 11.6 \rightarrow \text{pOH} = 2.4$$

$$E_{\text{eq}} = -0.24 + (0.059)(2.4) \rightarrow E_{\text{eq}} = -0.098 \text{ V}$$

3) For equation (4.19):



$$\Delta G^0 = 2G_{\text{NiO}_2}^0 + 4G_{\text{H}_2\text{O}}^0 - 2G_{\text{Ni}(\text{OH})_3}^0 - 2G_{\text{OH}^-}^0$$

$$\Delta G^0 = 2(-47.5) + 4(-56.690) - 2(-129.5) - 2(-37.595)$$

$$\Delta G^0 = 12.43 \quad E^0 = \frac{\Delta G^0}{nF}$$

$$E^0 = \frac{12.43 \times 10^3}{2 \times 23060} = 0.27$$

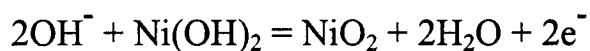
$$E^0 = 0.27 \text{ V} \quad E_{\text{eq}} = E^0 + (0.059/2)\log(1/a_{\text{OH}^-})$$

$$E_{\text{eq}} = E^0 + (0.059)\text{pOH}$$

$$\text{pOH} = 14 - \text{pH} \quad \text{pH} = 11.6 \rightarrow \text{pOH} = 2.4$$

$$E_{\text{eq}} = 0.27 + (0.059)(2.4) \rightarrow E_{\text{eq}} = 0.41 \text{ V}$$

4) For equation (4.20):



$$\Delta G^0 = G^0_{\text{NiO}_2} + 2G^0_{\text{H}_2\text{O}} - 2G^0_{\text{OH}^-} - G^0_{\text{Ni}(\text{OH})_2}$$

$$\Delta G^0 = -47.5 + 2(-56.690) - 2(-37.595) - (-108.3)$$

$$\Delta G^0 = 22.61$$

$$E^0 = \Delta G^0 / nF$$

$$E^0 = \frac{22.61 \times 10^3}{2 \times 23060}$$

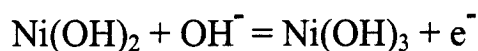
$$E^0 = 0.49 \text{ V} \quad E_{\text{eq}} = E^0 + (0.059/2)\log(1/a_{\text{OH}^-})$$

$$E_{\text{eq}} = E^0 + (0.059)\text{pOH}$$

$$\text{pOH} = 14 - \text{pH} \quad \text{pH} = 11.6 \rightarrow \text{pOH} = 2.4$$

$$E_{\text{eq}} = 0.49 + (0.059)(2.4) \rightarrow E_{\text{eq}} = 0.63 \text{ V}$$

5) For equation (4.21):



$$\Delta G^0 = G^0_{\text{Ni(OH)}_3} - G^0_{\text{Ni(OH)}_2} - G^0_{\text{OH}^-}$$

$$\Delta G^0 = -129.5 - (-108.3) - (-37.595)$$

$$\Delta G^0 = 16.395$$

$$E^0 = \frac{\Delta G^0}{nF}$$

$$E^0 = \frac{16.395 \times 10^3}{1 \times 23060} = 0.71$$

$$E^0 = 0.71 \text{ V} \quad E_{\text{eq}} = E^0 + (0.059/2)\log(1/a_{\text{OH}^-})$$

$$E_{\text{eq}} = E^0 + (0.059)\text{pOH}$$

$$\text{pOH} = 14 - \text{pH} \quad \text{pH} = 11.6 \rightarrow \text{pOH} = 2.4$$

$$E_{\text{eq}} = 0.71 + (0.059)(2.4) \rightarrow E_{\text{eq}} = 0.85 \text{ V}$$



## APPENDIX D:

**Table D.1 Peak potential difference vs. scan rate (mV/s).**

Scan rate (mV/s)	$E_{pc}-E_{pa}$ (V) pH 3.5	$E_{pc}-E_{pa}$ (V) pH 5.5	$E_{pc}-E_{pa}$ (V) pH 7.5	$E_{pc}-E_{pa}$ (V) pH 10.5
10	132	110	120	122
30	158	144	150	138
50	178	166	166	154
70	192	184	188	158
100	218	212	208	158
150	248	244	240	158
200	272	268	262	158
250	294	298	290	174
300	318	316	308	174
350	336	338	328	176
400	362	356	348	182
450	374	374	364	182
500	396	394	382	178